A STUDY OF STRUCTURAL PROPERTIES AND PERFORMANCE OF Ni-Co-Mg-Al-Ox CATALYST FOR CARBON DIOXIDE REFORMING OF METHANE

A Thesis Submitted to the College of

Graduate and Postdoctoral Studies

in Partial Fulfilment of the Requirements for

the Degree of Doctor of Philosophy in the

Department of Chemical and Biological Engineering

University of Saskatchewan

Saskatoon, Saskatchewan

By

Wahab Alabi Olaiya

PERMISSION TO USE

In presenting this thesis in partial fulfillment of the requirements for a Doctor of Philosophy Degree from the University of Saskatchewan, I agree that the libraries of this University may make this thesis freely available for inspection. I further agree that permission for copying of this thesis in any manner, in whole or in part, for scholarly purpose may be granted by the professors who supervised my thesis work or, in their absence, by the Head of the Department or the Dean of the College of Graduate and Postdoctoral Studies in which the thesis work was complete. It is understood that any copying or publication or use of this thesis or parts thereof for financial gain shall not be allowed without my written permission. It is also understood that due recognition shall be given to me and to the University of Saskatchewan in any scholarly use which may be made of any material in my thesis.

Requests for permission to copy or to make other use of material in this thesis in whole or parts shall be addressed to:

Head of the Department of Chemical and Biological Engineering

University of Saskatchewan

Saskatoon, Saskatchewan

S7N 5A9, Canada

OR

Dean

College of Graduate and Postdoctoral Studies

University of Saskatchewan

116 Thorvaldson Building, 110 Science Place

Saskatoon, Saskatchewan

S7N 5C9, Canada

ABSTRACT

Previous work from our group has established Ni-Co-Mg-Al-Ox catalyst to be an active and stable catalyst for CO_2 reforming of Methane, also known as dry reforming of Methane (DRM). Additionally, bimetallic Ni-Co showed better performance compared to individual monometallic catalysts of Ni or Co. Further studies revealed that Ni and Co showed different extent and kinetics of reduction. The relationship between the bulk structure and reducibility of active metals (Ni and Co) has not yet been studied. The individual interaction of the active metals with the component of the support is yet to be examined. Likewise, exploration of other feed source for DRM or dry reforming of higher hydrocarbon on Ni-Co-Mg-Al-Ox catalyst has not been studied. The primary aim of this research work is to study the effects of Mg/Al ratio (support) on the bulk structure, basicity, metal support interaction, metal site formation and site performance of Ni-Co-Mg-Al-Ox catalyst for CO_2 reforming of CH_4 (DRM).

The research plan for this project is divided into two parts. Part one focuses on understanding the relationship between bulk structure, site formation and catalytic performance of monometallic (Ni or Co) and bimetallic Ni-Co-Mg-Al-Ox for DRM, as the Mg/Al ratio in the support changes. The second part focuses on the exploration of DRM using simulated coal gas feed and CO_2 reforming of C_2H_6 (shale gas contains appreciable amount of C_2H_6).

For part one, the effects of Mg/Al ratio on the bulk structure, site formation and performance of Ni-Co-Mg-Al-Ox for dry reforming were studied. High Mg/Al ratio showed $NiCoO_2$ + MgO-solid phase + spinel structure, compared to the lower ratio that showed a complete spinel structure. This additional MgO phase improved the basicity and the easy of reduction of the active metals, leading to better activity and stability of catalyst to DRM reaction. With respect to the monometallic catalysts, supported Ni and Co showed similar structure, but different metal

reducibility and site performance for DRM. The Al-Ox supported Co catalyst showed no reducibility and activity, appreciable amounts of both properties was found in the corresponding Ni catalyst. Introduction of MgO into the support improved metal reduction and basicity of support, making the performance of the catalysts better. These observations were related to the different interaction and distribution of the metals within the support system.

For part two, DRM was studied using simulated coal feed gas at higher temperature (900 ^{o}C) using larger catalyst loading. Better activity, stability and product selectivity were observed in bimetallic Ni-Co with higher Mg/Al ratio compared to the lower ratio and monometallic Ni catalyst. Also, appreciable amount of activity was found using the coal gas feed, even though the amount of CO_2 and CH_4 were small compared to other components of the feed. The difference in the activity of catalysts using both feed was related to the difference in the composition of CH_4 and CO_2 in both feeds. For CO_2 reforming of Ethane (CRE), two main points were addressed in this study; C_2H_6 dissociation study and CO_2 reforming of C_2H_6. Results showed that the catalyst support, catalyst in oxide form and reduced catalysts can activate CO_2 reforming of C_2H_6, unlike DRM that needs reduced catalyst for the reaction to proceed. Additionally, higher Mg/Al ratio catalysts showed preference for CRE over C_2H_6 dissociation, while lower Mg/Al ratio catalysts showed preference for C_2H_6 dissociation over CRE.

In conclusion, variation of the composition of Mg/Al ratio in the support led to changes in the bulk structure, basicity, metal support interaction, active metal distribution, reducibility and performance of monometallic (Ni, Co) and bimetallic (Ni-Co) catalysts for DRM. Higher Mg/Al ratio improved the basicity of support leading to easy activation of CO_2, which helped in the conversion of deposited carbon to CO. The presence of sufficient active site helped (synergistically with support) in the activation of the CH_4, leading to better catalytic performance.

ACKNOWLEDGEMENTS

My sincere appreciation goes to my supervisor, Professor Hui Wang for his patience, guidance, encouragement and constructive criticism during research and thesis writing period. His mentorship and encouragement in making me apply for MITACS Globalink Research Award for a collaborative project at Taiyuan University of Technology, Shanxi, China is also appreciated.

I would like to thank the members of my advisory committee, Dr. Dalai, Dr. Scott, Dr. Hu and Dr. Soltan for their valuable feedback during my research work, as well as the thesis writing. Their comments and suggestions helped to improve the quality of my results presentation. I also appreciate the contribution of Dr. Christian Patzig (Centre of Applied Microstructure Diagnostic, Fraunhofer, Germany) in the STEM-EDX analysis and results interpretation.

I am grateful to the technical staff of the Department of Chemical and Biological Engineering, University of Saskatchewan, especially Richard Blodin, for his assistance with purchase of laboratory supplies, developing GC analytical method and troubleshooting of instruments. The Secretaries of the Department are also appreciated, especially Kelly Bader and Paul Meghan, you guys are such wonderful and understandable personalities.

Many thanks to the entire staff of Key Laboratory of Coal Science and Technology, Ministry of Education of China and Shanxi Province, Taiyuan University of Technology, Taiyuan, Shanxi, and more specifically, Professor Huang's group for allowing me to use their equipment and familiarising me with all the characterization equipment. Special thanks to Li Xiandong, Du Yali and Lu Xiaobo for their companionship in and out of the Laboratory. My greatest appreciation goes to Professor Huang, your gesture towards me was greatly appreciated and I would keep the memories forever.

I acknowledge NSERC and MITACS for providing the fund for this research work and appreciate the other members of Dr. Wang's group for their valuable advice at every stage of this research work.

Mention must be made of friends that gave me courage during the adversity period of my studies: Kazeem O. Sulaiman, Emma Bruce and Adewumi Adeshina. I appreciate you guys and value your contributions toward the completion of this research work.

I must not forget to mention the special people in my life; Oloyede Hairat Adejoke (my darling wife), Alabi Aminat (pretty sister), Alabi Habibat (baby sister), Alabi Jameel Oluwatawalore (adorable son), Alhaji and Alhaja Oloyede (lovely in-laws), thanks for all your support and prayers during the hardest time of my programme. I so much appreciate and love you all. To the entire members of Alabi's family, thanks for filling all voids during my absence.

To my mum, I miss you so much. I wish you are here today to see what your son has become, but to Allah we shall return. I love you so much, till we meet and part no more. I pray almighty Allah grant you Aljanat Firdaus (Ameen). To my Dad, thanks so much and may Allah make paradise your abode.

DEDICATION

To Almighty Allah, my source of life and the most knowledgeable.

To Prophet Muhammad (SAW), the light of guidance.

To my Mum (Alhaja Rukayat Alabi), who I loved and cherished more than life itself.

To my wife (Queen Oloyede Hairat Adejoke), who stood by me, encouraging and praying for me throughout this academic journey.

To my precious son (Alabi Jameel Oluwatawalore), whose birth gave me strength at the toughest period of this journey.

TABLE OF CONTENTS

LIST OF TABLES

LIST OF FIGURES

NOMENCLATURE

a, b, c, a_0, b_0, c_0	Constants
dp	Particle size
E_a, E_b, E_c	Apparent activation energy, kJ mol^{-1}
F	Volumetric flow rate (ml min^{-1})
h	Extent Ni reducibility (%)
k, k_0	Specific rate of reaction
L	Loading of the active metal (mol g^{-1})
m, n	Reaction order
n_i	Molar flow rate (mol min^{-1})
P	Pressure, kPa
pH	Potential of hydrogen
R	Ideal gas constant
r_i	Rate of reaction per unit weight of catalyst, mol g^{-1} s^{-1}
T	Temperature, (K, ^oC)
U_{CO}	CO uptake (μmol g^{-1})
x	Degree of spinel inversion
X	Conversion of reactant
$W_{catalyst}$	Weight of catalyst (g)
y	Extent of Co reducibility (%)

ABBREVATIONS

BE	Binding energy
BET	BET- Brunauer–Emmett–Teller
CN	Co-ordination number
CRE	CO_2 reforming of ethane
CRM	CO_2 reforming of methane
DRM	Dry reforming of methane
EDX	Energy dispersive X-ray
FCC	Face cubic centre
F-gases	Fluorinated gases
GC	Gas chromatography
HFCs	Hydrofluorocarbons
ICP-MS	Inductively coupled plasma mass spectrometry
IUPAC	International union of pure and applied chemistry
JCPDS	Joint committee on powder diffraction standard
Ksp	Solubility product constant
L-H	Langmuir- Hinshelwood
MFC	Mass flow controller
NMR	Nuclear magnetic resonance spectroscopy
PFCs	Perfluorocarbons
RWGS	Reverse water gas shift
STEM	Scanning transmission electron microscopy
Syngas	Synthesis gas
TCD	Thermal conductivity detector
TEM	Transmission electron microscopy

TOF	Turnover frequency
TOS	Time on stream
TPD	Temperature programmed desorption
TPO-MS	Temperature programmed oxidation-mass spectrometry
TPR	Temperature programmed reduction
XANES	X-ray absorption near edge structure
XPS	X-ray photoelectron spectroscopy
XRD	X-ray powder diffraction

CHAPTER ONE

HUMAN ACTIVITIES AND GLOBAL WARMING

The relationship between human activities, greenhouse gases emission and global warming is explained in this chapter. Ways of mitigating and the utilization of greenhouse gases are also highlighted. The last part of this chapter summarizes the content and organization of the entire thesis.

1.1 Global Warming and Greenhouse Gases.

Global warming is the increase in the earth's atmospheric and oceanic temperatures widely predicted to occur due to increase in greenhouse emission, resulting especially from pollution. The warming that happens when certain gases (greenhouse gases) in earth atmosphere traps heat is known as greenhouse effect. These gases let in infra-red light but prevent heat from escaping. Greenhouse gases include water vapour, CO_2, CH_4, N_2O and fluorinated gases. Over past decades, global warming has been a major concern due to the various changes it has caused in our environment and natural resources. Melting of glaciers, rising in sea levels, dying of cloud forests, scrambling of wild life to keep pace, changes in weather conditions in some parts of the world have been credited to global warming caused by the emission of greenhouse gases (National geography, 1996). Naturally, greenhouse gases are present in the atmosphere to sustain life on earth by trapping heat from the sun and warm the earth. Without naturally occurring heat-trapping gases (water vapour, carbon dioxide and methane), the earth would be too cold to sustain life (National geography, 1996). Expeditious increase of carbon dioxide and other greenhouse gases in the atmosphere has intensified this natural greenhouse effect, thereby creating a major environmental concern.

Human activities in modern days such as burning fossil fuels, deforestation, intensive agricultural practices have added huge quantities of carbon dioxide and other greenhouse gases emission into the atmosphere. Modern atmosphere contains 42 % more CO_2 than it did at the start of the industrial era. CH_4 and CO_2 levels have attained their highest level than they have been in nearly half a million years (Suzuki, 2014). The strength of the greenhouse effect and the extent of extra energy directed towards the earth's surface depend on how much greenhouse gas molecules in the atmosphere. When greenhouse gases concentration is high, they absorb a greater percentage of the earth's infrared energy emissions and more energy gets re-emitted back toward the earth's surface, raising its average surface temperature (Suzuki, 2014).

1.2 Emission of Greenhouse Gases

The two major ways greenhouse gases get into the atmosphere are human activities and natural processes. While human activities include burning of fossil fuels, deforestation, intensive livestock farming, use of synthetic fertilizers and industrial processes, natural processes entail animal and plant respiration (US Department of Energy, 2008). Plants and other photo-synthesizers can only remove finite amounts of greenhouse gases like CO_2 and almost all the photosynthetic capacity goes toward balancing out natural CO_2 emission. After all the CO_2 emitted by animal respiration and organic decomposition has been accounted for, there will be no sufficient photosynthetic capacity left to clear the CO_2 emitted through fossil fuel combustion (US Department of Energy, 2008). Considering the individual emission of the greenhouse gases, the use of fossil fuel is the major source of CO_2 emission. Direct human activity on land use and forestry can also lead to CO_2 emission, while its removal from the atmosphere can occur through reforestation, soil improvement and some other human activities.

The burning of biomass, energy use, waste management and agricultural activities can all contribute to the emission of CH_4 into the atmosphere. While the use of fertilizer for agricultural purposes is the primary source of N_2O emission, combustion of fossil fuels can also generate N_2O. Fluorinated gases (F-gases) are majorly emitted through industrial processes, refrigeration and the use of consumer products such as hydrofluorocarbons (HFCs), perfluorocarbons (PFCs), and sulfur hexafluoride (SF_6) (Environmental Protection Agency, 2014). The pie chart in Figure 1.1 shows the percentage of greenhouse gases emitted into the atmosphere via human activities. CO_2 and CH_4 are the major component of the emitted gases, with 76% of the total gases allotted to CO_2 and 16% to CH_4. Also, CO_2, CH_4, N_2O and the fluorinated gases are all well-mixed gases in the atmosphere and do not react to changes in either air pressure or temperature. Thus, they do not get removed easily like water that condenses to become rain or snow (Ramaswamy et al., 2001). Their long atmospheric lifetimes allow them to have a lasting effect on global warming and climate change. Since these gases have long atmospheric life time, there is need to limit their emission or other means of converting them to useful products should be devised.

1.3 Limiting the Emission of Greenhouse Gases

Upon realization that greenhouse gases are threat to our atmosphere, various researchers have been exploring ways or techniques of limiting the emission of these gases into the atmosphere. Since CO_2 and CH_4 are the major components of the greenhouse gases, more efforts have been devoted to finding ways to limit their emission or convert them to useful products.

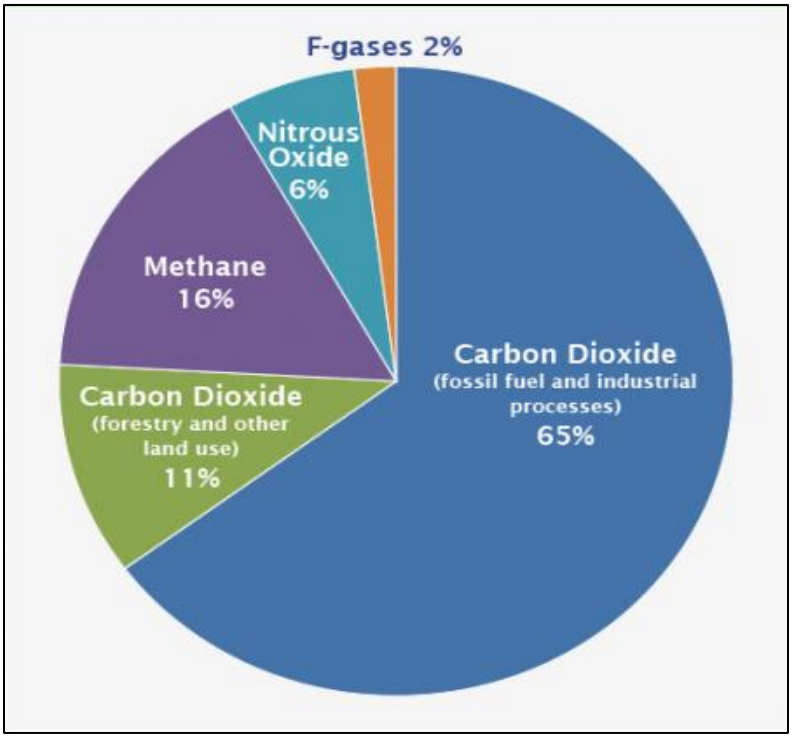

Figure 1.1. Greenhouse gases emission from human activities. (Intergovernmental panel on climate change (IPCC) report, 2014).

As per Choi and Cho, 2008; in most parts of the world, three kinds of mitigation process are in use or under consideration. They include:

1) Reduction of fossil energy consumption from industries;
2) Replacement of fossil energy by renewable energy sources and;
3) Effective utilization of CO_2 as a clean carbon raw material for carbon market products.

With proper agent, CO_2 can be converted to many useful hydrocarbon products as seen in Figure 1.2. All these products are useful for daily human needs, as well as having a good market value.

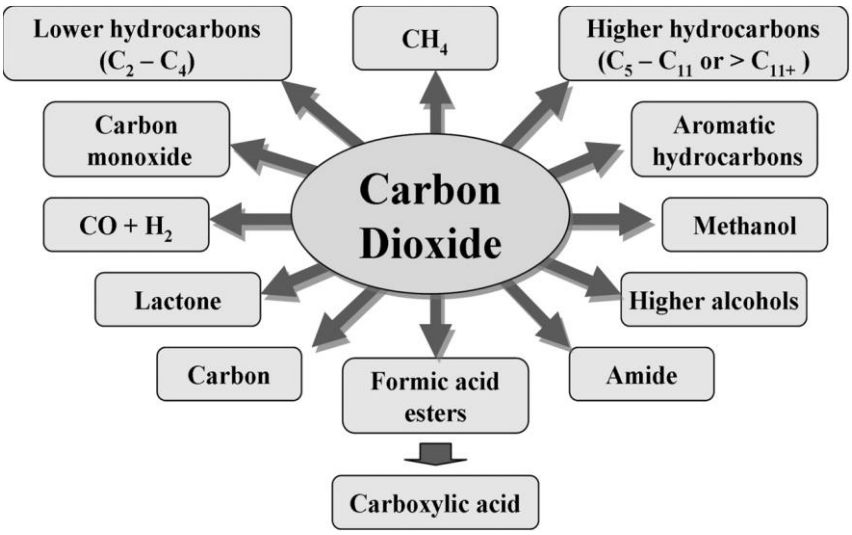

Figure 1.2. Chemicals that can be obtained from CO_2 (Choi and Cho, 2008).

1.4 Utilization of Greenhouse Gases

Utilization of greenhouse gases is one of the highlighted ways of mitigating the emission of greenhouse gases into the atmosphere. To achieve this goal, several methods have been investigated through biological and chemical means. Biological method involves the use of microbes in converting these gases (most especially CO_2) to useful products. Some of the biological methods highlighted by Choi and Cho, 2008; include but not limited to:

- Production of high value-added products from CO_2 by microalgae;
- Transfer system of CO_2 to fuel using cyanobacteria;
- Development of a biological fixation process of CO_2;
- Removal process of CO_2 and production of H_2 using Anabaena variabilis;
- Electrochemical conversion of CO_2 using microbial enzymes and;
- Fixation technology for CO_2 by electrochemical reduction.

On the other hand, the chemical method involves the conversion of these gases to useful products via chemical reaction. Some of the chemical methods highlighted by the same author (Choi and Cho, 2008) include:

- Manufacturing processes for methanol and Dimethyl ether from CO_2 using $Cu/Zn/Al_2O_3$ based catalyst;
- Production of dimethyl carbonate from CO_2;
- Ethylbenzene dehydrogenation using CO_2 oxidation;
- Hydrocarbon production using CO_2;
- A study for conversion of CO_2 over phase-transfer catalysts;
- Hydrogenation of CO_2 using the reverse water-gas shift reaction;
- Optimization of methanol synthesis and process development of methanol to olefin by catalytic hydrogenation of CO_2;

- CO_2 reforming of methane to syn-gas (CO and H_2);
- Synthesis of compounds from CO_2 by homogeneous reaction;
- Decomposition of CO_2 using a thermal plasma;
- Chemical fixation of CO_2 by catalysts and;
- Production technology of a substitute fuel by hydrogenation of CO_2.

Of all the technologies highlighted, only CO_2 reforming of CH_4 utilizes the two major greenhouse gases to give a highly useful industrial product called syngas. The differences between this method and other methods of producing syngas are discussed in section 1.5.

1.5 Methods of Producing Syngas

Syngas is one of the most important industrial feedstocks to produce different chemicals and it is a mixture of hydrogen (H_2) and carbon monoxide (CO). The downstream synthesis of these chemicals depends on the H_2/CO ratio of the syngas, as this ratio is usually dictated by the H/C ratio of the primary feedstock or the reaction routes of producing the syngas (Wu et al., 2005). The three most commonly used methods of producing syngas are:

- Steam reforming of CH_4

$$CH_4 + H_2O \rightleftharpoons 3H_2 + CO \qquad 1.1$$

- Partial oxidation of CH_4

$$CH_4 + 0.5O_2 \rightleftharpoons 2H_2 + CO \qquad 1.2$$

- CO_2 reforming of CH_4 (dry reforming reaction)

$$CH_4 + CO_2 \rightleftharpoons 2H_2 + 2CO \qquad 1.3$$

Different combinations of these three basic reactions can be utilized for different objectives.

Over time, steam reforming has been the most common and widely used technology for syngas production as stated by Cheng and Kung, (1994); LeBlanc et al., (1994); Adris et al., (1996). But the inherent drawback of this process originates from the fact that the H_2/CO ratio in the syngas is theoretically 3, which is usually too high compared to the ratio required by many downstream synthesis processes. Also, to avoid catalyst deactivation through carbon deposition, excess steam more than the stoichiometric requirement must be used (Armor, (1999); LeBlanc et al., (1994)), which leads to higher operational costs. Additionally, the reactor (that is of the high-temperature tubular heat exchanger type) is often inefficient and very expensive (Wu et al., 2005).

Partial oxidation of CH_4 can theoretically yield a syngas with a H_2/CO ratio of 2, which is suitable for many downstream synthesis processes. Non-catalytic CH_4 oxidation operates under the conditions of 30-100 atm and 1573 K (Armor, 1999), which translates to high operation costs (Wu et al, 2005). On the other hand, the catalytic CH_4 oxidation process can operate at relative lower temperatures. Although it is considered a promising technology, yet the economics of partial oxidation could be restricted by the cost of pure oxygen supply.

In recent years, CO_2 reforming CH_4 has attracted a lot of interests due to its industrial and environmental benefits. From industrial point of view, this reaction can yield H_2/CO ratio of 1, which is a desirable feedstock for Fischer-Tropsh synthesis (Gadalla and Bower, 1988) and for the synthesis of oxygenates (Burch and Petch, (1992); Alyea et al., (1993)). While from environmental point of view, this reaction offers a route for the conversion of two major greenhouse gases to useful product (syngas), limiting the emission of greenhouse gases that can cause global warming in the atmosphere. One major setback in the realization of these potentials is getting an affordable and long-lasting catalyst that can withstand the reaction condition (high temperature) without easy deactivation (Adris et al., (1996); Armor, (1999); Qin and Lapszewicz, (1994); Richardson,

(1989)). Thus, latest research efforts have been largely centered on modifying or developing catalysts that are active and stable for CO_2 reforming of CH_4 reaction.

1.6 Catalyst Development for CO_2 Reforming CH_4

Since the inception of CO_2 reforming of CH_4 (DRM) up till recent time, catalysts development has been an on-going research area towards industrialization of the process. Earlier publications have shown that group VIII transition metals (Ni, Ru, Rh, Pd, Ir, and Pt) show activity towards this reaction (Ferreira-Aparicio et al., (1998); Edwards and Maitra, (1995)), while noble metals (ruthenium and rhodium) show superiority in terms of activity and carbon deposition resistant (Bradford and Vannice, 1999). However, considering their high cost and restricted availability, scale-up toward industrial level of noble metals is not suitable economically.

Supported Ni catalysts have drawn remarkable attention in this area due to its high activity to the reaction and wide availability (Rostrup-Nielsen, 1997). However, Ni catalysts suffer more severe catalyst deactivation than noble metal-based catalysts due to sintering, metal oxidation (Slagtern, et al, 1997), and especially severe carbon formation (Ashcroft et al., (1991), Rostrup-Nielsen, (1997); Bradford and Vannice, (1999)) on the catalyst surface and/or on the tubes of the reactor, leading to deactivation of the catalyst and/or a plugging of the reactor tubes.

Supported cobalt catalysts have also been reported to show considerable activity for DRM (Ruckenstein and Wang, 2000). Although the catalytic performance is neither superior to Ni nor to the noble metal catalysts, but it is probable that the mechanism of carbon deposition on Co metal is different from that on Ni (Ferreira-Aparicio et al., 1998). Recent improvements in the performance of catalysts (Ni and Co) for this reaction have been achieved through changing the nature of support, improved dispersion of active metals, particle size adjustment, trying different supports, using composite support, preparation method, addition of promoters, improved metal-

metal interaction and metal support interaction (Chen et al., (2013); Garcia et al., (2010); Zhu et al., (2012); Ranjbar and Rezaei, (2012)). While a detailed literature review based on dry reforming catalyst is presented in chapter 2, our contribution towards good catalyst development, along with the objective of present study are presented in section 1.7.

1.7 Previous Work from this Group

Previous work from this group had reported that Ni-Co catalysts showed better activity and stability in a bimetallic catalyst system compared to Ni-Fe, Ni-Cu and Ni-Mn (Zhang et al., 2007). Variation of Ni/Co ratio and their composition in Ni-Co-Mg-Al-O bimetallic system resulted in different catalytic performance and resistance to carbon deposition (Zhang et al., 2008). Higher Ni-Co loading resulted in catalyst deactivation through carbon deposition (Zhang et al., 2007; 2008). Co-precipitation method of catalyst preparation showed better catalytic performance and enhanced Ni-Co interaction in forms of alloy compared to impregnation method. More Ni reduction was observed compared to Co in all the catalysts, irrespective of the preparation methods (Wang et al., 2012). Different extent of metal reduction, as well as different mechanism and kinetics of Ni and Co reductions were observed in impregnation and co-precipitation catalysts (Wang et al, 2012). These differences are believed to originate from the bulk structure of the catalysts and the interaction of the active metals with the component of the support. While Ni is known to be the main active metal for this reaction in the bimetallic catalyst system, the role of Co remains to be clearly defined or re-defined. Also, the individual interaction of Ni and Co with the component(s) of the support and detailed examination of monometallic Ni and Co catalysts for DRM remain unexamined in our catalyst system.

1.8 Research Objectives and Sub-objectives

The major objective and sub-objectives are listed below;

Objective:

- Study the effects of support on the catalytic properties and performance of Ni-Co-Mg-Al-Ox catalyst for DRM.

Sub-objectives

- Study the effect of Mg/Al ratio on the bulk structure, extent of metal reduction, site formation and the catalytic properties of monometallic (Ni and Co) and bimetallic Ni-Co-Mg-Al-Ox for DRM.
- Study the industrial application of DRM on Ni-Co-Mg-Al-Ox catalyst using coal gas feed as compared to pure gas feed.
- Explore CO_2 reforming of C_2H_6 and study the effect of support on the catalytic performance.

1.9 Structure of Thesis

The entire thesis consists of eight main chapters numbered 1 to 8, in addition to the reference and appendix sections. Chapter 1 relates global warming effect to human activities in this industrialization era. Mitigation efforts are also discussed leading to dry reforming reaction and catalyst development. Previous work and current research objectives from our group are stated in this chapter. Chapter 2 presents literature review with respect to catalysts modification for DRM. Experimental procedure as well as catalyst characterization methods and procedures are highlighted in Chapter 3. Extensive catalyst characterization results are discussed in Chapter 4. How changes in the nature, as well as compositional changes in the support affect the catalytic properties and site generation are the major highlights of this

Chapter. Experimental results with respect to the bulk structure and site performance are presented in Chapter 5. Comparison of DRM using ideal feed and coal delivered feed based on catalysts properties and feed composition are shown in Chapter 6. Chapter 7 is devoted to the study of CO_2 reforming of C_2H_6. Dissociation of C_2H_6 is also highlighted in this Chapter. Conclusions and recommendations for future work are highlighted in Chapter 8. The remaining part of the thesis consist of Appendices and References

Four publications are expected from this work. Two publications based on Chapters 3, 4 and 5. One publication from Chapter 6 (already in press with Catalysis Today Journal) and at least one publication from Chapter 7.

CHAPTER TWO

CATALYST DEVELOPMENT FOR DRY REFORMING REACTION

A brief review on catalyst development for DRM reaction is presented in this chapter. Progressive development towards modification of Ni and Co catalysts for this reaction is also highlighted. Contributions of Dr. Wang's group towards making stable catalysts for this reaction are also presented in this chapter.

2.1 Catalysts Development for Dry Reforming Reaction

Concern over global warming effect and continuous emission of greenhouse gases has led to extensive research over the past decades, regarding mitigation or utilization of these gases to useful products. Of all the methods investigated so far, chemical method using dry reforming reaction is one of the promising ways of utilizing these environmental unfriendly gases to get a useful product. Aside the fact that this reaction makes use of two major greenhouse gases (CH_4 and CO_2), it also converts them to useful industrial product called syngas. Despite the environmental and industrial potential benefits of this process, industrial technology for this reaction is not fully established. This is due to the problem of catalyst deactivation, majorly from carbon deposition.

Thermodynamic studies of Reitmeter et al., (1948); White et al., (1975); Gadalla and Bower (1998); revealed that high CO_2/CH_4 ratio above 1 and high temperature operation are required to avoid carbon deposition. But from industrial point of view, it is good to operate at lower temperature with CO_2/CH_4 feed ratio close to 1, to minimize operational cost. This can be achieved using catalyst that can inhibit carbon formation kinetically under conditions that favour carbon deposition (Hu and Ruckenstein, 2002).

Earlier reviewed work by Hu and Ruckenstein, 2002; had shown that Rh, Ru, Pt and Pd can catalyse this reaction. While non-noble supported metals such as Ni, Co and Fe had shown some potential to be a good catalyst for this reaction (Tokunaga and Ogasawara, 1989). Good activity, easy availability, as well as low cost make Ni a potential active element for the industrial application of this process. Thermodynamic studies indicated that Ni based catalysts are prone to carbon deposition (Gadalla and Bower, 1998) and carbon deposition is unavoidable under low CO_2/CH_4 ratio (Ashcroft et al., 1991). A suitable catalyst can kinetically enhance carbon free operation for this reaction under the high temperature reaction (Hu and Ruckenstein, 2002). A short review based on Ni and Co catalysts for this reaction are presented in subsequent sections.

2.2 Common Catalysts Support

Table 2.1 shows a list of common supports used for Ni and Co catalysts for DRM from the literature survey. Three major oxides were used as supports in earlier catalysts namely; Al_2O_3, SiO_2 and TiO_2. The common properties among these oxides are high melting point and high specific surface area. High melting point enhances stable catalyst surface at high reaction temperature and prevents sintering (Zhang, 2008). Even with high melting points of these supports, carbon deposition could not be totally suppressed. Ruckestein and Hu, 2000; recognized the two factors that contribute to carbon deposition as size of metal cluster and acidity of support. If the size of cluster is greater than a critical value (10 nm) and/or support is acidic, then carbon deposition will occur. Thus, to inhibit carbon formation, size of particle must be less than the critical value and support must be basic. The best way to reduce acidity of support is to introduce basic metal oxide into the support (Hu and Ruckestein, 2002).

Table 2.1. Catalyst development for dry reforming reaction

Active metal	Support	Reference and Year
Ni	Al_2O_3	Osaki et al., 1994; 1995; Takayasu, 1993; Vernon et al., 1992; Swaan et al., 1994; Zhang et al., 1994; 1995; Kim et al., 1994; Tang et al., 1995; Chen et al., 1994; Bhattacharyya et al., 1994; Ruckenstein et al., 1995; 1996; Hu et al., 1996; 1997; Ashcroft et al., 1991; Blom et al., 1994; Seshan et al.,1994; Takano et al., 1994; Chang et al., 1996; Horiuchi et al., 1996 Tang et al., 2000; Osaki et al., 2001; Seok et al., 2002; Tomishige et al., 2002; Hou et al., 2003; Huang et al., 2005
	SiO_2	Osaki et al., 1994; Takayasu, 1993; Bradford et al.,1996; 1997 1998; Kim et al., 1994; Tang et al., 1995; Ruckenstein et al., 1996; 1997; Hu et al., 1996; 1997; Takano et al., 1996; Gronchi et al., 1996; Fei et al., 2004
	TiO_2	Osaki et al., 1994; 1996; 1997; Bradford and Vannice, 1996; Takanabe et al., 2005
Co	Al_2O_3	Ruckenstein and Wang, 2002; Ji et al., 2001; Cho et al., 2012 Wang and Ruckestein , 2001;
	SiO_2	Takanabe et al., 2005; Nagaoka et al., 2003
	TiO_2	Wang et al., 1996; Ferreira-Aparicio et al., 1998; Song et al., 2008

Alkaline earth metals (MgO, CaO, SrO or BaO) are good oxides that can be used to increase basicity of support, and the size of oxide crystal can help reduce the metal particle size (Hu and Ruckenstein, 2002). Thus, catalyst improvement has been achieved majorly through support modification, addition of promoter or both. Other factors such as preparation method, catalyst pre-treatment and metal loading can affect catalyst performance and extent of carbon deposition on the catalyst.

2.3 Modification of Conventional Catalysts Support

Introduction of modifiers into the conventional catalyst supports can mitigate carbon deposition for dry reforming of methane. Table 2.2 shows a list of reported metal oxide modifiers for conventional supports in literature. All the authors reported that the introduction of the corresponding modifiers mitigated carbon deposition to some extent in both supported Ni and Co catalyst systems.

2.4 Modification of Active Metal using Promoter

Promoters can concurrently improve the performance of both active metal sites and support. Introduction of second metal as a promoter is believed not to only facilitate better catalytic properties, but also to mitigate carbon deposition. A list of publications that reported better catalytic performance with the introduction of second metal (promoter) are presented in Table 2.3. The high possibility of alloy formation between the active metal and the promoter is believed to facilitate smaller metallic site and inhibit carbon deposition.

Table 2.2. Catalyst improvement with modifiers

Active Metal	Support	Modifier	References and Year
Ni	Al_2O_3	CaO	Quincoces et al., 2001; Dias et al., 2003; Lemonnidou et al., 2002;
		K_2O	Juan-Juan et al., 2004;
		MgO	Guo et al., 2005; 2010; Koo et al., 2008;
		ZrO_2	Hao et al., 2004; Therdthianwong et al., 2008; Souza et al.,2004; Pompeo et al.,2007;
		K, Ca	Hou et al., 2003
		Na, Mg, Ca Ce oxides	Wang et al., 2000
		Li, K, Mg, La oxides	Suzuki et al., 2001
	SiO_2	BaO	Jing et al., 2004;
		CaO	Jing et al., 2004;
		MgO	Jing et al., 2004;
		La_2O_3	Mo et al., 2005;
		La, Mg, Co, Zn oxides	Zhu et al., 2011;
Co	Al_2O_3	K, Sr oxides	SanJose´-Alonso et al., 2011;
	TiO_2	Ru, Pt oxides	Nagaoka et al., 2004;

Table 2.3. Catalyst improvement using promoter

Active metal	Support	Second metal	Reference and Year
Ni	Al_2O_3	Cu	Lee et al., 2004
		Mo	Quincoces et al., 2002
		Sn	Nichio et al., 2000
	SiO_2	Cu	Michalkiewwicz et al., 2009
		Ru	Crisafulli et al., 2002
		Rh	Jozwiak et al., 2005
	TiO_2	Co	Takanabe et al., 2005
Co	Al_2O_3	K, Sr	San Jose´-Alonso et al., 2011
	TiO_2	Ru, Pt	Nagaoka et al., 2004

2.5 Other Factors Contributing to Carbon Deposition

Catalyst synthesis method, pre-treatment condition and percentage loading of the active metal are other factors that can affect the performance and resistance to carbon deposition of catalyst in dry reforming reaction. Ji et al., 2001 reported a good performance and better resistance to coking of Co/Al_2O_3 catalyst prepared by sol gel method, as compared to the catalyst prepared using conventional impregnation method. Wang and Ruckenstein, (2001); Takanabe et al., (2005); reported that calcination and reduction condition affected the interaction of the active metal with the support. This consequently affected the activity and stability of catalyst for DRM. In addition to studying effect of pre-treatment condition, Cho et al., (2012), Wang and Ruckenstein, (2001; 2002); established that higher metal loading led to the formation of bigger particles that could facilitate carbon deposition.

2.6 Contribution of Our group to the Development of Stable Catalyst

After detailed literature review, Dr. Wang's group started developing bimetallic Ni-Co-Mg-Al-Ox for dry reforming reaction. From literature analysis, it was understood that a good and stable catalyst should have the following properties as proposed by Wang and Sameen, 2013:

- Good thermal stability at high temperature;
- Good surface area and pore structure;
- Appreciable metal-support interaction;
- Appreciable metal site dispersion and;
- Smaller and stable active metal site.

Low cost, availability of material and simple synthetic procedure were taken into consideration when choosing the component of catalyst, as well as the catalyst preparation method. The catalyst design involves the introduction of both modifier (MgO) and promoter (CoO) into the conventional

support and active metal (Al_2O_3) and (Ni) respectively. Al_2O_3 provides high surface area, MgO provides the required thermal stability and Co-precipitation method facilitates a strong metal - support interaction needed by a good catalyst (Zhang, 2008). The choice of second metal during screening was based on metals close to Ni in the periodic table. A summary of results from previous work done by the group on catalyst development for DRM are highlighted below:

- Mg-Al-Ox supported bimetallic Ni-Co catalyst showed better activity and resistance to carbon deposition compared to Ni-Cu, Ni-Fe and Ni-Mn (Zhang et al., 2007);
- Bimetallic Ni-Co showed enhanced activity and stability compared to the individual monometallic Ni and Co catalysts for DRM (Zhang et al., 2007);
- Study of the optimum Ni-Co loading and Ni/Co ratio showed that a ratio close to 1 is good for an active and stable Ni-Co bimetallic catalyst for DRM (Zhang et al., 2008);
- Impregnation prepared catalysts reduced better than co-precipitation catalysts, while co-precipitation catalysts showed better activity and stability (Wang et al., 2012);
- Ni showed better reduction than Co, and both showed different reduction kinetics in the bimetallic catalyst system (Wang et al., 2012), and;
- Kinetic modelling study using bimetallic Ni-Co catalysts for DRM (Zhang et al., 2009).

After all these findings, the following points still require further examination:

- Effect of support composition on the structure, metal reduction and catalytic performance of bimetallic Ni-Co-Mg-Al-Ox catalysts for dry reforming reaction;
- What controls Ni and Co reduction in the catalyst structure;
- Study of individual interaction of the active metals with the support for DRM;
- Industrial application of dry reforming reaction on our catalyst using coal gas feed and;
- CO_2 reforming of higher hydrocarbons.

All these led to the objective of this present study as stated in Chapter one.

CHAPTER THREE

EXPERIMENTAL

The focus of this chapter is on the experimental procedures and studies carried out in this research work. This chapter covers the catalysts synthesis method, catalyst evaluation methods and the catalysts characterization techniques.

3.1 Experimental Procedure

The procedures used for the experimental parts of this work were grouped into catalyst synthesis method and catalyst evaluation method for the reactions studied in this research work. Two groups of catalysts (monometallic and bimetallic) with different metal and support compositions were synthesized using co-precipitation method. The target of study is to know the effects of the nature and composition of support on the structure and catalytic properties of catalysts for DRM. Catalyst evaluation and reactions studied were conducted at two different research centres. The initial CO_2 reforming of methane and ethane reaction studies were carried out at the Department of Chemical and Biological Engineering, University of Saskatchewan, Saskatoon, Saskatchewan, Canada. While the other part of research on dry reforming using coal gas feed was done at Key Laboratory of Coal Science and Technology at Taiyuan University of Technology, Taiyuan, Shanxi, China.

3.1.1 Catalyst preparation method

The synthesis of catalysts was done using the co-precipitation method. For each group of catalysts synthesized, the intended amount of the active metals Ni and/or Co in each catalyst is 3.26 % based on mole composition, while the balance 96.74 % is meant for Mg and/or Al. For the bimetallic catalysts system of Ni-Co-Mg-Al-Ox, four samples with different Mg/Al ratio were

prepared by co-precipitation of aqueous solutions of aluminum nitrate nanohydrate (98-102 %, Alfa Aesar Chemical Company, USA), magnesium nitrate hexahydrate (99+ %, Acros Organic, USA), nickel (II) nitrate hexahydrate (98 %, Alfa Aesar Chemical Company, USA) and cobalt (II) nitrate hexahydrate (98-102 %, Alfa Aesar Chemical Company, USA). Samples were prepared to have equal amount of Ni and Co but variable Mg/Al ratio in the Mg-Al-Ox support. Precipitation was conducted at room temperature and pH 8.6 which was adjusted by titrating aqueous ammonia solution (50 % NH_4OH + 50 % H_2O). To control the rate of precipitation of the metal hydroxide over time, the flow rate of the salts solution mixture was maintained between 15-18 ml min^{-1} (under controlled addition of the NH_3 solution to maintain the pH) and the precipitate obtained was filtered, washed with deionized water and dried overnight in oven at 120^{o}C. Calcination was done in air at 800^{o}C for 6 hours at a ramping rate of 5^{o}C/min in a 79400 thermolyne tube furnace and the solid catalyst obtained was crushed and sieved to the desire size for DRM. The monometallic catalysts of Ni and Co were prepared using the same procedure. While maintaining 3.26 mole % for the active metal (Ni or Co), the composition of supports depends on whether it is Al-Ox or Mg-Ox only, or both Mg-Al-Ox. Other groups of monometallic and bimetallic were synthesized using this same procedure and a schematic representation of the catalyst synthesis procedure is shown in appendix A. The catalysts naming system used is CopCat-NixCoy-Mg/Al-z., where CopCat represent the method of catalyst preparation (Co-precipitation catalyst), x and y are the respective mole % of Ni and Co in the catalysts after calcination, and z is the actual ratio of Mg/Al after calcination.

3.1.2 Catalysts evaluation procedure

The evaluation procedure of catalysts follows the same pattern for all the reactions studied, except that the experimental condition was slightly varied at times. For the dry reforming reaction

using pure feed gas, evaluation of the catalyst activity and stability was carried in a fixed-bed quartz reactor (Autoclave Engineers) with ID 3.9 mm, OD 6.35 mm and length 30 cm. For each experimental run, 10 mg of catalyst (with particle size 250 microns) was mixed with 50 mg of silicon carbide and equimolar reactant feed composition of CH_4 (99.2 %), CO_2 (99.9 %) and N_2 (99.9 %) mixture was introduced into the reactor at atmospheric pressure and GHSV = 1.2×10^6 mL g^{-1} h^{-1} (flow rate 200 ml min^{-1}). Catalyst was activated in H_2 (99.9 %) and N_2 (99.9 %) mixture with a molar ratio of 1:4 at 800 ^oC for 4 h before activity test. All the gases were supplied by Praxair Canada Inc. Evaluation test was carried out at 755 ^oC with the mixture of catalyst and silicon carbide loaded in the middle of the reactor during evaluation test. The product gas from the DRM reaction was analyzed by an on-line Agilent 6890N GC equipped with TCD and a GS-GASPRO capillary column (J&W Scientific) of 60 m in length and 0.32 mm in inner diameter using GC Chemstation software. Helium (Ultra high purity 5.0, PRAXAIR Canada Inc.) was used as the carrier gas.

For the experiments carried out in China, evaluation of catalyst performance was done in a fixed–bed quartz reactor (Tianjin Tian Yi Technology Co. Ltd) with ID 8 mm, OD 12 mm and length 60 cm. For each experimental run, 150 mg of catalyst (with particle size 250 microns) was mixed with 750 mg of sand. Equimolar reactant feed composition of CH_4 (99.99 %), CO_2 (99.99 %) and N_2 (99.99 %) mixture was introduced into the reactor at atmospheric pressure, 900 ^oC and a GHSV = 1.2×10^5 mL g^{-1} h^{-1}. The coal gas feed composed of CH_4 (6.6 %), CO_2 (6.7 %), N_2 (2.6 %), CO (32.36 %), H_2 (51.34 %) and O_2 (0.4 %). Catalyst was activated in H_2 and N_2 gas mixture with a molar ratio of 1:4 at 900 ^oC for 4 h before activity test. All gases were supplied by Jining Xieli Special Gas Co. Ltd. Evaluation was carried out at 900 ^oC with the mixture of catalyst and sand loaded at the middle of the reactor. The product gas from the DRM reaction (for both coal and pure gas) was analyzed using a gas chromatography (Haixin GC-950) on packed column

(TDX-01) with Ar as carrier gas, equipped with a thermal conductivity detector after passing a cold trap.

The experimental procedure for CO_2 reforming of C_2H_6 is like the dry reforming reaction except for some changes in the reaction conditions. For each experimental run, 40 mg of catalyst (with particle size of 250 microns) was mixed with approximately 200 mg of silicon carbide and reactant feed composition of C_2H_6 (99.0 %), N_2 (99.9 %) and CO_2 (99.9 %) mixture at molar ratio 1:1.5:2 was introduced into the reactor at atmospheric pressure and GHSV = 6×10^5 mL g^{-1} h^{-1} (flow rate 200 ml min^{-1}). Catalyst was activated in H_2 (99.9 %) and N_2 (99.9 %) mixture with a molar ratio of 1:4 at 800 ^oC for 4 h before activity test. All the gases were supplied by Praxair Canada Inc. Evaluation test was carried out at 800 ^oC with the mixture of catalyst and silicon carbide loaded in the middle of the reactor during evaluation test. The product gas from the CO_2 reforming of C_2H_6 reaction was analyzed by an on-line Agilent 6890N GC equipped with TCD and a GS-GASPRO capillary column (J&W Scientific) of 60 m in length and 0.32 mm in inner diameter using GC Chemstation software. Helium (Ultra high purity 5.0, Praxair Canada Inc.) was used as the carrier gas.

All experimental conditions were chosen such that internal and external mass transfer limitations had been overcome as shown in Appendix E.

3.2 Catalysts Characterization Procedure

Different characterization techniques were used to understand some properties of the catalysts from after synthesis, through reduction steps and after reaction. The characterization techniques used are presented in subsequent sub-sections.

3.2.1 Inductively coupled plasma mass spectrometry (ICP-MS)

Elemental composition of catalysts was determined using ICP-MS analysis at Saskatchewan Research Council, Saskatoon. For each analysis, sample was crushed and a subsample was split out using a sample riffler. The subsample was pulverized using a puck and ring grinding mill. The pulp was then transferred to a barcode labeled plastic snap top vial. An aliquot of pulp was digested to dryness in a hot block digestion system using a mixture of concentrated HF: HNO_3: $HClO_4$. The obtained residue was subsequently dissolved in diluted HNO_3. Analysis was carried out using PerkinElmer Optima 5300 DV/Optima 8300 DV and instrument was calibrated using certified commercial solution before analysis. A quality control sample was also prepared and analyzed with each sample.

3.2.2 N_2 adsorption and desorption experiment

Textural properties of the catalysts were determined using this method. N_2 adsorption was carried out at temperature of -196 ^oC using Micrometric ASAP 2000 and approximately 175 mg of catalyst was used for each analysis. Before analysis, each sample was evacuated at 200 ^oC and 500 µmHg (66.6 Pa) to remove any moisture or other adsorbed gases. Subsequent evacuation was then carried out at 20 µmHg (2.67 Pa) before N_2 adsorption. BET method was used to calculate the surface area, while the pore size distribution was obtained from adsorption branch of the N_2 isotherm by Barret –Joyner-Halenda (BJH) method.

3.2.3 X-ray powder diffraction experiment (XRD)

XRD was used to determine the crystallinity and bulk phase of the catalysts. The diffraction pattern was studied using Rigaku/Rota flex Cu rotating anode X-ray diffraction instrument, equipped with generation voltage of 40 kV and tube current of 40 mA. For each study,

catalyst was powdered and mixed with methanol to form a mud which was loaded to the coarse side of a glass plate and placed under ambient drying condition. The dried catalyst plate was then loaded in the analysis chamber. Each catalyst was scanned at a rate of 4 ^{o} min^{-1} with 2θ varying between 10 ^{o} and 90 ^{o}

3.2.4 Mg and Al K-edge X-ray absorption near edge structure (XANES)

This characterization method was used to study the co-ordination number (CN) of Mg and Al in the catalysts system. The X-ray absorption spectroscopy (XAS) for Mg (1305 eV) and Al (1560 eV) K-edge XANES spectra were collected on the SGM beamlines at Canadian Light Source, Saskatoon. Measurements were made in fluorescence mode using Si drift detectors, with the ionization chambers optimized for the maximum current at the SGM beamline. For the XAS scan, 8–10 mg oxide catalysts were loaded on to a rectangular sample holder, which was later transferred into a holder on the beam line. All scans were acquired before catalyst reduction.

3.2.5 ^{27}Al nuclear magnetic resonance spectroscopy (NMR)

The degree of spinel inversion in the catalysts system was measured using this characterization technique. ^{27}Al Magic Angle Spinning (MAS) NMR experiment was carried out at the Saskatchewan Structural Sciences Centre using a Bruker AVANCE III HD spectrometer operating at 130.32 MHz (^{1}H frequency at 500.13 MHz), with a 4 mm DOTY CP-MAS probe. The samples were spinning at a MAS rate of 13 kHz and a 90 ^{0} pulse of 1.2 µs was used for the ^{27}Al channel, with no ^{1}H decoupling. For all the samples, 760 scans were accumulated, with a recycle delay of 1s. Chemical shifts are referenced to 1 M Al $(NO_3)_3$ aqueous solution at 0ppm.

3.2.6 X-ray photoelectron spectroscopy (XPS)

This technique was used to determine the oxidation state of the active metal ions and their distribution within the phases present in the catalyst systems. This characterization was done at Taiyuan University of Technology, China and analysis was done by X-ray XPS, Thermo Fisher, using an Escalab 250 scanning microprobe instrument with Al Kα radiation (30 kV, hν = 1486.6eV) in steps of 0.1 eV under ultrahigh vacuum (2.0×10^{-7} Pa), calibrated internally using the carbon deposit C 1s (Eb = 284.6 eV). Background was subtracted using Shirley method.

3.2.7 Scanning transmission electron microscopy with energy dispersive X-ray (STEM-EDX)

STEM-EDX analysis was done at Fraunhofer Institute for Mechanics of Materials IWM, Germany, and this technique involves the scanning of defined area of the catalysts sample by an electron beam. The beam is localized on a certain point in the image and used to measure an EDX. Area mapping was easily done using this technique, and information regarding the distribution/interaction of active metals with the support was obtained.

3.2.8 H_2 temperature programmed reduction (TPR)

Reduction of active metal(s) within bulk phase of the catalysts over a temperature range was studied by H_2-TPR, using a TP-5000 (Xianquan China) at Taiyuan University of Technology, China. Instrument was equipped with a thermal conductivity detector to establish the appropriate reduction temperature or measure the hydrogen consumption. The tests were performed using a quartz reactor containing the catalyst (50 mg) in 5 % H_2 (balanced with N_2) at 20 mL min^{-1} and a heating rate of 10 °C min^{-1}, from room temperature to 900 °C.

3.2.9 Ni and Co K-edge X-ray absorption near edge structure (XANES)

The extent of reduction of Ni and Co in the catalyst systems was determined using this technique. The X-ray absorption spectroscopy (XAS) for Ni (8333 eV) and Co (7709 eV XANES spectra were collected on the SXRMB beamline at Canadian Light Source, Saskatoon. Measurements were made in transmission mode with the ionization chambers optimized for the maximum current at the SXRMB beam line. For the XAS scan, in a wet lab, 8–10 mg oxide catalysts were loaded into a 6-hole stainless steel shooter, which was later installed in a quartz reactor. The catalysts were heated to 800 °C then maintained at this temperature while H_2/N_2 gas (H_2 5 %, v/v) was passed through for 4 h, followed by Co and Ni K-edge scan. One scan each was acquired before and after reduction (scan after reduction was also done at room temperature after the reactor cooled down after the reduction process).

3.2.10 CO chemisorption

Dispersion of active metals on the support was studied using this technique**.** CO chemisorption was measured using the Micromeritics ASAP-2020 instrument for the determination of Co and /or Ni dispersion, after samples had been reduced in hydrogen at 800 °C for 4 h. Prior to CO chemisorption, sample was evacuated at 110 °C for 0.5 h, followed by in-situ CO chemisorption. Lastly, isotherm of CO chemisorption was conducted at 35 °C.

3.2.11 CO_2 temperature programmed desorption (CO_2-TPD)

Basicity of catalysts was determined using CO_2-TPD. The pulse chemisorption and temperature programmed desorption (CO_2-TPD) measurements were performed in QIC-20 analytical instrument (HIDEN). Catalyst sample was pretreated at 280 °C for 0.5 h in a He atmosphere to remove physically adsorbed and/or weakly bound species, and then the CO_2

adsorption was carried out at 50 °C to saturation. Afterwards, CO_2 desorption was carried out under He flow and desorption signal was recorded by a QIC-20 analytical instrument (HIDEN) with linear temperature increase up to 900 °C at a rate of 10 ° min^{-1}.

3.2.12 Transmission electron microscopy (TEM)

Transmission electron microscope (TEM) images of the reduced catalysts were obtained on a Hitachi HT7700 High Resolution digital TEM operated at an accelerating voltage of 100 kV. The sample was prepared by dropping and drying the reduced catalyst which was dispersed in anhydrous ethanol, on a 300 mesh formvar/carbon coated copper grid. Images were subsequently obtained, from which particles sizes were measured.

3.2.13 Temperature-programmed oxidation-mass spectrometry (O_2-TPO-MS)

Oxidation properties of deposited carbon on the used catalysts were investigated by O_2-TPO-MS), using a QIC-20 analytical instrument (HIDEN). The used catalyst was pretreated at 150 °C for 0.5 h in a He atmosphere, cooled to 50 °C, and then the atmosphere was switched to 5 % O_2 (Ar balance). The temperature was increased linearly to 900 °C at 10 °C min^{-1}. CO_2 (m/z = 44) in the effluent was measured by a mass spectrometer (QIC-20, HIDEN) and recorded as a function of temperature, which can be used to determine the type of carbon species.

3.3 Data Analysis, Reactant Conversion and Product Selectivity

The presence of inert N_2 is used as an internal reference for the calculation of reactants conversion rate, as well as the products selectivity in our reforming reaction study. Since N_2 is an inert gas for this reaction, the molar flow rate of N_2 is the same before and after reaction,

i.e $F^{i}_{N_2}=F^{f}_{N_2}=F_{N_2}$ 3.1

where F = volumetric flow rate, i = initial and f = final

Thus, the flow rate of every species in product stream can be calculated using equation 3.2 based on the results of the gas chromatography (GC) analysis.

$$F_j = \frac{f_j^f}{f_{N_2}^f} \times F_{N_2} \qquad 3.2$$

where f_j^f is the fraction of specie j in the product obtained from the GC analysis.

Reactant conversion (X), product selectivity (S), rate of conversion (reactant) and formation (product), -r, r are calculated using Equations 3.3-3.7

$$X_j = \frac{F_j^i - F_j^f}{F_j^i} \times 100 \qquad 3.3$$

$$S_{H_2} = \frac{F_{H_2}^f}{2 \times (F_{CH_4}^i - F_{CH_4}^f)} \times 100 \qquad 3.4$$

$$S_{CO} = \frac{F_{co}}{(F_{CH_4}^i - F_{CH_4}^f) + (F_{CO_2}^i - F_{CO_2}^f)} \times 100 \qquad 3.5$$

$$-r_i \ (\text{mol g}^{-1}\text{s}^{-1}) = \frac{n_j^i - n_j^f}{60 \times m_{cat}} \qquad 3.6$$

$$r_i \ (\text{mol g}^{-1}\ \text{s}^{-1}) = \frac{n_j^f}{60 \times m_{cat}} \qquad 3.7$$

m_{cat} = weight of catalyst used for reaction (gram), n_j^i, n_j^f = initial and final molar flow rate of specie j respectively (mol min^{-1}).

MFC calibration, GC calibration data and repeatability of some data are presented in Appendices C, D and F respectively.

CHAPTER FOUR

CATALYST CHARACTERIZATION RESULTS

Majority of the catalyst characterization results are discussed in this chapter. Catalysts were subjected to three characterization stages namely: characterization after calcination (before reduction), after catalyst reduction and after reaction. The results of the first two (before and after reduction) are discussed in this chapter, while catalysts characterization results after reaction are presented in chapter 5.

4.1 Catalyst Characterization Results before Reduction

The elemental composition of catalysts, N_2 adsorption – desorption isotherm, bulk structure and distribution of the active metal on the support are some of the catalytic properties discussed in this section.

4.1.1 Elemental composition of catalysts

The results of the elemental composition of the calcined precipitates for the monometallic catalysts determined by ICP-MS are presented in Table 4.1. Based on the amount of the metal salts, the intended ratio of the active metal (Ni and /or Co) to the total metal (active + support) on mole basis is 3.26 %.

$$\frac{\text{Active metal}}{\text{Total metal}} * 100 = 3.26\ \% \qquad 4.1$$

Al-Ox supported monometallic Ni and Co catalysts showed a value close to the target value as seen in Table 4.1. Introduction of Mg seemingly made the value far from target value and similar trend was also observed in the results of the bimetallic catalysts in Table 4.2.

Table 4.1. Elemental composition of monometallic catalysts

Catalyst	Mole (%)				Mg/Al
	Ni	Co	Mg	Al	
CopCat-Ni3-Mg/Al-0.0	3.0	0.0	0.0	97.0	0.0
CopCat-Co4-Mg/Al-0.0	0.0	3.6	0.0	96.4	0.0
CopCat-Ni5-Mg/Al-1.60	4.8	0.0	59.0	36.2	1.6
CopCat-Co6-Mg/Al-1.55	0.0	6.1	56.8	37.1	1.5
CopCat-Ni84-Mg/Al-#	83.9	0.0	16.1	-	-
CopCat-Co87-Mg/Al-#	-	87.1	12.9	-	-

Table 4.2. Elemental composition of bimetallic catalysts

Catalyst	Mole (%)				Mg/Al
	Ni	Co	Mg	Al	
CopCat-Ni2Co2-Mg/Al-0.30	1.6	1.7	21.5	75.2	0.3
CopCat-Ni2Co2-Mg/Al-1.00	1.7	1.8	45.6	50.9	1.0
CopCat-Ni3Co3-Mg/Al-1.75	2.6	3.2	59.9	34.3	1.8
CopCat-Ni4Co5-Mg/Al-2.00	3.9	4.9	60.8	30.4	2.0
CopCat-Ni2Co2-Mg/Al-0.00	1.5	1.9	-	96.6	0.0
CopCat-Ni39Co53-Mg/Al-#	39.5	53.0	8.50	-	-

Increasing the ratio of Mg/Al resulted in having more active metal(s) than the intended amount in the precipitated solid after calcination. This observation could be related to either more precipitation of the active metals or insufficient precipitation of the support metal (Mg or Al). With respect to the values of the solubility product (Ksp), Al $(OH)_3$ has the lowest value compared to the other metal hydroxides (employed in this study), and 100% precipitation was expected based on equilibrium calculation. The Ksp values of the metal hydroxides are Al (1.3×10^{-33}), Co (1.65×10^{-15}), Ni (2.0×10^{-15}) and Mg (1.8×10^{-11}) as reported by Euler, 2006. Comparison between the target and actual ratio of Ni/Al and Co/Al (Tables 4.3 and 4.4) showed that almost all Ni and Co were precipitated from the salt solutions. Thus, the difference in the composition of the active metal(s) in the catalysts system could only be due to the difficulty of $Mg(OH)_2$ precipitation as revealed by the difference between the target and actual values of Mg/Al ratio in all the catalysts. $Mg(OH)_2$ has the highest Ksp, and equilibrium calculations showed that higher pH would be required to precipitate appreciable amount of $Mg(OH)_2$ compared to the target. This is also substantiated by the difference between the target and the actual values of the active metals in the MgO only supported catalysts (Table 4.2). Since less $Mg(OH)_2$ was precipitated compared to $Co(OH)_2$ and $Ni(OH)_2$ in these catalysts (MgO supported catalysts), no further consideration was given to these catalysts in this study. Additionally, more Co precipitation was observed compared to Ni in all the catalysts system. The salt solution of Co has higher initial pH value compared to the corresponding salt of Ni and the trend observed was that the closer the initial salt pH to the precipitating pH, the easier it was to precipitate the active metals, and more difficult it was to precipitate $Mg(OH)_2$. Even though the order and extent of metal precipitation depend on the Ksp value of the metal hydroxide, the initial pH of the salt solution, pH of the co-precipitation process and the concentration of the metal ions in the precipitating solution seem to have influence on the metal hydroxide precipitation as shown in Appendix E.

Table 4.3. Mole ratio comparison for monometallic catalysts

Catalyst	Target mole ratio			Actual mole ratio		
	Ni/Al ($\times10^{-1}$)	Co/Al ($\times10^{-1}$)	Mg/Al ($\times10^{0}$)	Ni/Al ($\times10^{-2}$)	Co/Al ($\times10^{-2}$)	Mg/Al ($\times10^{0}$)
CopCat-Ni3-Mg/Al-0.00	0.3	0.0	0.0	0.3	0.00	0.0
CopCat-Co4-Mg/Al-0.00	0.0	0.3	0.0	0.00	0.4	0.0
CopCat-Ni5-Mg/Al-1.60	1.5	-	3.6	1.4	-	1.6
CopCat-Co6-Mg/Al-1.55	-	1.5	3.6	-	1.5	1.5
CopCat-Ni84-Mg/Al-#	-	-	-	-	-	-
CopCat-Co87-Mg/Al-#	-	-	-	-	-	-

Table 4.4. Mole ratio comparison for bimetallic catalysts

Catalyst	Target mole ratio			Actual mole ratio		
	Ni/Al ($\times10^{-1}$)	Co/Al ($\times10^{-1}$)	Mg/Al ($\times10^{0}$)	Ni/Al ($\times10^{-1}$)	Co/Al ($\times10^{-1}$)	Mg/Al ($\times10^{0}$)
CopCat-Ni2Co2-Mg/Al-0.30	0.2	0.2	0.3	0.2	0.2	0.3
CopCat-Ni2Co2-Mg/Al-1.00	0.3	0.3	1.0	0.3	0.4	0.9
CopCat-Ni3Co3-Mg/Al-1.75	0.9	0.9	4.0	0.8	0.9	1.7
CopCat-Ni4Co5-Mg/Al-2.00	1.5	1.5	8.0	1.8	1.6	2.0
CopCat-Ni2Co2-Mg/Al-0.00	0.2	0.2	-	0.2	0.2	0.0
CopCat-Ni39Co53-Mg/Al-#	-	-	-	-	-	-

In summary, the difference in the composition of the active metal in the catalyst system as Mg/Al ratio increased, was related to the difficulty of precipitating Mg $(OH)_2$ at the pH of the co-precipitation process.

4.1.2 Textural properties of catalysts

The results of the isotherms from N_2 adsorption-desorption experiments for both monometallic and bimetallic catalysts are shown in Figures 4.1 and 4.2, while the textual properties are summarized in Tables 4.5 and 4.6 respectively. In line with IUPAC classification of Sing et al., 1985; all the catalysts exhibit type-IV isotherm which is typical of mesoporous material, but different types of hysteresis loop. Al-Ox supported monometallic Ni and Co catalysts displayed H1 type hysteresis loop, which is related to solid material with narrow pore size distribution. Introduction of MgO changed the hysteresis loop to H4-type, which is associated with pores in form of slits with uniform pore size in the Mg-Al-Ox supported monometallic catalysts. Similar trend was observed in the isotherms of the bimetallic catalysts. As the Mg/Al ratio increases, a change from type H1 to type H4 was observed in the hysteresis loop. The presence of significant amount of MgO seems to enhance the uniformity of the pores based on the hysteresis loops.

Notable difference was also observed in the textural properties as the nature and composition of support changes in catalysts system (Tables 4.5 and 4.6). A decrease in BET surface area was observed with the introduction of MgO into the monometallic catalysts. There was also a trend in the reduction of the BET surface area as the Mg/Al ratio changed from 0.3 to 2 in the bimetallic catalysts. Obviously, the presence of MgO reduced the BET surface area of the catalysts system.

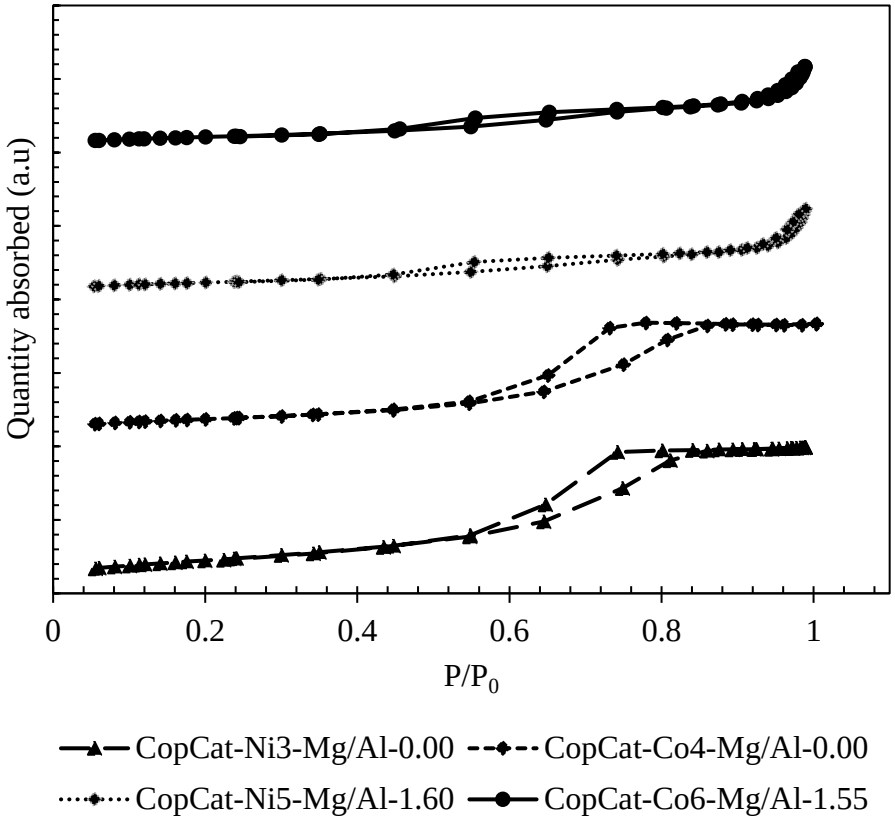

Figure 4.1. N_2 adsorption-desorption isotherms of monometallic catalysts

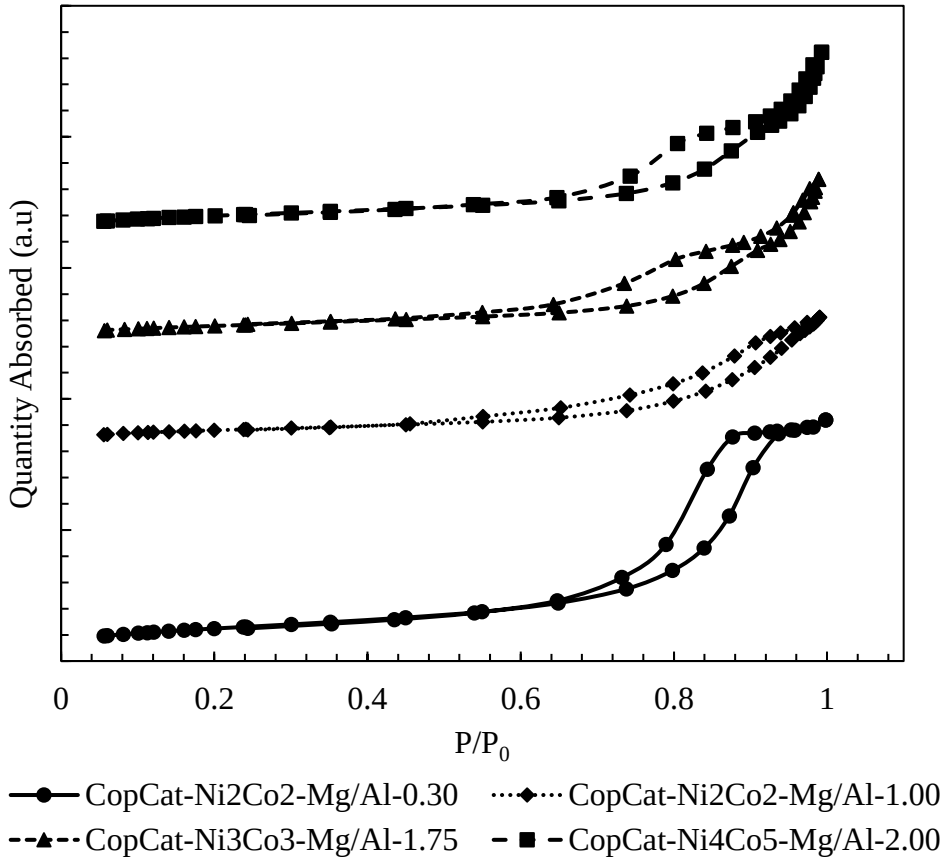

Figure 4.2. N_2 adsorption-desorption isotherms of bimetallic catalysts

While there was increase in pore size, a decrease in pore volume was observed with increase in MgO loading in the catalysts. Comparison between monometallic CopCat-Ni5-Mg/Al-1.6 and bimetallic CopCat-Ni3Co3-Mg/Al-1.75 catalysts showed that incorporation of Co into the bimetallic catalyst system in a MgO rich catalyst system caused a slight decrease in BET surface area, while both pore size and pore volume increased. Sufficiently uniform mesoporous property is necessary for the stability of catalyst in a high temperature reaction like dry reforming reaction (Hu et al., 2007).

Table 4.5. Textural properties of monometallic catalysts

Catalyst	BET surface Area (m^2/g)	Pore Volume (cm^3/g)	Pore size (Å)
CopCat-Ni3-Mg/Al-0.00	182	0.34	75.8
CopCat-Co4-Mg/Al-0.00	142	0.29	80.6
CopCat-Ni5-Mg/Al-1.60	91	0.19	84.0
CopCat-Co6-Mg/Al-1.55	84	0.18	88.0

Table 4.6. Textural properties of bimetallic catalysts

Catalyst	BET surface Area (m^2/g)	Pore Volume (cm^3/g)	Pore size (Å)
CopCat-Ni2Co2-Mg/Al-0.30	95	0.32	116.3
CopCat-Ni2Co2-Mg/Al-1.00	81	0.28	120.5
CopCat-Ni3Co3-Mg/Al-1.75	77	0.25	126.8
CopCat-Ni4Co5-Mg/Al-2.00	74	0.22	130.4

4.1.3 Crystallinity and bulk phase of catalysts

The observed pattern for the XRD study of both monometallic and bimetallic catalysts are shown in Figures 4.3 and 4.4 respectively. Using the procedure of Foot et al., 2012, some of the possible processes and interactions that could occur during calcination include:

$$2Al(OH)_3 \rightarrow 3H_2O + Al_2O_3 \text{ (Spinel structure)} \quad 4.2$$

$$Mg(OH)_2 \rightarrow H_2O + MgO \quad 4.3$$

$$Ni(OH)_2 \rightarrow H_2O + NiO \quad 4.4$$

$$Co(OH)_2 \rightarrow H_2O + CoO \quad 4.5$$

$$CoO + NiO \rightarrow NiCoO_2 \quad 4.6$$

$$CoO + MgO \rightarrow CoO - MgO \text{ (Solid structure)} \quad 4.7$$

$$NiO + MgO \rightarrow NiO - MgO \text{ (Solid structure)} \quad 4.8$$

$$Al_2O_3 + MgO \rightarrow {}^{[4]}(Al_x,Mg_{1-x})^{[6]}(Al_{2-x},Mg_x)O_4 \text{ (Spinel structure)} \quad 4.9$$

$$Al_2O_3 + NiO \rightarrow {}^{[4]}(Al_x,Ni_{1-x})^{[6]}(Al_{2-x},Ni_x)O_4 \text{ (Spinel structure)} \quad 4.10$$

$$Al_2O_3 + CoO \rightarrow {}^{[4]}(Al_x,Co_{1-x})^{[6]}(Al_{2-x},Co_x)O_4 \text{ (Spinel structure)} \quad 4.11$$

$$Al_2O_3 + MgO + NiO \rightarrow {}^{[4]}(Al_x,(Ni, Mg)_{1-x})\ {}^{[6]}(Al_{2-x},(Ni, Mg)_x)O_4 \text{ (Mixed spinel structure)} \quad 4.12$$

$$Al_2O_3 + MgO + CoO \rightarrow {}^{[4]}(Al_x,(Co, Mg)_{1-x})\ {}^{[6]}(Al_{2-x},(Co, Mg)_x)O_4 \text{ (Mixed spinel structure)} \quad 4.13$$

where $^{[4]}( )$ and $^{[6]}( )$ represent the tetrahedral site and octahedral sites of the spinel respectively. x is the degree of spinel inversion. A complete regular spinel structure is equivalent to x = 0, while x = 1 represents a completely inverted spinel.

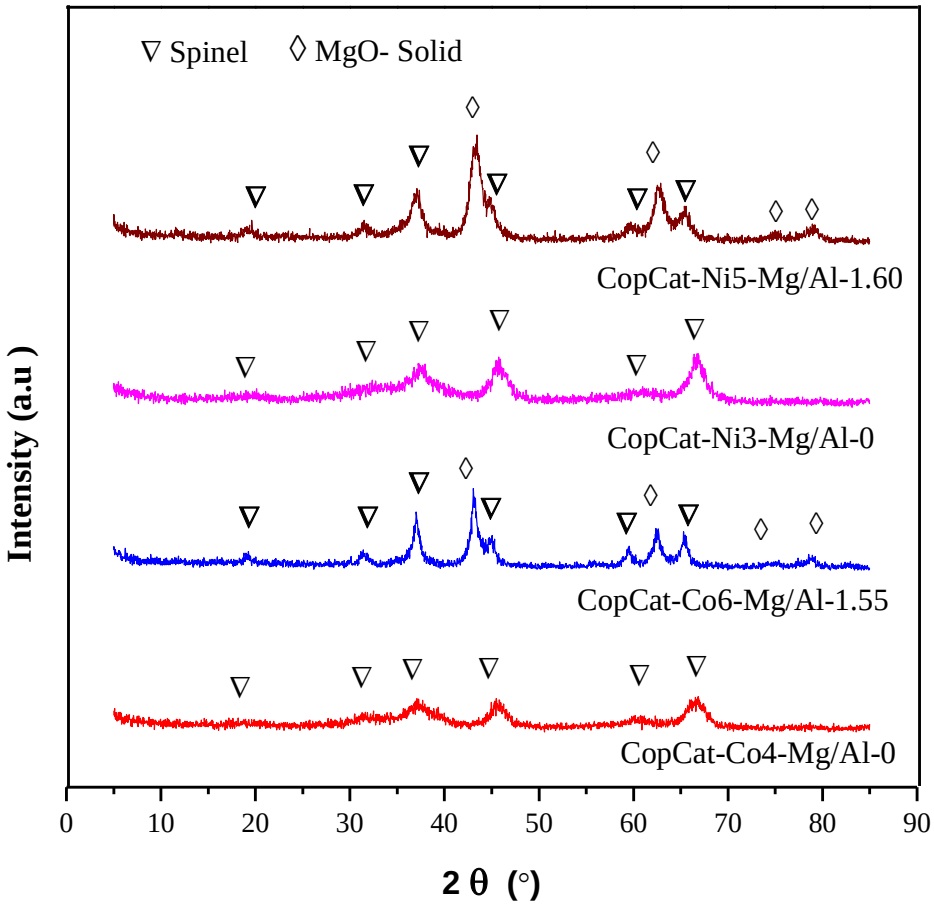

Figure 4.3. XRD plot of monometallic catalysts

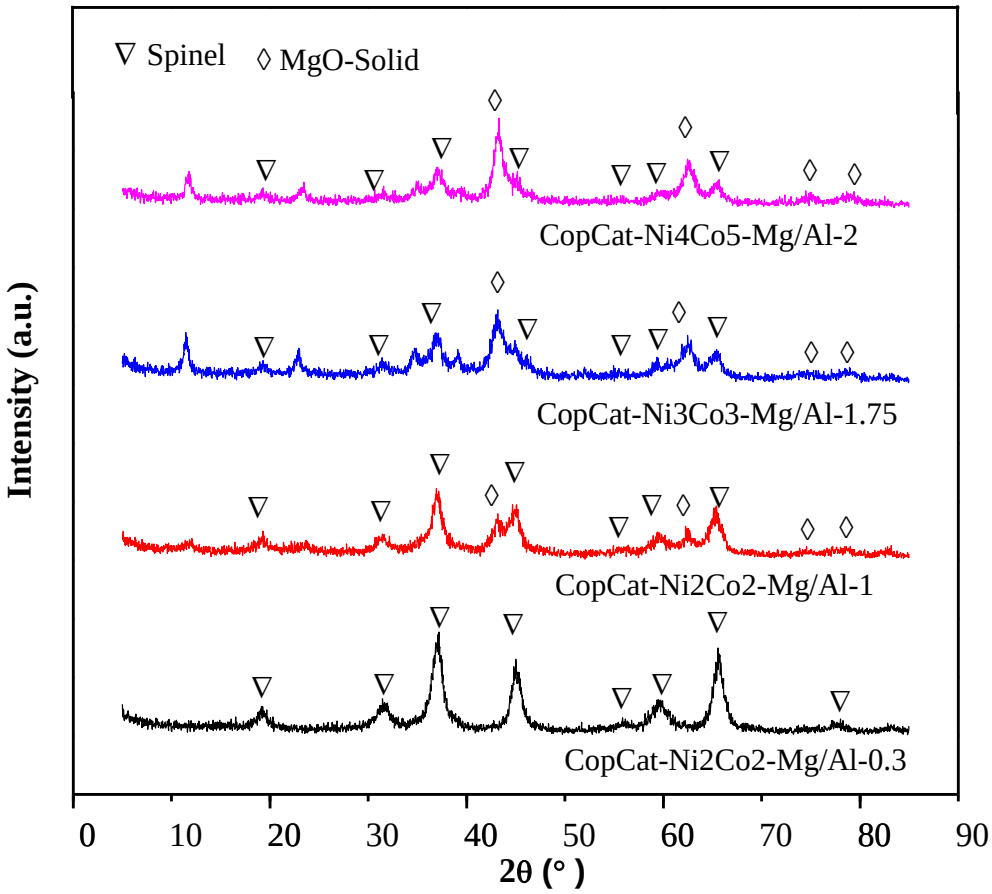

Figure 4.4. XRD plot of bimetallic catalysts

For the Al-Ox supported monometallic catalysts, phase assigned to spinel structure with characteristic diffraction peaks 2θ at 19.4 º, 32.5 º, 38.1 º, 46 º, 59.8 º and 65.6 º was observed in the XRD results (Figure 4.3). The associated diffraction planes relative to these angles are (111), (220), (311), (422), (511) and (440) respectively. The nature of the spinel could be $^{[4]}(Al_x,Ni_{1-x})^{[6]}(Al_{2-x},Ni_x)O_4$ in (CopCat-Ni3-Mg/Al-0), $^{[4]}(Al_x,Co_{1-x})^{[6]}(Al_{2-x},Co_x)O_4$ in (CopCat-Co4-Mg/Al-0), γ-Al_2O_3 spinel or their respective composites ,which are indistinguishable in XRD due to their similar morphology (Tichit et al., 1997). Two phases, notably MgO-solid and spinel phases, were observed in the Mg-Al-Ox supported composite catalysts. The intensity of the spinel peaks decreased with the introduction of MgO and a shift to lower angle was observed in the spinel peaks. This possibly indicated that the chance of forming $^{[4]}(Al_x,Ni_{1-x})^{[6]}(Al_{2-x},Ni_x)O_4$, $^{[4]}(Al_x,Co_{1-x})^{[6]}$ $(Al_{2-x},Co_x)O_4$ and γ-Al_2O_3 was reduced with the introduction of MgO or the type of spinel might be different. The formations of $^{[4]}(Al_x,Mg_{1-x})^{[6]}(Al_{2-x},Mg_x)O_4$, or mixed spinel [$^{[4]}(Al_x,(Ni, Mg)_{1-x}{}^{[6]}(Al_{2-x},(Ni, Mg)_xO_4$, $^{[4]}(Al_x,(Co, Mg)_{1-x}{}^{[6]}(Al_{2-x},(Co, Mg)_xO_4$] are also favourable in the Mg-Al-Ox supported catalysts during calcination. This is due to the presence of MgO and the preparation method as previously stated by Guo et al., (2004); Son et al., (2014). The diffraction peaks relative to MgO-solid phase at 2θ are given as 43.2º, 62.9º, 76º and 79.2º. The associated diffraction planes are (200), (220), (311) and (222) respectively. MgO, NiO and CoO all have fcc structures, with a very close lattice parameter and the combination of MgO and CoO/NiO at any molar ratio can form solids, which are indistinguishable in the XRD (Hu, 2009). When the Mg/Al ratio was less than 1 in the bimetallic catalysts, a completely spinel structure was displayed by CopCat-Ni2Co2-Mg/Al-0.33, and as the Mg/Al ratio increased, the spinel phases decreased, while MgO solid phase increased as seen in Figure 4.4.

Additional peaks were found in the XRD of the bimetallic catalysts with Mg/Al ratio > 1 when compared to their corresponding monometallic catalysts. Peaks around 36.6 ^{o} and 42 ^{o} with diffraction plane (111) and (200) could be ascribed to $NiCoO_2$ (JCPDS 10-0188) in these catalysts system. Thus, the introduction of MgO changed the phases and bulk structure of the catalysts system.

A semi-quantitative analysis (using integration area in Origin software) was carried out to quantify the relative phases of MgO and spinel as the Mg/Al ratio changed from 0 to 2 in the catalysts system. The phase percentage was calculated using the formula:

$$\% \text{ Spinel } = \frac{\text{Peak area of spinel}}{\text{Peak are of spinel+MgO}} * 100 \qquad 4.14$$

$$\% \text{ MgO } = \frac{\text{Peak area of MgO}}{\text{Peak are of MgO+spinel}} * 100 \qquad 4.15$$

The results of the analysis presented in Tables 4.7 and 4.8 for both group of catalysts showed that increase in Mg/Al brought about a corresponding increase in the MgO phase and a decrease in the spinel phase.

Table 4.7. Phase quantification of the monometallic catalysts

Catalyst	MgO Phase (%)	Spinel Phase (%)
CopCat-Ni3-Mg/Al-0.00	0	100
CopCat-Co4-Mg/Al-0.00	0	100
CopCat-Ni5-Mg/Al-1.60	55	45
CopCat-Co6-Mg/Al-1.55	52	48

Table 4.8. Phase quantification of the bimetallic catalysts

Catalyst	MgO Phase (%)	Spinel Phase (%)
CopCat-Ni2Co2-Mg/Al-0.30	0	100
CopCat-Ni2Co2-Mg/Al-1.00	22	78
CopCat-Ni3Co3-Mg/Al-1.75	53	47
CopCat-Ni4Co5-Mg/Al-2.00	62	38

4.1.4 Mg K-edge XANES

The normalized results of the Mg K-edge XANES study are presented in Figures 4.5 and 4.6 for the monometallic and bimetallic catalysts respectively. The edge region is characterized by three main peaks in the energy range 1305-1318 eV and a broad peak around 1325-1330 eV. The peaks are labeled A, B, C and D with regards to their energy positions. Only CopCat-Ni2Co2-Mg/Al-0.30 catalyst showed an additional peak at 1321 eV, labeled D'. All catalyst samples with Mg/Al ratio greater than 1 showed similar spectra with respect to the features and energy positions. The spectrum of CopCat-Ni2Co2-Mg/Al-0.30 is characterized by a sharp peak A, whose intensity is almost equal to peak C, a weak feature B and D', and a broad peak D. The two higher Mg/Al ratio catalysts had spectra that were characterized by sharp peaks A and C (C slightly higher than A), an unresolved peak B and a broad peak D. CopCat-Ni2Co2-Mg/Al-1.0 spectrum had features and peaks energy between CopCat-Ni2Co2-Mg/Al-0.3 and the two catalysts with Mg/Al greater than 1. The energy positions of peaks A and B for CopCat-Ni2Co2-Mg/Al-1.0 and CopCat-Ni2Co2-Mg/Al-0.3 catalysts were at lower energy, while peaks C and D are at higher energy compared to the corresponding peaks of the other catalysts. Comparing these spectra with the work of Trcera et al., (2009); Yoshimura et al., (2013); CopCat-Ni2Co2-Mg/Al-0.3 has a spectrum that matches the CN of Mg in a normal spinel with a major value of 4. The two catalysts with Mg/Al ratio greater 1 have spectra that resemble a coordination environment of Mg with a major CN of 6. While CopCat-Ni2Co2-Mg/Al-1.0 shows a spectrum in between both with an Mg CN 5 on the average (i.e part of the Mg in this catalyst has CN 6 and the other ones has CN 4).

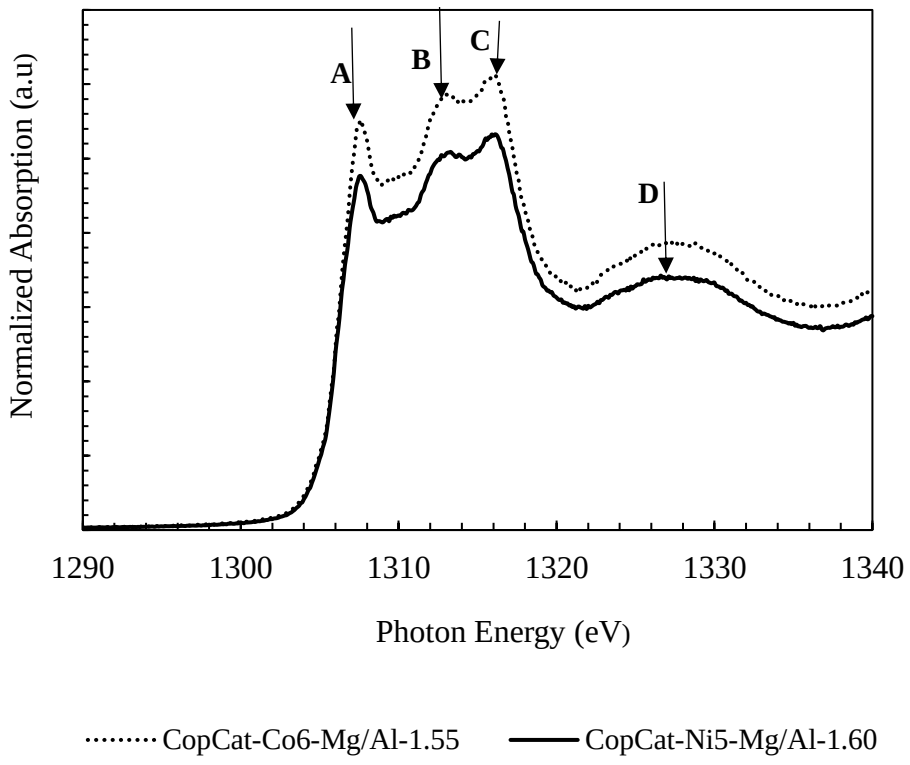

Figure 4.5. Mg K-edge XANES of monometallic catalysts

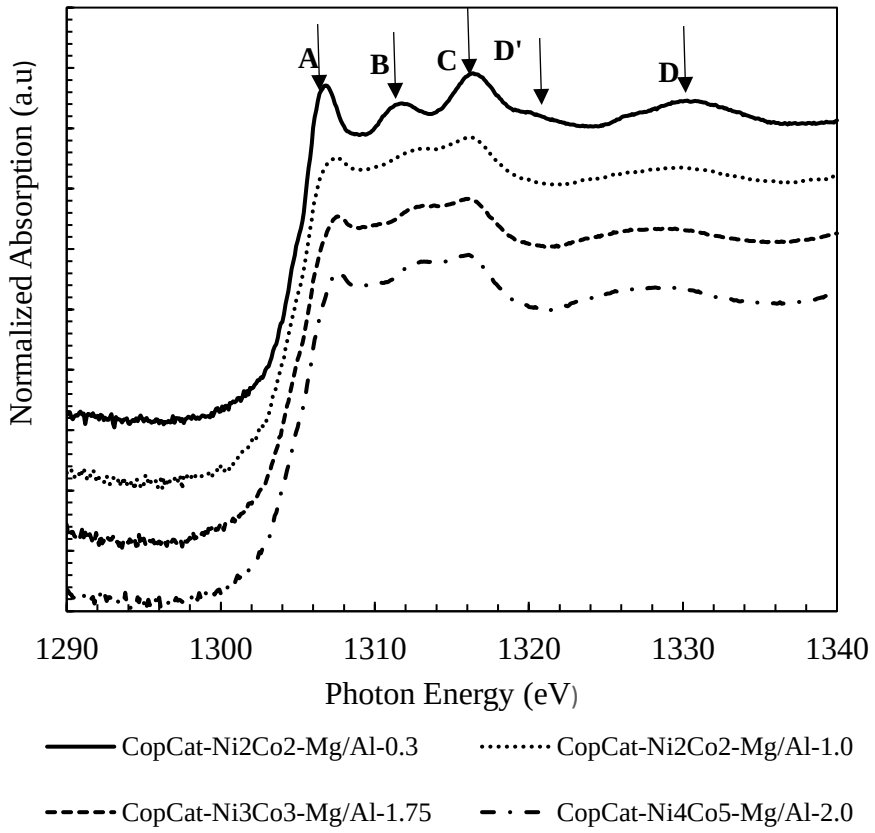

Figure 4.6. Mg K-edge XANES of bimetallic catalysts

The position of the first peak of XANES spectra is related to both the coordination and polyhedron distortion change as related by Trcera et al., 2009. It can be seen from Figure 4.6 that there was a change in the energy position of the first XANES peak (peak A) to higher energy from CopCat-Ni2Co2-Mg/Al-0.3, through CopCat-Ni2Co2-Mg/Al-1.0 upto CopCat-Ni4Co5-Mg/Al-2.0. Such changes in the energy position is attributed to increase in CN (Trcera et al., 2009). The spectra of the higher Mg/Al ratio catalysts compared well with the spectrum of MgO reported by Yoshimura et al., 2013; in terms of feature and energy position of the peaks. But unlike their spectrum, there are no small peaks at 1311.5 and 1322 eV in our catalysts. This difference could result from the interaction of Mg with other atoms such as Ni, Co and Al in the spinel phase within the structure of the catalysts. A CN of 4 is related to tetrahedral site occupancy in a spinel structure, while CN 6 signifies an octahedral site occupancy. A CN 6 for Mg in the higher Mg/Al ratio catalysts could result from the MgO phase or octahedral site occupancy in the spinel or both. Summarily, from the Mg K-edge XANES results, a progressive increase in the CN was observed as the Mg/Al ratio increased from 0 to 2 in the catalyst systems.

4.1.5 Al K-edge XANES

The Al K-edge XANES results for the monometallic catalysts are presented in Figure 4.7, while the results of the bimetallic catalysts are shown in Figure 4.8. For the Al-Ox supported Ni and Co monometallic catalysts (CopCat-Ni3-Mg/Al-0.00 and CopCat-Co4-Mg/Al-0.00), the edge region can be described by four peaks in the energy range 1565-1576 eV and a broader peak around 1588-1592 eV. The four main peaks were labelled a, b, c, d and the broader peak e with respect to their energy positions.

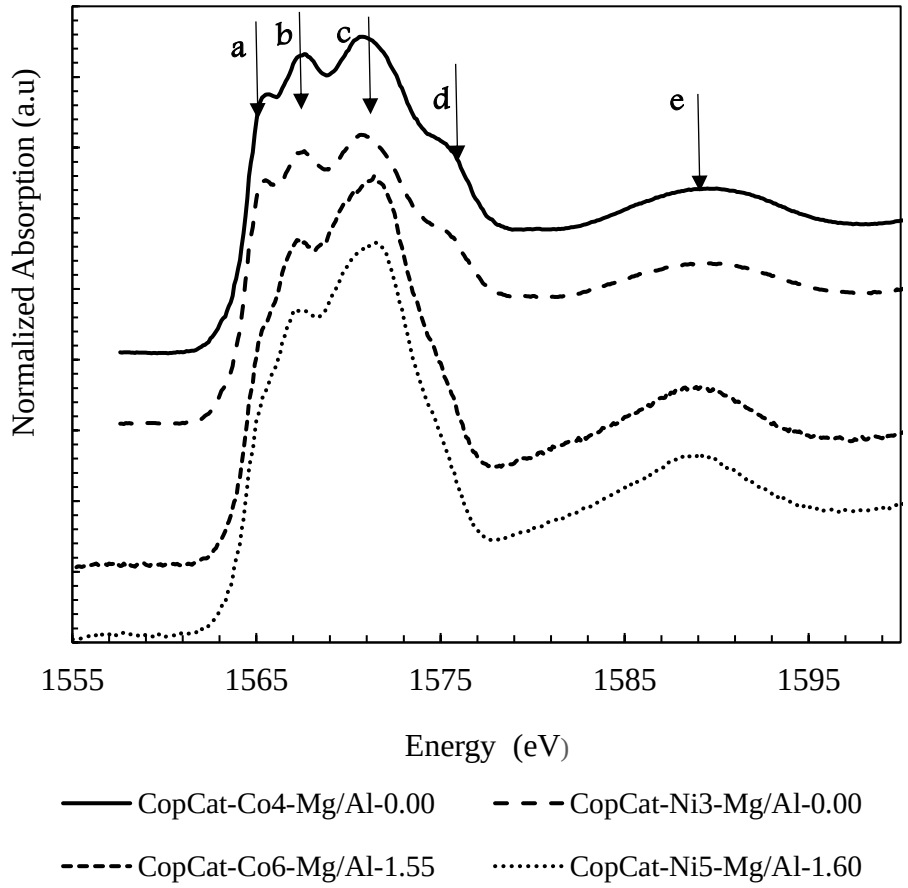

Figure 4.7. Al K-edge XANES of monometallic catalysts

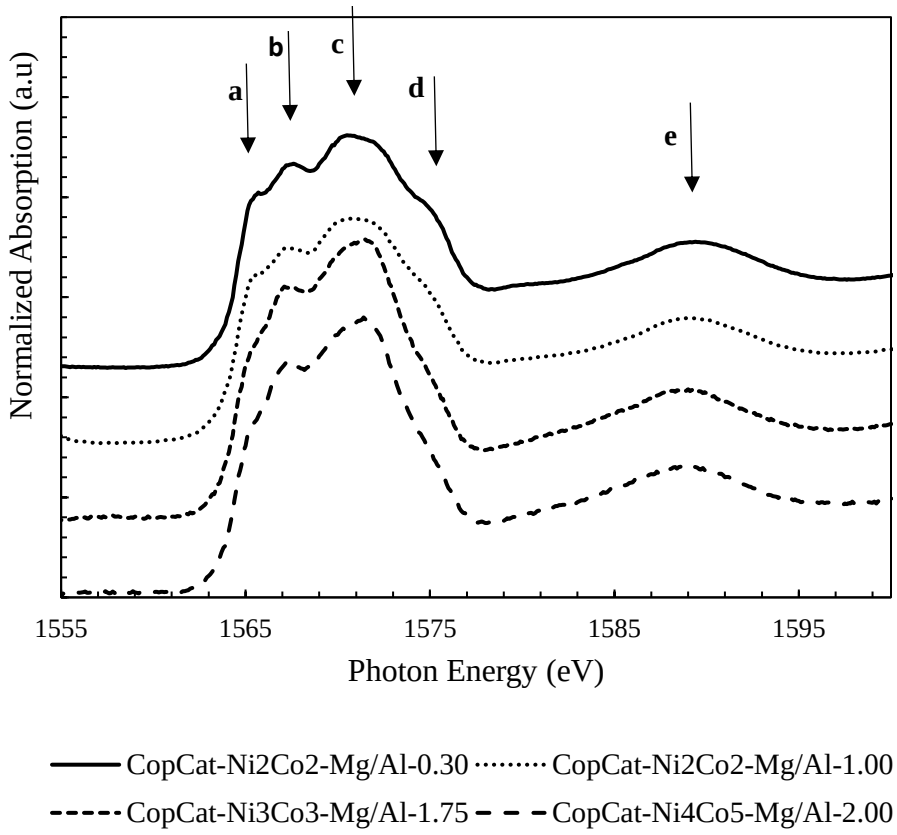

Figure 4.8. Al K-edge XANES of bimetallic catalysts

The intensities of the first three peaks in these two catalysts increased slightly with increase in energy, followed by a decrease to peak d up to e. With the introduction of MgO, peaks a and d disappeared, while peak e became more defined. Similar trend was observed in the Al K-edge XANES results of the bimetallic catalysts with respects to the spectra features and peak positions. A progressive decrease was observed in peaks a and d, which finally disappeared as the Mg/Al ratio increased from 0.3 to 2 in the bimetallic catalysts. Comparing these spectra results with the work of Hu et al., (2008); Neuville et al., (2009); Al-Ox supported Ni and Co monometallic catalysts (CopCat-Ni3-Mg/Al-0.0 and CopCat-Co4-Mg/Al-0.0) had spectra which matched the spectrum of gamma alumina with Al having CN 4 and 6 (occupying tetrahedral and octahedral sites in the spinel structure). For the Mg-Al-Ox supported monometallic catalysts (CopCat-Ni5-Mg/Al-1.60 and CopCat-Co6-Mg/Al-1.55), their spectra matched the spectrum of Al in an $MgAl_2O_4$ spinel with considerable degree of inversion (meaning part of Al ions take the tetrahedral sites rather than the octahedral site where they are supposed to be). For the bimetallic catalysts, result of CopCat-Ni2Co2-Mg/Al-0.30 matched the spectrum of Al rich spinel of $MgAl_2O_4$ reported by Treca et al., 2009, with Al having mostly a CN of 6. The results of CopCat-Ni3Co3-Mg/Al-1.75 and CopCat-Ni4Co5-Mg/Al-2.0 were closely related to that of Mg-Al-Ox supported Ni and Co monometallic catalysts in this study. These results closely matched the spectra of $MgAl_2O_4$ spinel published by Treca et al., 2009; with appreciable degree of inversion; a situation which causes interchange of sites between the M^{2+} and M^{3+} metal in the spinel, thereby making some Al^{3+} to occupy the tetrahedral site. The CopCat-Ni2Co2-Mg/Al-1.0 showed a result like CopCat-Ni2Co2-Mg/Al-0.3 catalyst.

A summary of the CN of Mg and Al from the K-edge XANES study of the catalysts are presented in Tables 4.9 and 4.10.

Table 4.9. Summary of CN from Mg and Al K-edge XANES for monometallic catalysts

Catalysts	CN of Mg	CN of Al
CopCat-Ni3-Mg/Al-0.00	-	4 and 6
CopCat-Co4-Mg/Al-0.00	-	4 and 6
CopCat-Ni5-Mg/Al-1.60	Majorly 6	4 and 6
CopCat-Co6-Mg/Al-1.55	Majorly 6	4 and 6

Table 4.10. Summary of CN from Mg and Al K-edge XANES for bimetallic catalysts

Catalysts	CN of Mg	CN of Al
CopCat-Ni2Co2-Mg/Al-0.30	Majorly 4	Majorly 6
CopCat-Ni2Co2-Mg/Al-1.00	4 and 6	Majorly 6
CopCat-Ni3Co3-Mg/Al-1.75	Majorly 6	4 and 6
CopCat-Ni4Co5-Mg/Al-2.00	Majorly 6	4 and 6

A simultaneous change was observed in the CN of both Mg and Al as the Mg/Al ratio changes in the catalyst systems (Tables 4.9 and 4.10). While a CN 6 for Mg could result from the MgO-phase, a concurrent change in CN of Mg and Al could represent a gradual inversion in the spinel phase, with increase in Mg/Al ratio. When the Mg/Al ratio was less than the stoichiometry value of spinel (0.5), the Al majorly occupied the octahedral site. But incorporation of Mg, seemingly displaced some Al ions into the tetrahedral site.

4.1.6 ^{27}Al MAS NMR

This characterization technique was purposely carried out to check for spinel inversion and determine the extent of inversion if there is any. The results obtained from the technique are presented in Figures 4.9 and 4.10 for the monometallic and bimetallic catalysts respectively. All the spectra showed two peaks around 68 ppm and 9 ppm attributed to tetrahedral (Al_4) and octahedral (Al_6) aluminium respectively as reported by Millard et al., (1992); Louise et al., (2014). Area integration method was then used to determine the ratio of octahedral aluminium (Al_6) to tetrahedral aluminium (Al_4). For a spinel $^{[4]}(A_{1-x}B_x)\ ^{[6]}[B_{2-x}A_x]\ O_4$, the inversion parameter (x) can also calculated using the formulas below as proposed by Millard et al., (1992); and Schreyeck et al., (2001);

$$\%\ Al_4 = \frac{\text{Area of peak at 68ppm}}{\text{Total peak Area}} * 100 \qquad 4.16$$

$$\%\ Al_6 = \frac{\text{Area of peak at 9ppm}}{\text{Total peak Area}} * 100 \qquad 4.17$$

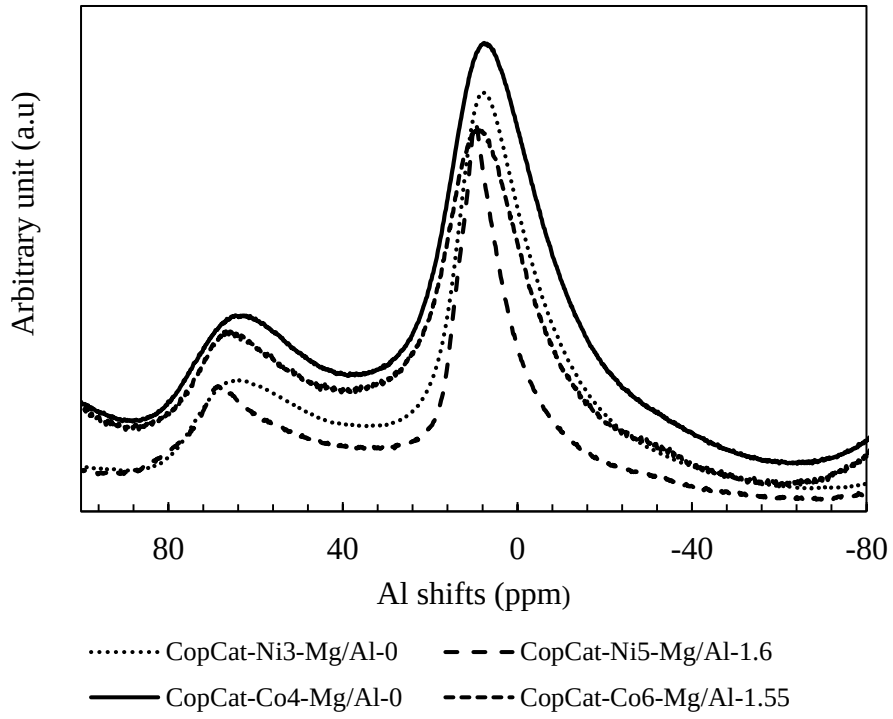

Figure 4.9. Al NMR spectra of monometallic catalysts

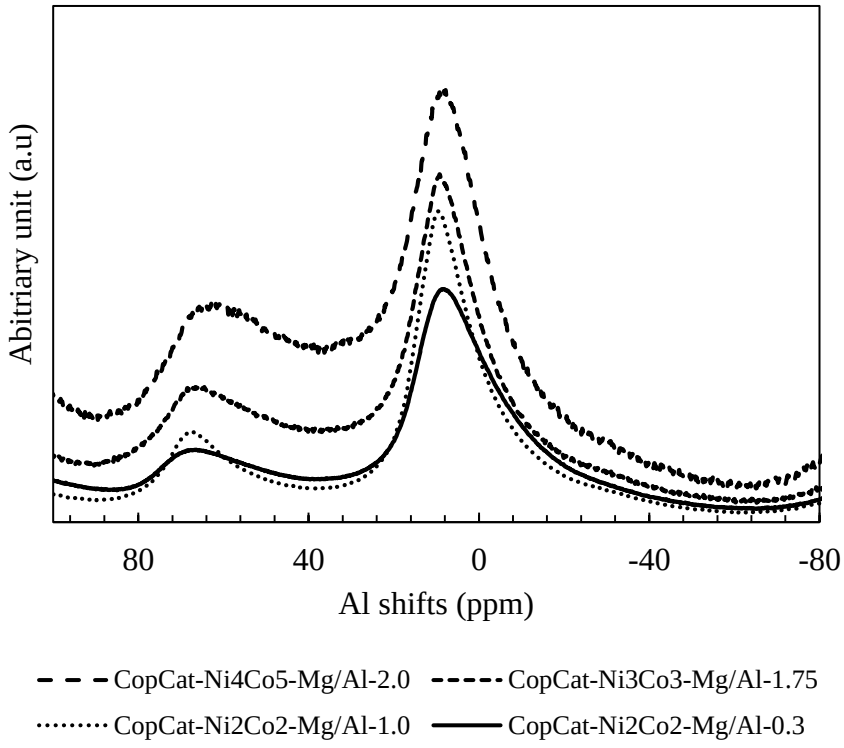

Figure 4.10. Al NMR spectra of bimetallic catalysts

The ratio of octahedral to tetrahedral aluminium correspond to;

$$\frac{Al_6}{Al_4} = \frac{2-x}{x} \qquad 4.18$$

This leads to;

$$x = \frac{2}{\left[1+\left(\frac{Al_6}{Al_4}\right)\right]} \qquad 4.19$$

where A = M^{2+} (Mg, Ni, Co) , B = (Al^{3+}) , ^{4}( ) = Tetrahedral site, ^{6}( ) = Octahedral site , and x = inversion parameter.

The results obtained from the calculation of the area integration and the inversion parameter are presented in Tables 4.11 and 4.1.12. A progressive increase in value of x was observed as the Mg/Al ratio increased from 0 to 2 in both monometallic and bimetallic catalysts. Additionally, Ni catalysts showed more inversion than Co catalyst, signifying that their desire for the octahedral sites are different. Obviously, incorporation of Mg causes inversion in the spinel structure and Ni ions occupy more octahedral site than Co ions.

Table 4.11. Inversion parameter for monometallic catalysts

Catalysts	Al_6/Al_4	x
CopCat-Ni3-Mg/Al-0.00	3.54	0.44
CopCat-Co4-Mg/Al-0.00	4.01	0.40
CopCat-Ni5-Mg/Al-1.60	2.70	0.54
CopCat-Co6-Mg/Al-1.55	3.32	0.46

Table 4.12. Inversion parameter for bimetallic catalysts

Catalyst	Al_6/Al_4	x
CopCat-Ni2Co2-Mg/Al-0.30	5.60	0.30
CopCat-Ni2Co2-Mg/Al-1.00	4.09	0.39
CopCat-Ni3Co3-Mg/Al-1.75	3.17	0.48
CopCat-Ni4Co5-Mg/Al-2.00	2.57	0.56

4.1.7 XPS of Ni and Co 2p

Information about the oxidation state and interaction of the active metal with the support were obtained using this characterization technique. The Ni 2p spectra of the monometallic catalysts are presented in Figure 4.11, while the Co 2p spectra are shown in Figure 4.12. The spectra of both Ni and Co 2p are characterized by two major peaks related to $2p_{3/2}$ and $2p_{1/2}$ with an associated satellite peak. The energy separation between the main and satellite peak of the 2p XPS spectra, in addition to the binding energy (BE), give information about the environment of metals according to Dillard et al., 1983. From Figures 4.11 and 4.12, the $2p_{3/2}$ BE of the Al supported monometallic Ni and Co are 856 eV and 781 eV respectively. While this BE value of the Co catalyst correspond to that of $CoAl_2O_4$ spinel 781 eV reported by Chin and Hercules, 1982; Xiong et al., 2005; a slight difference was observed in the BE of the Ni catalyst compared to $NiAl_2O_4$ spinel value of 856.2eV stated by Stöcker et al., 1988. The decrease in BE value could be related to the presence of some isolated or loosely bonded Ni on the Al-Ox support. Introduction of MgO into the support caused a decrease in the value of $2p_{3/2}$ BE in the Mg-Al supported catalyst compared to the Al-Ox only supported catalysts. The value of the Ni catalyst decreased to 854.8 eV, while that of Co went down to 780 eV. These reductions in value could be related to reduced interaction of the active metals with Al, and the presence of considerable amount of the metals in the MgO phase as earlier stated by Juan-Juan et al., 2009.

The 2p XPS spectra of both Ni and Co in the bimetallic catalysts are presented in Figures 4.13 and 4.14 respectively. The spectra features are like the monometallic catalysts in terms of the major and satellite peaks. The trend observed was that the $2p_{3/2}$ BE energy decreased as the Mg/Al ratio increased, which could signify more interaction of the active metals with MgO-phase as the ratio increased.

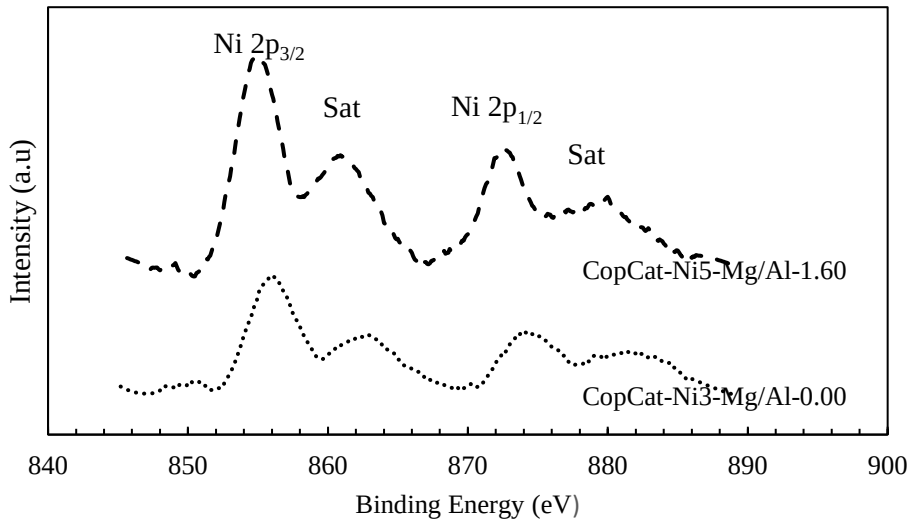

Figure 4.11. Ni 2p XPS spectra of monometallic catalysts

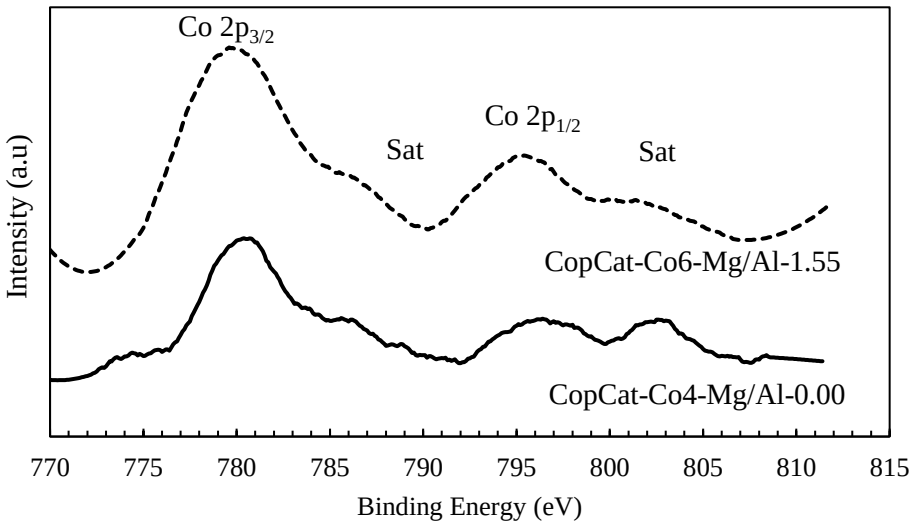

Figure 4.12. Co 2p XPS spectra of monometallic catalysts

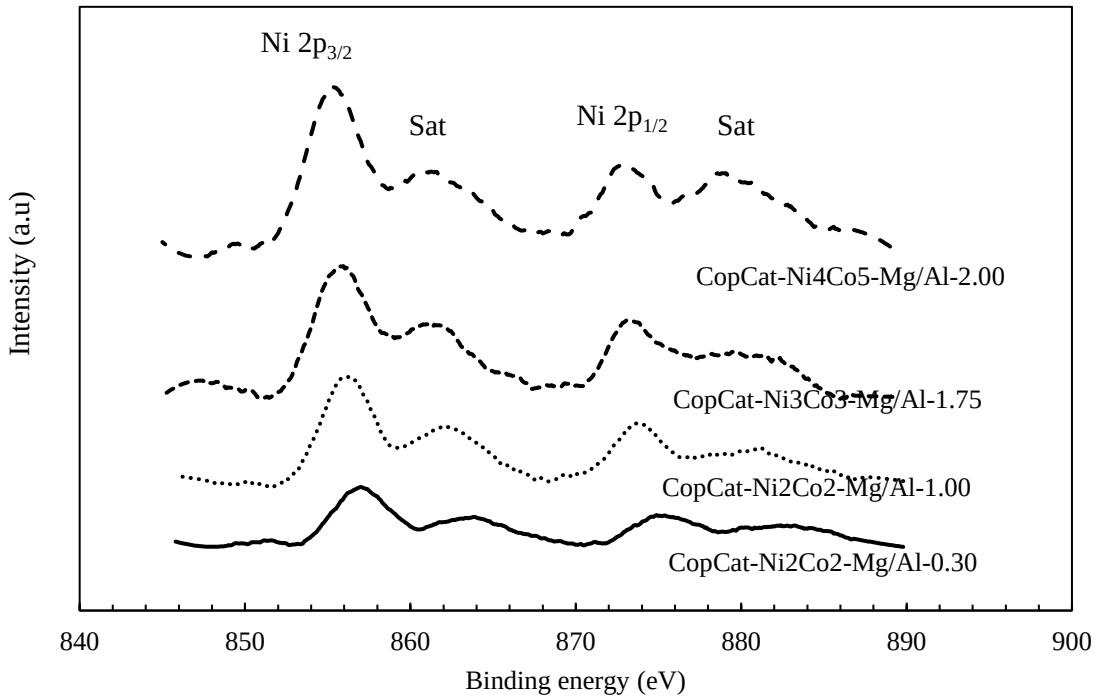

Figure 4.13. Ni 2p XPS spectra of bimetallic catalysts

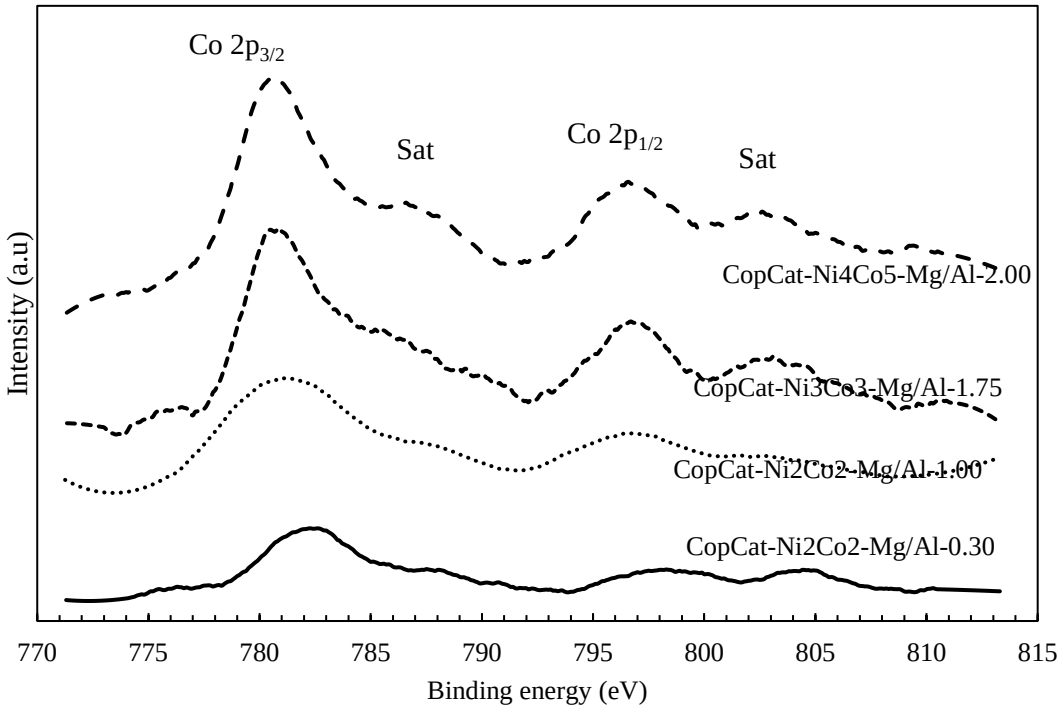

Figure 4.14. Co 2p XPS spectra of bimetallic catalysts

A difference was observed in the $2p_{3/2}$ BE of the Mg-Al-Ox supported bimetallic catalysts when compared with the corresponding monometallic catalysts. With the similar support composition, this difference could only be related to the interaction of support with Ni and Co. An increase in peak intensity was also observed as the Mg/Al ratio increased in the Mg-Al supported composite catalysts. Such increase in XPS peak intensity could be related to decrease in particle size because of better dispersion (Oh et al., 2003). Also, the intense satellite structure on the high binding energy side of the main photo peaks shows that Ni and Co are present mostly in +2 states (Dillard et al., 1983). A summary of the important features of the spectra are highlighted in Table 4.13 for the monometallic catalysts, while Tables 4.14 and 4.15 are for Ni and Co in the bimetallic catalysts.

Regarding the distribution of the metal within the bulk phases of the support, some features of the spectra were compared with pure standard metal oxide (purely octahedral) and metal spinel (purely tetrahedral). $Co2p_{1/2} - Co2p_{3/2}$ energy split of approximately 16 eV shows Co is present as Co (II) in high spin for the catalysts (Brinen and Armstrong, 1978). From Table 4.13, the $2p_{3/2}$ BE (781 eV) and ΔBE Co $2p_{3/2}$ (sat-main) value of 5.0 eV for CopCat-Co4-Mg/Al-0.0 catalyst compare well with the values of 781 and 4.7 eV reported by Dillard et al., 1983; for Co^{2+} in a complete tetrahedral site of $CoAl_2O_4$ spinel. These values of 780 and 6.0 eV for CopCat-Co6-Mg/Al-1.55 composites falls between $CoAl_2O_4$ and CoO (780.1 and 6.3 eV that is in purely octahedral geometry) (Dillard et al., 1983). Additionally, a shift of the $2p_{3/2}$ binding energy to higher value has been attributed to more tetrahedral site occupancy of metal ions (Wu and Hercules, 1979).

Table 4.13. Summary of XPS (Ni 2p and Co 2p) spectra of monometallic catalysts

Catalyst	Binding Energy (BE)$2p_{3/2}$ (eV)	ΔBE ($2p_{1/2}$-$2p_{3/2}$) (eV)	ΔBE $2p_{3/2}$ (sat –main) (eV)
CopCat-Ni3-Mg/Al-0.00	856.0	17.0	5.0
CopCat-Ni5-Mg/Al-1.60	854.8	17.5	5.9
CopCat-Co4-Mg/Al-0.00	781.0	15.5	4.9
CopCat-Co6-Mg/Al-1.55	780.0	15.7	6.0

Table 4.14. Summary of Co 2p XPS spectra of bimetallic catalysts

Catalyst	Binding Energy Co $2p_{3/2}$ (eV)	ΔBE Co ($2p_{1/2}$-$2p_{3/2}$) (eV)	ΔBE Co $2p_{3/2}$ (sat –main) (eV)
CopCat-Ni4Co5-Mg/Al-0.30	782.0	16.1	5.0
CopCat-Ni2Co2-Mg/Al-1.00	781.2	16.1	5.6
CopCat-Ni3Co3-Mg/Al-1.75	781.0	16.0	5.9
CopCat-Ni4Co5-Mg/Al-2.00	781.0	16.0	5.9

Table 4.15. Summary of Ni 2p XPS spectra of bimetallic catalysts

Catalyst	Binding Energy Ni $2p_{3/2}$ (eV)	ΔBE Ni ($2p_{1/2}$-$2p_{3/2}$) (eV)	ΔBE Ni $2p_{3/2}$ (sat – main) (eV)
CopCat-Ni2Co2-Mg/Al-0.30	856.4	17.3	5.1
CopCat-Ni2Co2-Mg/Al-1.00	856.0	17.1	5.7
CopCat-Ni3Co3-Mg/Al-1.75	855.5	17.1	6.0
CopCat-Ni4Co5-Mg/Al-2.00	855.4	17.1	6.0

In case of Ni, Stoker et al., 1988; reported a value of 856.2 and 854.6 eV for $2p_{3/2}$ BE of $NiAl_2O_4$ (purely tetrahedral) and NiO (purely octahedral) respectively. A ΔBE Ni ($2p_{1/2} - 2p_{3/2}$) and ΔBE Ni 2p3/2(sat-main) values of 18 and 6.1 eV were reported by Matienzo et al., 1973; for pure octahedral Ni. The values reported for our Ni catalysts in Table 4.13 falls between the purely octahedral and tetrahedral Ni. CopCat-Ni3-Mg/Al-0.0 has values a bit above $NiAl_2O_4$, while CopCat-Ni5-Mg/Al-1.6 has value close to that of NiO as reported by Stocker et al., (1988); Matienzo et al., (1973). The above results show that while Co^{2+} could be strictly distributed in the tetrahedral site in CopCat-Co4-Mg/Al-0.0, and appreciable amount of Co^{2+} occupies the octahedral site in CopCat-Co6-Mg/Al-1.55 monometallic composite. In case of Ni monometallic catalysts, Ni^{2+} is distributed between both sites in the Ni composite catalysts or there could be some isolated or loosely bonded Ni in the catalysts. For the bimetallic catalysts (Table 4.14), the ΔE Co $2p_{3/2}$(sat-main) values for all the catalysts range from 5.0 to 5.9 eV. These values fall between 4.7 eV for complete tetrahedral Co ions (Dillard et al., 198)] and 6.3 eV for octahedral Co ions (Kim, 1975). Additionally, this value became closer to the octahedral Co value as the Mg/Al ratio increased in the catalyst. Similar trend was observed in these values for Ni in the bimetallic catalysts as shown in Table 4.15. The difference in the value of ΔE Ni $2p_{3/2}$ (sat-main) in the catalysts shows that the distribution of Ni between the tetrahedral and octahedral sites is not the same, even though ΔBE ($2p_{1/2}$-$2p_{3/2}$) value shows the state of Ni is the same in all the catalysts.

Summarily, the XPS results show that with the introduction of MgO, there was reduced interaction between the active metals and Al in the spinel phase. Also, the active metals were present in both the MgO and spinel phase in the Mg-Al-Ox supported catalysts. Additionally, there was more octahedral occupancy of the active metals with the introduction of Mg, indicating that spinel inversion could offer more octahedral occupancy of the active metals.

4.1.8 STEM-EDX of monometallic catalysts

To understand the interaction of the active metals with the support, STEM-EDX mapping was done on the monometallic catalysts of Ni and Co, and the results obtained for the Al-Ox supported monometallic Co (CopCat-Co4-Mg/Al-0.00) and Ni (CopCat-Ni3-Mg/Al-0.00) catalysts are shown in Figures 4.15 and 4.16 respectively. Co showed a homogenous distribution with good dispersion on the support. Co particle size also appear smaller with no phase segregation on the Al-Ox support. Unlike Co, Ni displayed a non-homogeneous distribution, with slightly bigger particle size and a phase segregation of NiO on the Al-Ox support (Figure 4.16). The isolated phase is an indication of less stronger interaction of Ni with Al, when compared to Co and Al. Modification of the support with MgO changed the distribution of the active metals on the supports as revealed by the STEM-EDX results of the Mg-Al-Ox supported catalysts (Figures 4.17 and 4.18). There was an even distribution of between Mg and Al (Figures 4.17 c and 4.18 c) in both Ni and Co catalysts, an indication of stronger interaction between Mg and Al in the catalysts system. Co showed a stronger interaction with Al (Figure 4.17 a) than with Mg (Figure 4.17 b), while Ni showed similar distribution on both Al (Figure 4.17 a) and Mg (Figure 4.17 b). These are substantiated by the brightness and size of circled spot in the STEM-EDX results.

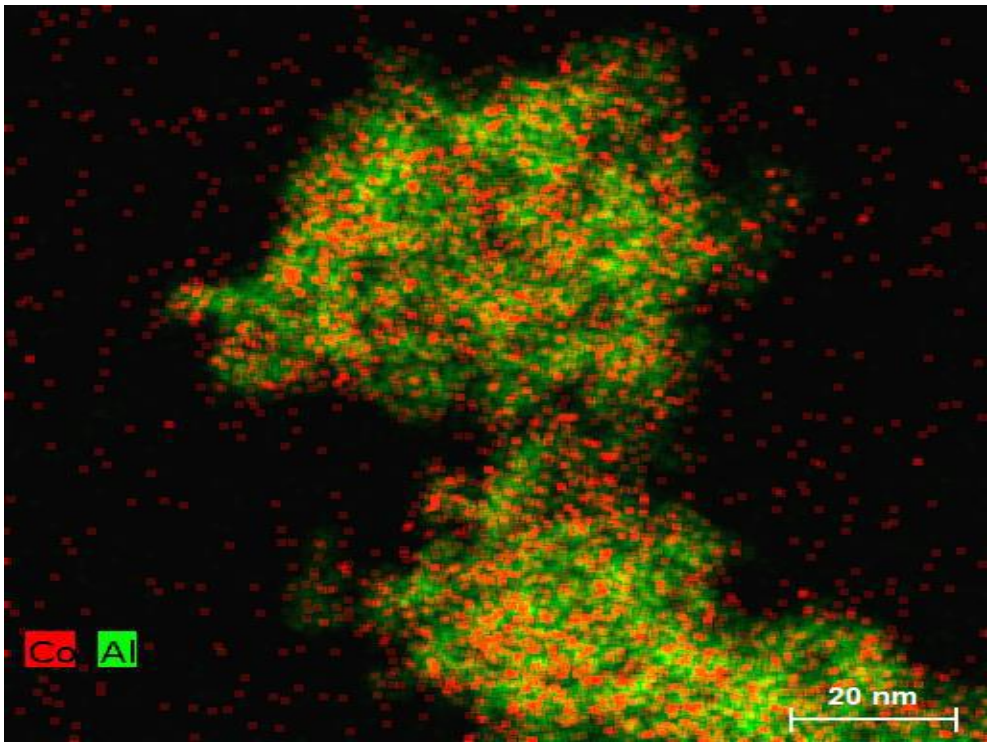

Figure 4.15. STEM-EDX of Al-Ox supported monometallic Co catalyst (CopCat-Co4-Mg/Al-0.0)

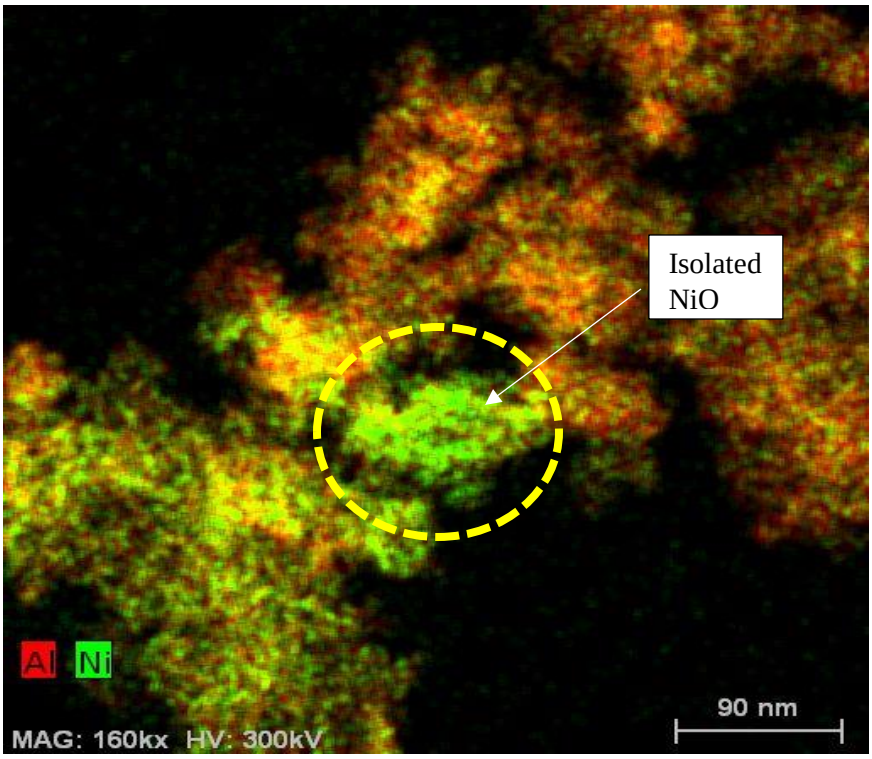

Figure 4.16. STEM-EDX of Al-Ox supported monometallic Ni catalyst (CopCat-Ni3-Mg/Al-0.0)

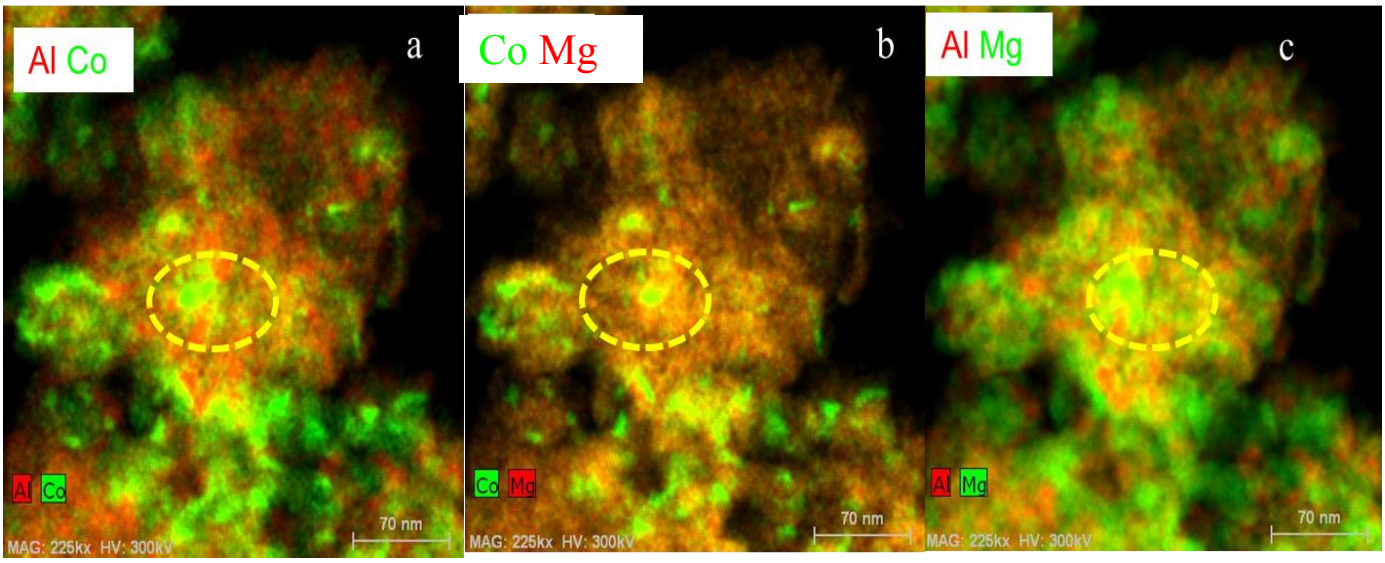

Figure 4.17. STEM-EDX of Mg-Al-Ox supported monometallic Co catalyst (CopCat-Co6-Mg/Al-1.55)

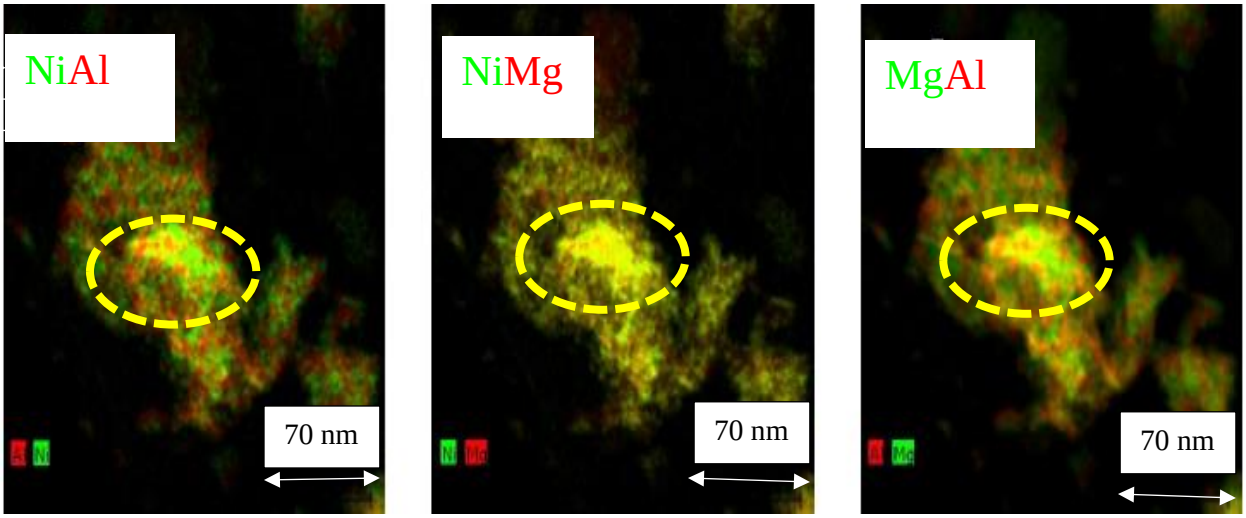

Figure 4.18. STEM-EDX of Mg-Al-Ox supported monometallic Ni catalyst (CopCat-Ni5-Mg/Al-1.6)

In summary, Ni and Co showed different distribution on similar support, as well as different level of interaction with the components of the support system

4.1.9 Basicity of catalysts from CO_2-TPD

This property tells us the capability of the catalysts for the adsorption and desorption of the reactant (CO_2) on the surface of the catalysts. The desorption pattern exhibited by the catalysts are shown in Figures 4.19 and 4.20 for the monometallic and bimetallic catalysts respectively. The profile of the catalysts is defined by three desorption peaks at temperatures around 100, 400 and 650 ^oC, suggestive of different basic sites. These peaks are assigned to weak, intermediate and strong basic sites respectively (Debecker et al., (2009); Di-Cosimo et al., (1998)). The basicity of the Al-Ox supported monometallic Co (CopCat-Co4-Mg/Al-0.0) and Ni (CopCat-Ni3-Mg/Al-0.0) catalysts are approximately equal, with both profiles characterized by distinct weak and strong basic sites, with a very faint intermediate basic site. The introduction of MgO into catalyst composites significantly increased the basicity of the catalysts, most especially the intermediate basic sites. This became obvious from the increase in the peak area of the profiles of the Mg-Al-Ox supported monometallic Co (CopCat-Co6-Mg/Al-1.55) and Ni (CopCat-Ni5-Mg/Al-1.6) catalysts as compared to the profile of the corresponding Al supported catalysts (CopCat-Ni3-Mg/Al-0.0 and CopCat-Co4-Mg/Al-0.0). Additionally, Co catalyst exhibited stronger basic site compared to the corresponding Ni catalyst in the Mg-Al supported catalyst. This could be related to stronger interaction of Co with the MgO in the support. The result of the bimetallic catalysts (Figure 4.20) showed progressive increase in peak area as the Mg/Al ratio increased from 0.3 to 2. The strength of the strong basic site became more obvious and intense in the higher Mg/Al ratio bimetallic catalysts.

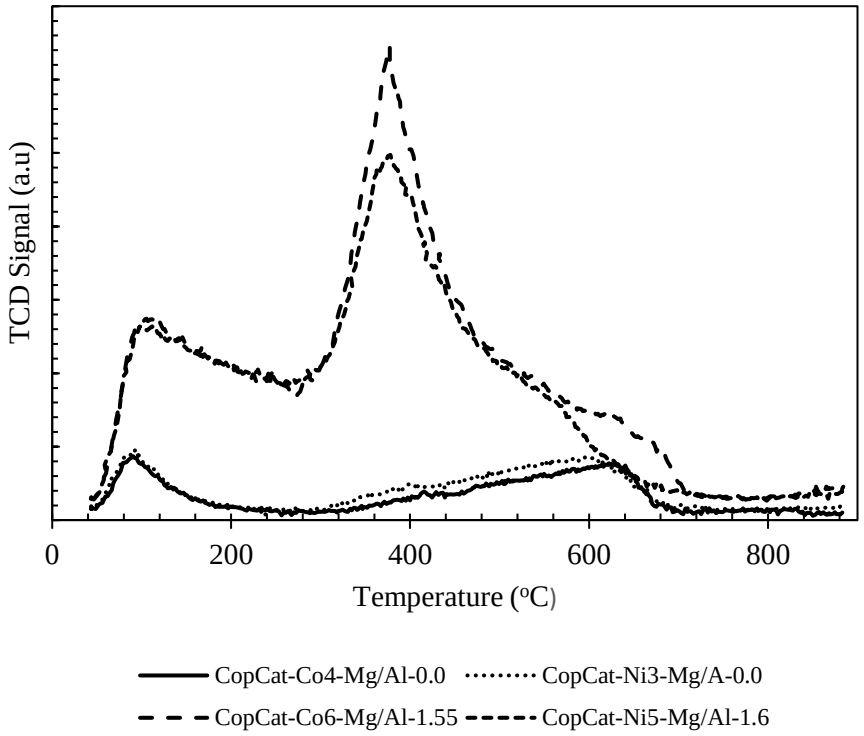

Figure 4.19. CO_2 -TPD result of the monometallic catalysts

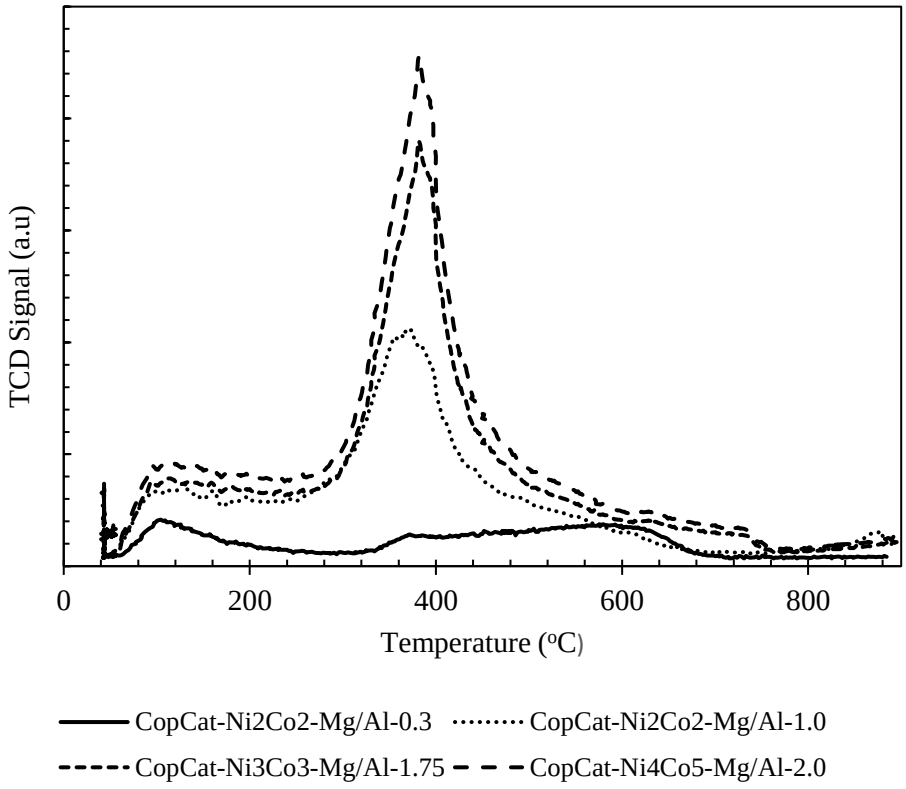

Figure 4.20. CO_2 -TPD result of the bimetallic catalysts

Weak basic site could be associated with the presence of (OH^-) where CO_2 probably adsorbed as bicarbonate species. Intermediate basic site is where CO_2 is adsorbed on Mg-O pairs, forming bidentate species. The adsorption of CO_2 over low coordination oxygen anions to form unidentate carbonates is related to the strong basic site respectively (Debecker et al., (2009); Di-Cosimo et al., (1998). Metal interaction, chemical composition, nature of surface specie, as well as local and bulk structure affect the basicity of catalyst (Munoz et al., 2012). Surface species can alter the strength of metal-Oxygen bond (Mg-O, Al-O, Ni-O and Co-O), resulting in diverse types of basic site (Munoz et al., 2012). Incorporation of sufficient MgO changed the bulk structure (from XRD result) and consequently affected the basicity. Basic sites promote the adsorption and conversion of more CO_2 during dry reforming reaction (Hu, (2009); Wang et al, (2009)) and enhance the elimination process of coke through the reaction of CO_2 with C to produce CO (Xu et al., (2011); Zhu et al., (2011)). Obviously, the compositional change as well as changes in the bulk phase affected the basicity of the catalysts.

4.2 Catalyst Characterization Results after Reduction

Discussions about active metal(s) reduction from bulk phases, extent of reduction, site formation and particle size of metal after reduction are presented in this section.

4.2.1 H_2-TPR profile

The H_2-TPR profile of the bimetallic catalysts are presented in Figure 4.21. Reduction peaks range between 200-850 ^oC suggest various types of interaction between the metal oxides and the support.

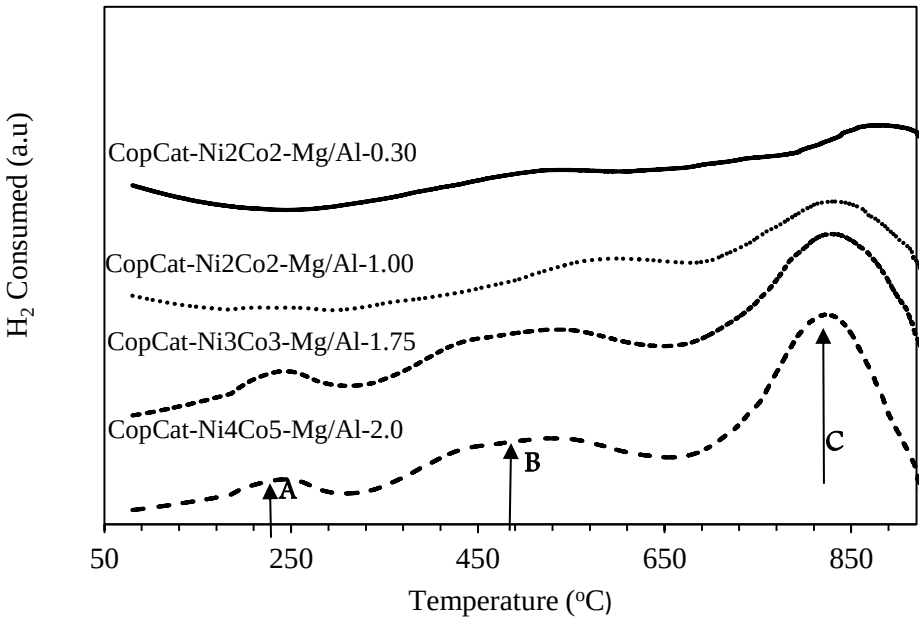

Figure 4.21. H_2-TPR profile of bimetallic catalysts

The profiles of the higher Mg/Al ratio catalysts (CopCat-Ni4Co5-Mg/Al-2.0 and CopCat-Ni3Co3-Mg/Al-1.75) are characterized by three different reduction peaks namely A, B, C at temperatures 200-300 ^{o}C, 400-600 ^{o}C and 750-850 ^{o}C, respectively. Only peak C with a shift to higher temperature was seen in the profile of the lower Mg/Al ratio catalyst (CopCat-Ni2Co2-Mg/Al-0.30). CopCat-Ni2Co2-Mg/Al-1.0 profile falls between these two groups of catalysts. Peak A can be attributed to the reduction of free surface or loosely bonded metal oxides (Ni) that have weak interaction with the support (Munoz et al., (2012); Arena et al., (1990); Yu et al., (2006); Koo et al., (2008)). These species are readily accessed by H_2 and are easily reduced. Peak B is related to the reduction of octahedral metal oxides from both surface and bulk having intermediate interaction with the support. Peak C can be ascribed to the reduction of metal oxides that have stronger interaction with the support and are hard to reduce (Munoz et al., (2012), Wu and Hercules, (1979); Al-Fatesh, (2015); Arena et al., (1990); Yu et al., (2006)). The profiles revealed more intense reduction peak area with increasing Mg/Al ratio. This shows that more reducible species are present in the higher Mg/Al catalysts. Also, a shift in reduction peak to higher temperature was observed as the Mg/Al ratio decreased, most especially peak C in CopCat-Mg/Al-0.30. Such a shift is attributed to the nature of spinel structure as Mg^{2+} facilitates easier reduction of the metal oxide, bringing about a shift in reduction peak to lower temperature (Koo, et al., 2008).

4.2.2 Ni and Co XANES

The extent of Ni and Co reduction was determined using Ni and Co K-edge XANES studies. Their K-edge XANES after reduction at 800 ^{o}C for 4hrs were compared with their respective metal foil and XANES before reduction. Sample plots for Al supported monometallic Co and Ni catalysts are shown in Figures 4.22 and 4.23 respectively. No full reduction of Ni or Co was seen in any of the catalysts after 4hrs reduction in N_2/H_2 gas mixture.

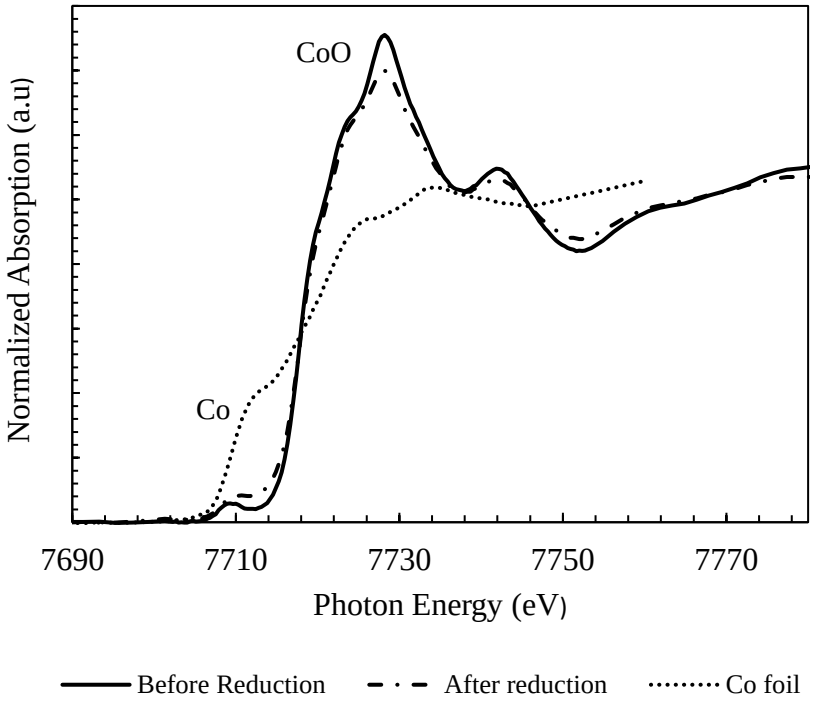

Figure 4.22. Normalized Co K-edge XANES for CopCat-Co4-Mg/Al-0.0

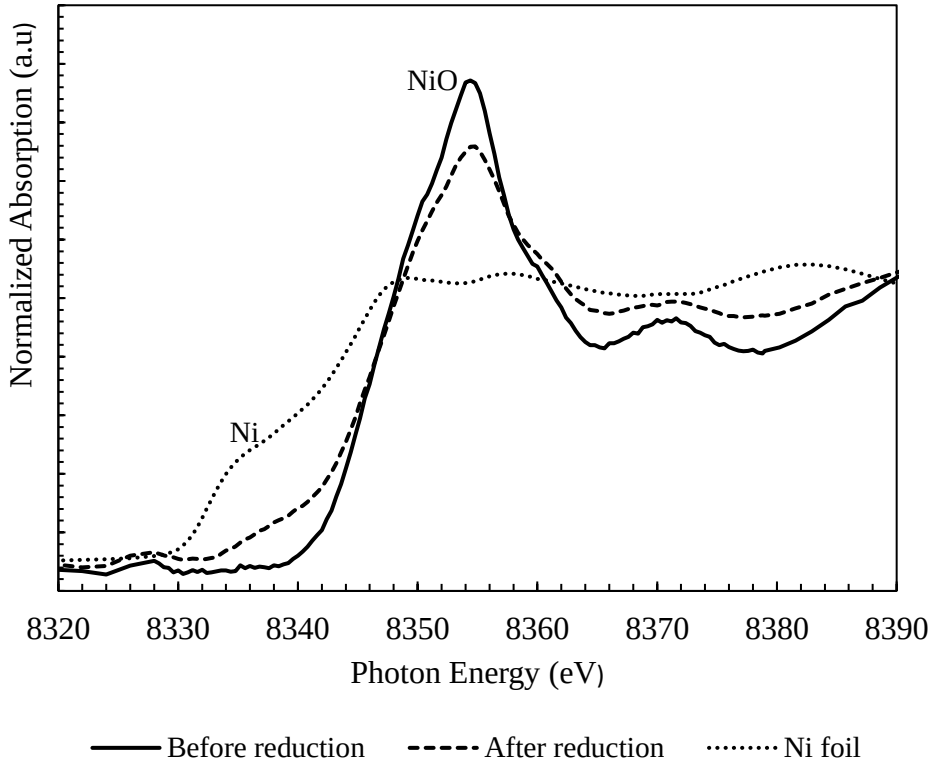

Figure 4.23. Normalized Ni K-edge XANES for CopCat-Ni3-Mg/Al-0.0

Linear combination fitting of XANES was then used to determine the extent of reduction of Ni^{2+} and Co^{2+} to their respective metal in all the catalysts. The results of XANES fittings for the reduced catalysts are shown in Table 4.16 for the monometallic catalysts. From the data presented in the Table 4.16, Al-Ox supported monometallic Co catalysts (CopCat-Co4-Mg/Al-0.0) showed no Co^{2+} reduction, while appreciable Ni^{2+} reduction up to 33 % was observed in the Al-Ox supported Ni catalyst (CopCat-Ni3-Mg/Al-0.0). The introduction of MgO into the catalyst composite improved the reducibility of the metal ions. Ni^{2+} reduction increased to 88 %, while Co^{2+} attained 54 % reduction. But in all the corresponding catalyst samples, Ni reduction was found to be higher than Co in the monometallic catalysts.

How the phase composition and Mg/Al ratio affect active metal reducibility was studied using the bimetallic catalysts. The results obtained for the metal reducibility is shown in Table 4.17, with the average metal reduction rate was calculated using Equation 4.20 below;

$$\text{Average reduction (\%)} = [\text{Ni reduction rate (\%)} * \frac{\text{\% Ni in sample}}{\text{\%Ni+\% Co}}] + [\text{Co reduction rate (\%)} * \frac{\text{\% Co in sample}}{\text{\%Ni+\% Co}}] \quad 4.20$$

Table 4.16. Extent of Ni and Co reduction in monometallic catalysts

Catalyst	Ni (%)	NiO (%)	Co (%)	CoO (%)
CopCat-Co4-Mg/Al-0.00	-	-	0	100
CopCat-Ni3-Mg/Al-0.00	33	67	-	-
CopCat-Co6-Mg/Al-1.55	-	-	54	46
CopCat-Ni5-Mg/Al-1.60	88	12	-	-

Table 4.17. Extent of Ni and Co reduction in bimetallic catalysts

Catalyst	Ni	NiO	Co	CoO	Average metal reduction
	%				
CopCat-Ni2Co2-Mg/Al-0.3	12	88	2	98	7
CopCat-Ni2Co2Mg/Al-1.0	35	65	7	93	21
CopCat-Ni3Co3-Mg/Al-1.75	85	15	28	72	57
CopCat-Ni4Co5-Mg/Al-2.0	90	10	32	68	61

From the fitting results shown in Table 4.17, the reduction rate of both Ni and Co increased with increase in the Mg/Al ratio in the catalysts. This result agreed with the H_2-TPR that showed more reduction peaks and phases in the higher Mg/Al ratio catalysts. Comparison between the reduction results of monometallic Ni (CopCat-Ni3-Mg/Al-1.60) and bimetallic Ni-Co (CopCat-Ni3Co3-Mg/Al-1.75 and CopCat-Ni4Co5-Mg/Al-2.0) showed that the extent of Ni reduction is similar in both group of catalysts. Thus, the presence of Co did not seem to have any effect on the reduction extent of Ni^{2+} in the bimetallic Ni-Co catalysts with sufficient MgO loading. But different trend was observed in Co^{2+} reduction, when compared the reduction results of monometallic Co catalysts (CopCat-Co6-Mg/Al-1.55) and bimetallic Ni-Co catalysts (CopCat-Ni3Co3-Mg/Al-1.75 and CopCat-Ni4Co5-Mg/Al-2.00). More Co reduction was observed in the monometallic catalysts compared to bimetallic Ni-Co catalysts with sufficient MgO. Additionally, while no reduction of Co was observed in the Al-Ox supported monometallic catalyst, appreciable amount of Ni^{2+} was observed in the corresponding catalysts. These results showed that interaction of the active metal(s) with the support, as well as the composition of the bulk phase, affected the reducibility of the active metals (Ni and Co) in this study.

The phase composition of catalyst after calcination was related to the extent of active metal reduction. The correlation results (Figures 4.24 and 4.25) showed that the extent of active metal reduction was directly proportional to the MgO-solid phase, with an inverse relationship to spinel phase. Additionally, the average metal reduction was found to be approximately equal to the MgO phase, an indication that the average metal reduction was determined by the MgO phase in the Ni-Co-Mg-Al-Ox catalyst system in this present study.

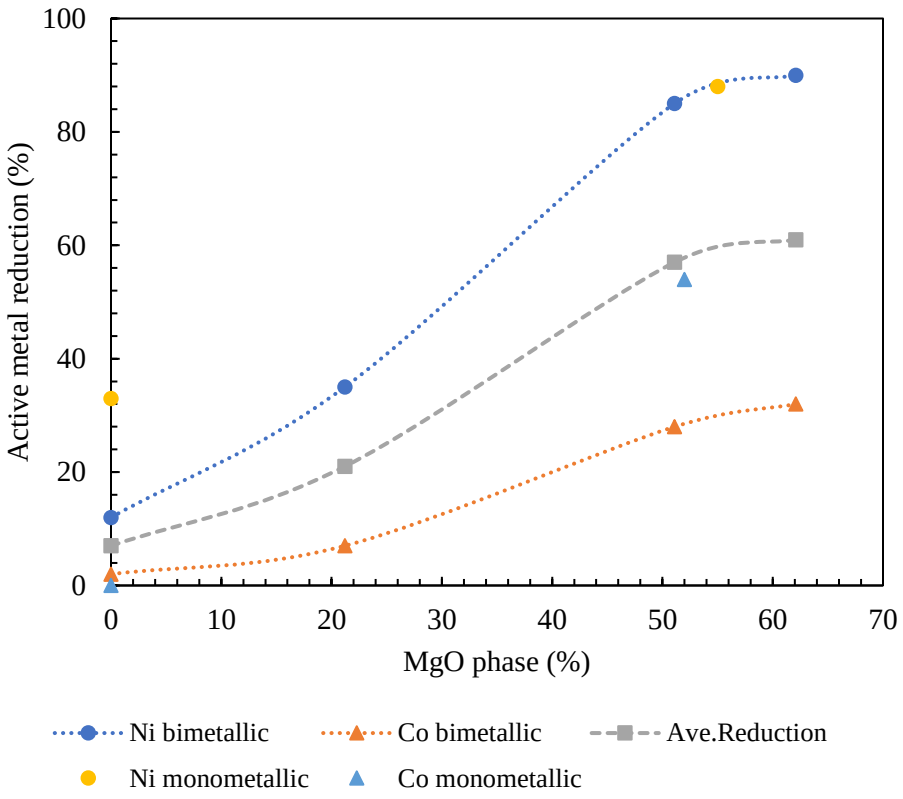

Figure 4.24. Correlation between metal reduction and MgO phase in the catalysts

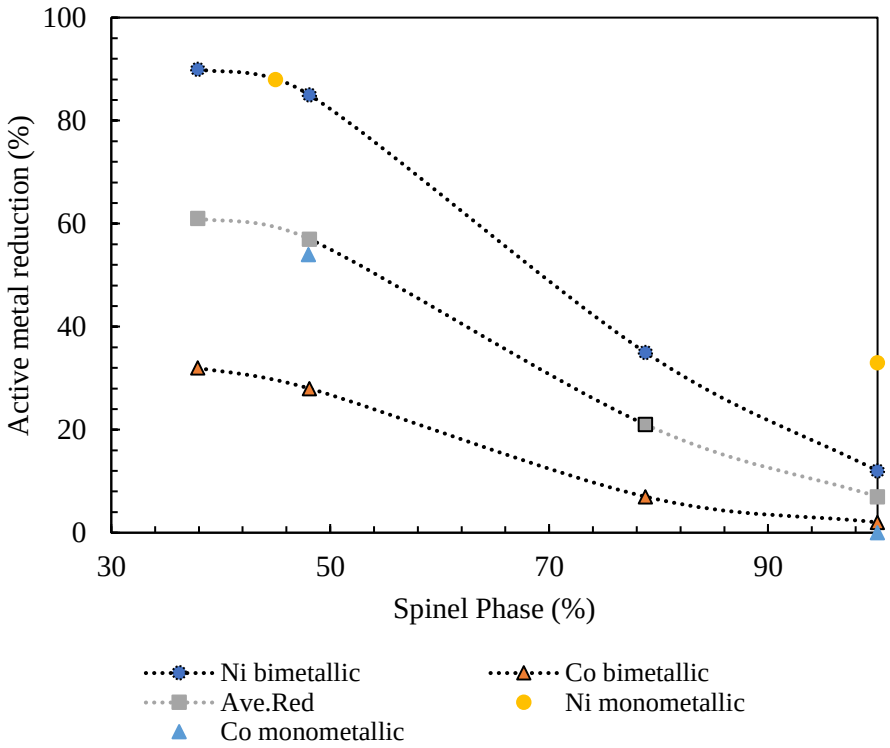

Figure 4.25. Correlation between metal reduction and spinel phase in the catalysts

Assuming Ni and Co were distributed equally in both phases (MgO and spinel) or percentage distribution of the active metals in each catalyst was equal to the percentage MgO and spinel in each catalyst (i.e for CopCat-Ni4Co5-Mg-Al-2, 62 % active metal in MgO and 38 % in spinel phase), it could be observed that percentage reduction of Co^{2+} was either less than or equal to the MgO phase, while the extent of Ni^{2+} reduction was greater than the MgO phase. This show that Co^{2+} reduction could be solely from the MgO-solid phase, while Ni^{2+} reduction was from both MgO-solid and spinel phase. This was substantiated by the reduction results of both Ni (33 %) and Co (0 %) in the Al supported monometallic catalysts. Thus, why Ni reduced more than Co could be related to the nature of oxides or how they interact with the support.

4.2.3 Catalyst structure, site preference and metal reducibility

From the textural and bulk characterization results, the catalysts can be classified into two groups. The first group has sufficient MgO (Mg/Al >1), while the other group has less or no MgO (0 <Mg/Al <1). Catalysts in each group showed similar properties (textural and bulk), except for some additional features caused by the presence of Co in the bimetallic catalysts. The presence of Mg and Co increased the mesoporous property and facilitated the formation of more uniform pores, in addition to improved basicity recorded in the catalysts. A progression from spinel to spinel + MgO and finally to spinel + MgO + $NiCoO_2$ was observed in the XRD results. The spinel phase resulted from the interaction of the active metals with Al, MgO-solid was due to their interaction with Mg, while the interaction between the active metals (in the presence of sufficient MgO) could have led to the formation of $NiCoO_2$ phase. A change in type of spinel and distribution of active metal was also observed from the combined Mg and Al K-edge XANES, Al-NMR and XPS results.

Besides the textural properties and crystal structure, factors such as nature of oxides, metal-metal interaction, metal-support interaction (Wang et al., (2012); Wang and Ruckenstein, (2001)), composition and distribution of the active metals within the structure of the catalysts (Wu and Hercules, 1979) can affect the reducibility of the active metals in a catalyst system. Based on the reduction potential value, Ni^{2+} (-0.25 V) would be easily reduced compared to Co^{2+} (-0.28 V). Additionally, isolated or loosely bonded NiO was observed in the catalyst (STEM-EDX), which could contribute to more Ni^{2+} reduction compared to Co^{2+}. Also, from the structures revealed by both XRD and Mg, Al K-edge XANES, there were two major sites namely tetrahedral and octahedral available for Ni^{2+} and/or Co^{2+} to occupy. The extent of metal reduction depends on these sites placement, and while octahedral site metal ions are easily reduced, tetrahedral are not (Wu and Hercules, 1979). The site preference of the metal ions and their distribution within these sites depend on factors such as electronic configuration, size of ions, lattice energy, ligand field stabilization energy and the interaction between the ions presents (Aditya, 2011). The amount of M^{2+} in the octahedral site and M^{3+} in the tetrahedral site is a measure of the inversion parameter. The choice of Ni^{2+} and Al^{3+} for octahedral site is due to their electronic configuration ($3d^8$) and lattice energy respectively. The less preference of Co^{2+} for the octahedral site is due to its $3d^7$ configuration, while site occupancy of Mg^{2+} depends on the affinity of the other ions for a site (Aditya, 2011). Then it is likely that MgO-solid phase offered the active metal ions more octahedral occupancy, leading to more metal ion reductions that was observed in the catalysts as Mg/Al ratio increased. Thus, the reduction of more active metal ions in the higher Mg/Al spinel could be related to the increase in inversion parameter (x).

Regarding the Al-Ox supported monometallic catalysts, gamma alumina support only showed a spinel structure (defective spinel) with appreciable amount of inversion up to 0.48. Incoming Ni and Co (3.26 %) would have to go into the octahedral or tetrahedral sites, with choice

of site depending on their electronic structure and interaction with Al-Ox. With Ni^{2+} preferring the octahedral and Co^{2+} tetrahedral sites, this could explain the difference in Ni and Co reduction in the Al-Ox supported catalysts. Thus, the inversion of gamma alumina spinel was solely due to the random distribution of Al^{3+} within the sites of the spinel.

In addition to site preference, the difficulty of Co^{2+} reduction compared to Ni^{2+} in the catalyst system could also result from the stronger interaction between Co and the support (CO_2-TPD result), resulting in the formation of a more stable structure (in both MgO and spinel phase), which could be totally reduced at higher temperature greater than 1000 °C (Wang et al., 2001). To confirm this, reduction study was conducted at different temperatures in the next sub-section.

4.2.4 Effect of temperature on active metals reduction

The reduction results of Ni and Co study at different temperatures using linear combination fitting of XANES are presented in Figures 4.26 and 4.27 for Ni and Co respectively. The results showed that the reduction of the metals increased with increase in reduction temperature, and Ni showed superior reduction than Co in all the catalysts at all the reduction temperatures studied. Looking at the reduction trend in the catalysts, Ni^{2+} showed little reduction (7 %), while no Co^{2+} reduction was observed in CopCat-Ni2Co2-Mg/Al-0.3 at 600 ^oC, and increase in temperature to 800 ^oC had no significant effect on the metal reducibility. A further increase in temperature to 900 ^oC increased both Co and Ni reduction significantly to 23 % and 75 % respectively. On the other hand, CopCat-Ni4Co5-Mg/Al-2 and CopCat-Ni3Co3-Mg/Al-1.75 experienced a linear increase in metal reducibility, when temperature increased from 600 ^oC to 800 ^oC, even up to 900 ^oC for Co^{2+}. Reduction extent of Ni in these catalysts increased from around 23 % to 85 % when temperature increased from 600 to 800 ^oC.

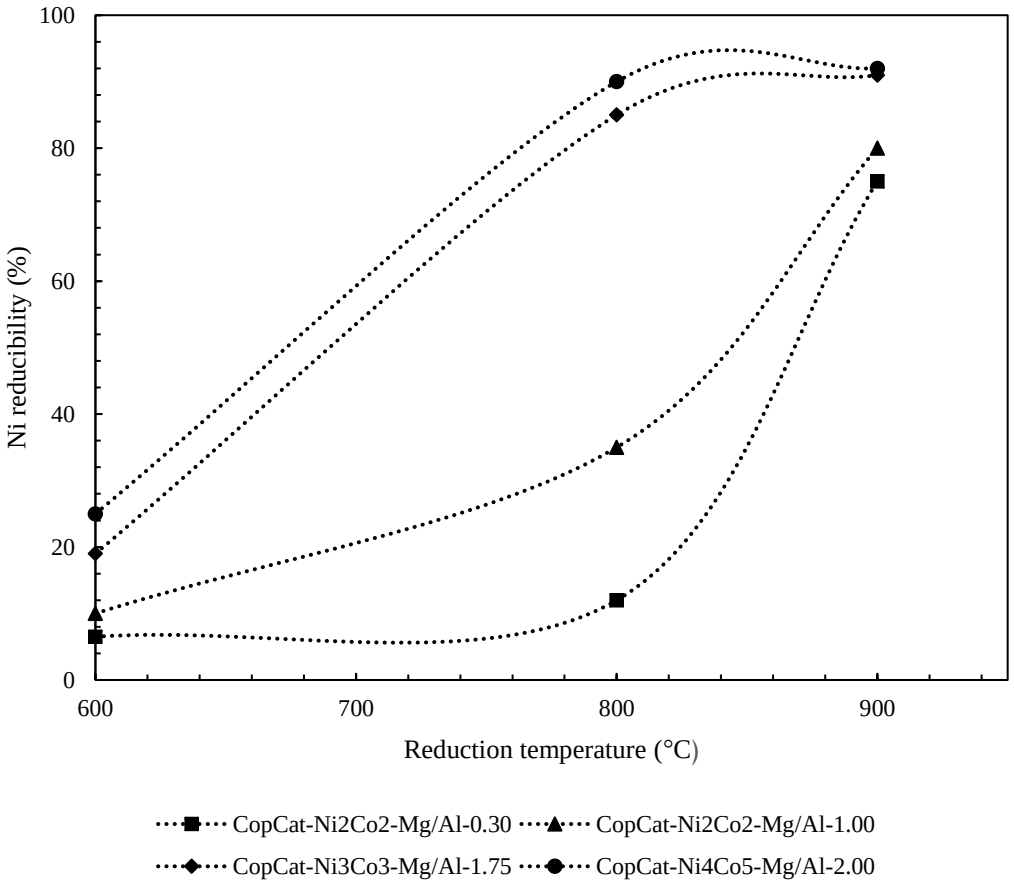

Figure 4.26. Extent of Ni reduction vs reduction temperature for bimetallic catalysts

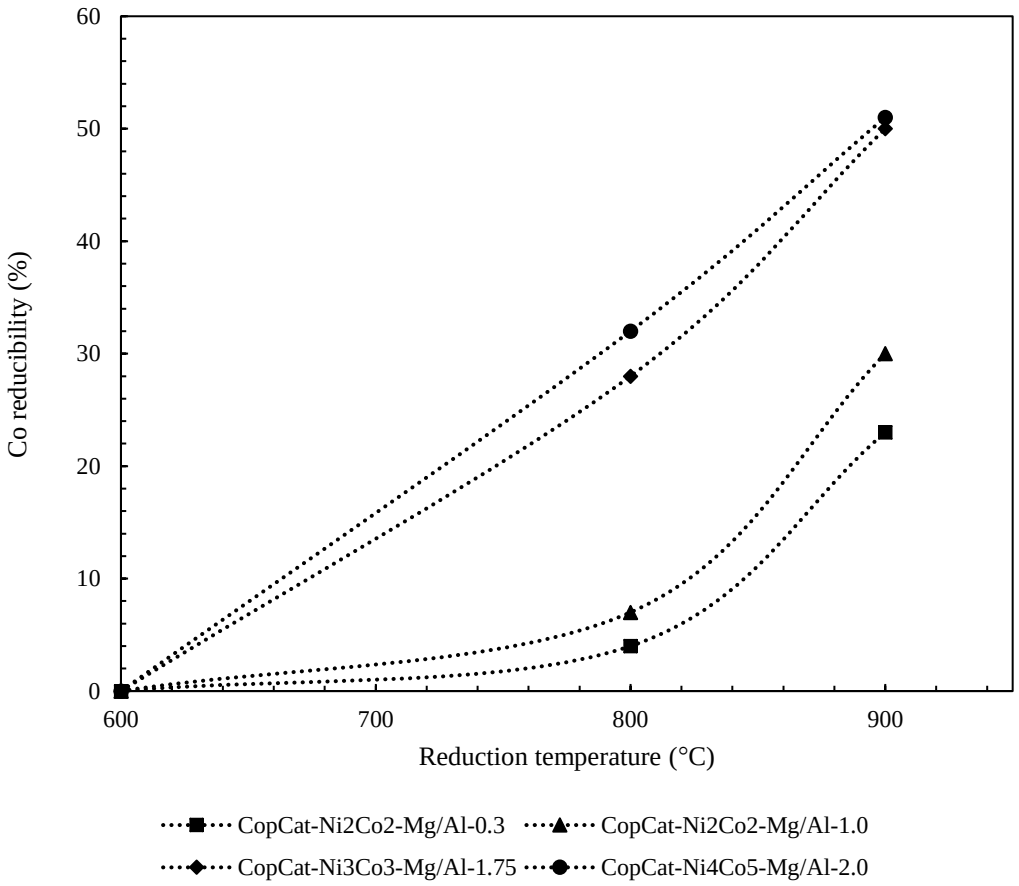

Figure 4.27. Extent of Co reduction vs reduction temperature for bimetallic catalysts

The flat-out for Ni from 800 ^{o}C to 900 ^{o}C in these catalysts could be related to absence of more accessible Ni^{2+} to be reduced in these catalysts. Co^{2+} showed a different reduction trend in these catalysts (CopCat-Ni4Co5-Mg/Al-2 and CopCat-Ni3Co3-Mg/Al-1.75). There was an average increase of 25 % percent when reduction temperature increased from 600 to 800 ^{o}C, and a subsequent increase to 50 % with further increase in temperature from 800 to 900 ^{o}C. For CopCat-Ni2Co2-Mg/Al-1.0, 7 % Co reduction was achieved when the reduction temperature increased from 600 ^{o}C to 800 ^{o}C. With further increase in temperature to 900 ^{o}C, the reduction of Co increased to 30 %. A significant 25 % Ni reduction was achieved when temperature increased from 600 ^{o}C to 800 ^{o}C, while a further increase in temperature raised Ni reduction to 80 %. These results showed that Ni and Co displayed different reduction trends, which further suggested their mechanism of reduction could be different as previously reported by Wang et al., 2012; or they were being reduced from different structures. Additionally, catalysts with similar structure displayed similar reduction features as well as reduction extent. Most of the Ni^{2+} reduction occurred between 600-800 ^{o}C, while Co^{2+} reduced mostly at around 900 ^{o}C in all the catalysts. These results showed that the difficulty of active metals reduction in CopCat-Ni2Co2-Mg/Al-0.3, could be due to the stability experienced by the metal ions in the normal spinel structure. An improved Co reduction was also seen in all the catalysts at 900 ^{o}C, which supported the claim that structure, stability and site occupancy govern the metals reduction in this study. Increase in temperature to 900 ^{o}C likely destabilized the structure of the catalysts, which could lead to the migration of the metal ions from the tetrahedral to the octahedral site, thus facilitated more reduction of metals in the lower Mg/Al ratio catalysts at 900 ^{o}C. This also explained the improved reduction in Co in the catalysts with increase in reduction temperature. Similar result was reported by Cimino et al., 1975; that increase in reduction temperature could promote more reduction of metals, due to the increased $[Ni]_{oct}/[Ni]_{tetra}$ ratio.

4.2.5 Dispersion results from CO chemisorption

Due to the endothermic nature of the reaction, sintering is one of the major problem of dry reforming catalyst. A well dispersed active metal on the right support can prevent sintering and carbon deposition (Damyanova et al., 2009). The dispersion results of the active metal(s) and CO uptake of the catalysts from the CO chemisorption experiment are shown in Tables 4.18 and 4.19 for the monometallic and bimetallic catalysts respectively. Since no Co reduction was seen in the CopCat-Co4-Mg/Al-0 catalyst, no CO-chemisorption study was conducted on this catalyst. Introduction of MgO into Al-Ox supported catalyst increased the CO uptake of monometallic Ni catalyst from 4.9 to 15.2 μmol g^{-1}, indicating the presence of more metallic sites on the Mg-Al-Ox supported catalyst. Similar trend was also observed in the bimetallic catalysts as CO uptake increased from 9.3 to 24.3 μmol g^{-1} as the Mg/Al ratio increased from 0.3 to 2. Comparison between the two groups of catalysts showed better CO adsorption in the bimetallic catalysts. This could be related to the interaction between Ni-Co, leading to stronger site performance with regards to CO adsorption. Additionally, all these results agree with the Ni and Co K-edge XANES reduction results. The presence of MgO also increased Ni dispersion from 0.9 to 1.5% in the monometallic catalysts. Similar trend was also observed in the results of the bimetallic catalysts system as increase in the Mg/Al ratio from 0.3 to 2 resulted in corresponding increase in dispersion from 1.4 to 2.0 %. Comparison between the mono and bimetallic catalysts showed that more dispersion was achieved in the bimetallic catalysts with similar support system (rich in MgO). A higher dispersion also corresponds to smaller particle size based on the relationship:

$$D \alpha 1/d_p \qquad (D = \text{dispersion and } d_p = \text{particle size}) \qquad 4.21$$

This was also verified from the TEM results. Thus, slightly better dispersion was achieved with higher Mg/Al ratio in this study.

Table 4.18. Metal dispersion results of the monometallic catalysts

Catalysts	Metal dispersion (%)	CO uptake ($\mu mol\ g^{-1}$)
CopCat-Co4-Mg/Al-0.00	-	-
CopCat-Ni3-Mg/Al-0.00	0.9	5
CopCat-Ni5-Mg/Al-1.60	1.5	15
CopCat-Co6-Mg/Al-1.55	1.3	8

Table 4.19. Metal dispersion results of the bimetallic catalysts

Catalysts	Metal dispersion (%)	CO uptake ($\mu mol\ g^{-1}$)
CopCat-Ni2Co2-Mg/Al-0.30	1.4	9
CopCat-Ni2Co2-Mg/Al-1.00	1.3	9
CopCat-Ni3Co3-Mg/Al-1.75	2.0	19
CopCat-Ni4Co5-Mg/Al-2.00	1.7	24

4.2.6 TEM results for particle size

The TEM images of the reduced catalysts are shown in Figures 4.28 and 4.29 for the mono and bimetallic catalysts respectively. For the Al-Ox supported monometallic Ni and Co catalysts, the images showed strictly rod-like crystals. Modification of the support with MgO reduced these rod- like crystals, and spot-like/ grain type crystals became dominant structure. Similar trend was also observed in the images of the bimetallic catalysts (Figure 4.29). As the Mg/Al ratio increased from 0.3 to 2, there was an obvious change from rod-like type dominated crystals to spot-like/grain like dominated. Additionally, the rod-like crystals became isolated, scattered and smaller. In combination with the XRD and XANES results of Mg and Al, the rod-like crystals were attributed to spinel, while the spot-like/grain type crystals were related to the MgO-solid phase. Also, no metal particle (black spot) was observed in the Al-Ox supported Co catalysts. This corresponds to no metal reduction in this catalyst as previously observed in the Co XANES results. Some Ni particles were seen in the Al-Ox supported Ni catalysts. Smaller and more reduced particles were observed in these catalysts with the introduction of MgO into the catalysts system. At higher Mg/Al ratio, more spot-like crystals, more reduced particles and smaller particle sizes were observed. These results agreed with the Ni and Co XANES results. The average crystallite size of catalysts was calculated from multiple images of the reduced catalysts. For the monometallic catalysts, the sizes of the crystals are in the order of CopCat-Ni5-Mg/Al-1.6 (6.7 nm) < CopCat-Co6-Mg/Al-1.55 (7.0 nm) < CopCat-Ni3-Mg/Al-0 (11.7 nm). The crystallite sizes of the bimetallic catalysts are in the order of 6.0 nm < 6.2 nm < 10.5 nm < 13.2 nm for Mg/Al ratio of 2, 1.75,1.0, and 0.3 respectively, with standard deviation of $\pm$0.2. Thus, the average crystallite sizes of the reduced metals became smaller as the Mg/Al ratio increased from 0.3 to 2.0

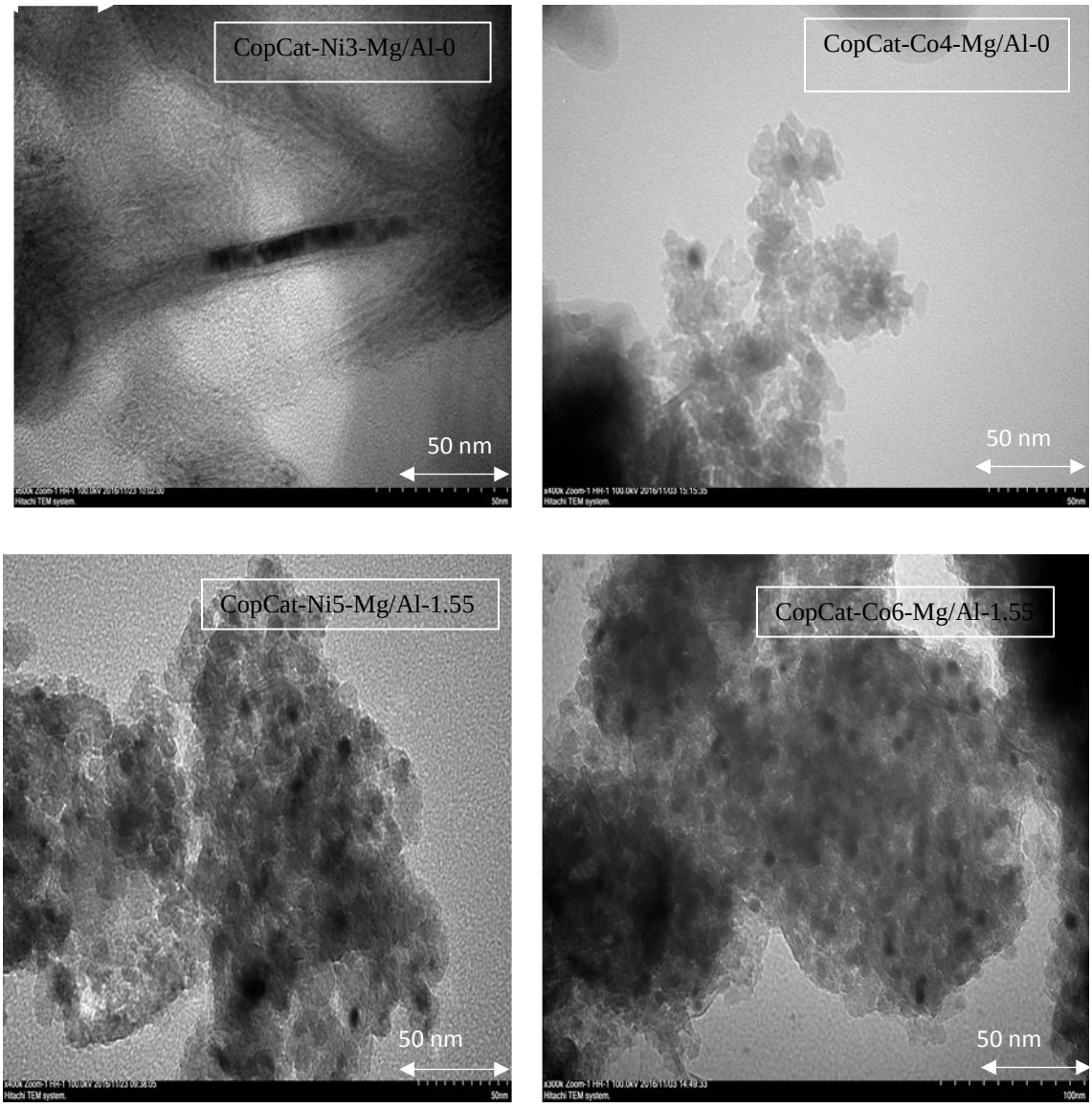

Figure 4.28.TEM images of reduced monometallic catalysts

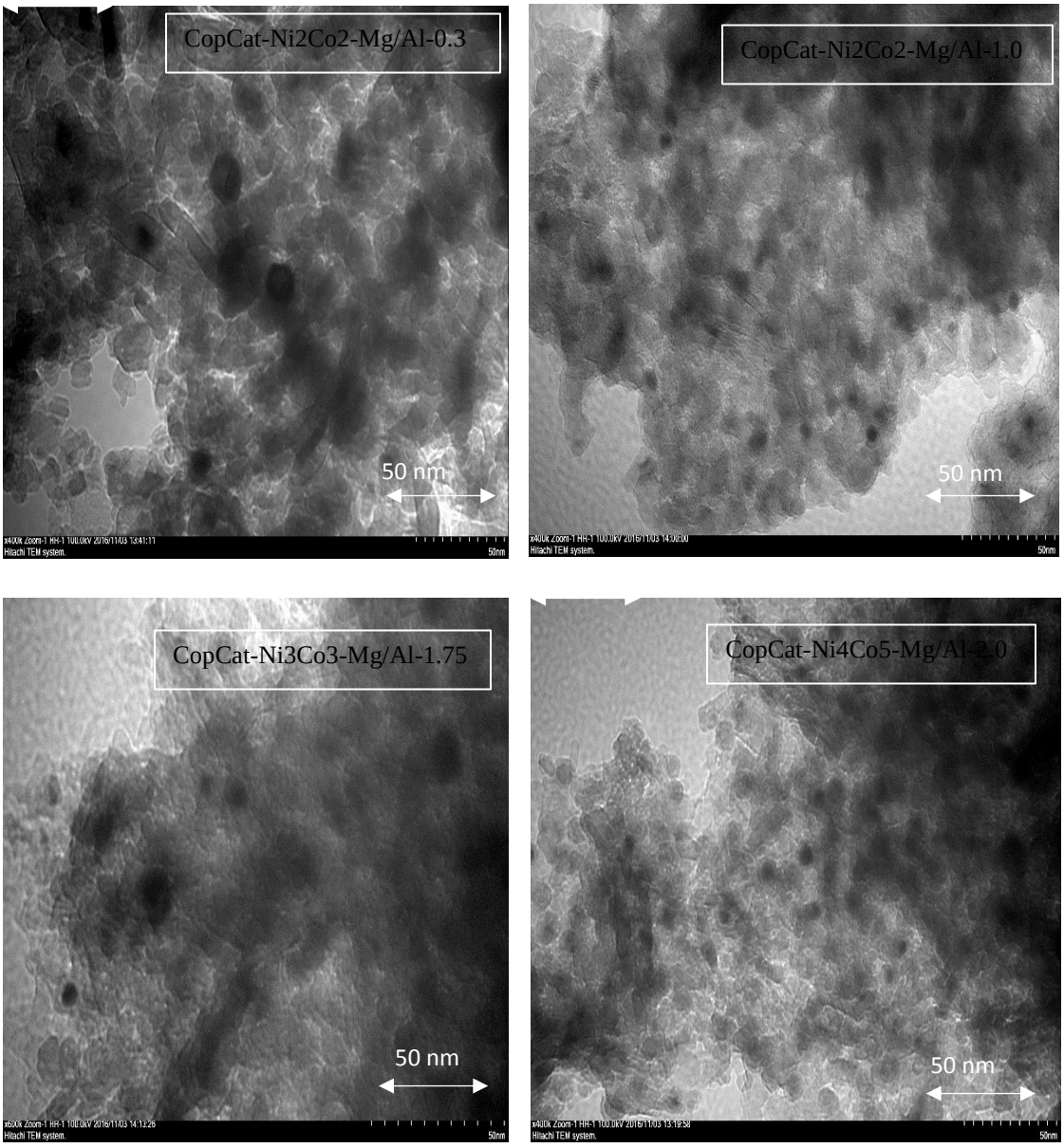

Figure 4.29.TEM images of reduced bimetallic catalysts

4.3 Conclusions

Based on the catalysts characterization results discussed so far, the following conclusions were made:

- A change in the bulk structure of the catalyst was observed, from complete spinel to (spinel + MgO-solid) and finally to spinel + MgO-solid + $NiCoO_2$ (bimetallic catalysts) as the Mg/Al ratio changed from 0 to 2.
- The relative composition of MgO and spinel phase varied with the composition of the support.
- The nature of spinel changed from majorly normal to more inverse spinel as the Mg/Al ratio changes from 0 to 2.
- More active metals were distributed in the octahedral sites as the Mg/Al ratio increased, due to spinel inversion and more MgO-solid phase.
- Ni and Co interacted differently with the support and showed different extent of reduction.
- Ni reduced on both MgO and spinel phase, while Co reduced strictly on the MgO-solid phase.

CHAPTER FIVE

CATALYTIC PERFORMANCE FOR DRY REFORMING REACTION

This chapter discusses the activity and stability of the catalysts for CO_2 reforming of CH_4. To know the major source of catalyst deactivation, characterization results of catalysts after reaction are also highlighted in this chapter.

5.1 Reactant Conversion and Product Selectivity

The performance of catalysts for DRM was measured by the rate of CO_2 and CH_4 conversion, as well as catalyst selectivity towards the desired products, CO and H_2. The reactants conversion and products selectivity were calculated using the formulas below:

$$\text{Reactant conversion (\%)} = (F_{in} - F_{out}) \times 100 / F_{in} \quad 5.1$$

$$H_2 \text{ Selectivity (\%)} = [(F_{out,\,H2,\,out} - F_{H2,\,in}) \times 100] / 2\times (F_{in,}\, c_{H4} - F_{out,\,CH4}) \quad 5.2$$

$$\text{CO Selectivity (\%)} = [(F_{out,\,CO} - F_{in,\,CO}) \times 100] / [(F_{in,}\, c_{H4,\,in} - F_{CH4,\,out}) + (F_{in,}\, c_{O2,\,in} - F_{CO2,\,out})] \quad 5.3$$

F = Volumetric flow rate

5.1.1 Rate of Conversion of CO_2 and CH_4

The activity results of the catalysts for the rate of conversion of CO_2 and CH_4 are presented in Figures 5.1 and 5.2 for the monometallic catalysts over 15 h TOS. No detectable activity was observed on the Al-Ox supported monometallic Co catalyst (CopCat-Co4-Mg/Al-0.0) for CH_4 conversion, which can be related to the absence of accessible active metal as observed in the Co XANES reduction result.

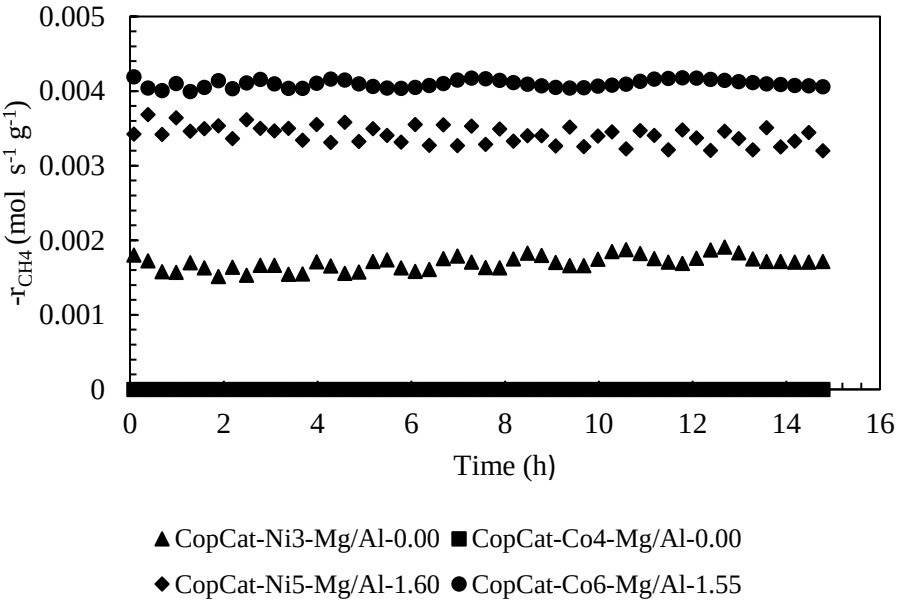

Figure 5.1. Rate of CH_4 conversion over the monometallic catalysts

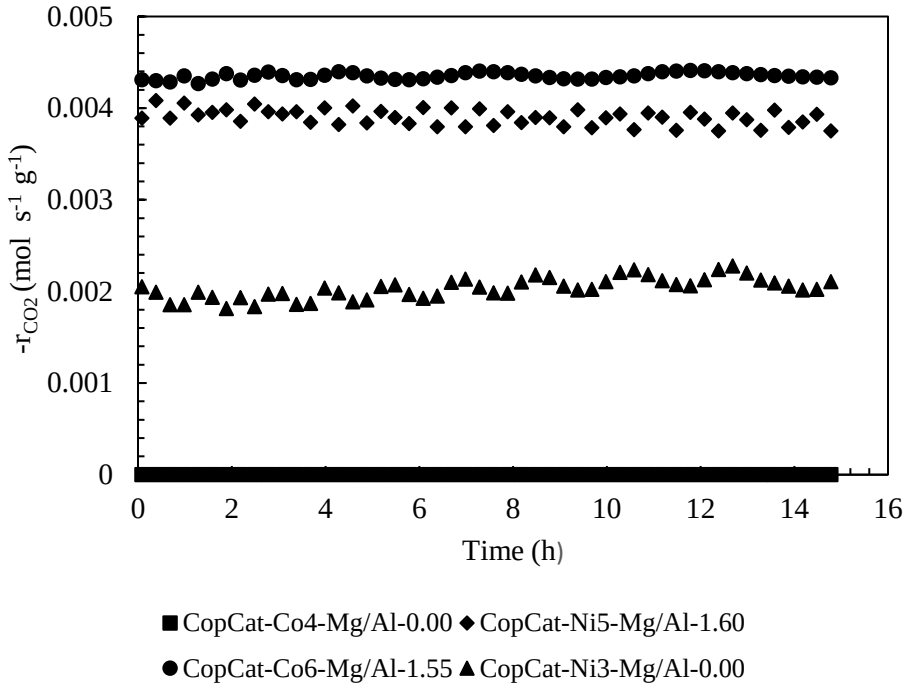

Figure 5.2. Rate of CO_2 conversion over the monometallic catalysts

While appreciable amount of activity was observed in the Al-Ox supported monometallic Ni catalyst (CopCat-Ni3-Mg/Al-0), higher activities were observed with the introduction of MgO (in CopCat-Ni5-Mg/Al-1.6 and CopCat-Co6-Mg/Al-1.55) for the same reaction, under the same reaction conditions. This could be expected based on the XANES reduction results, which showed the presence of more active Ni and Co in these catalysts. It is believed that CH_4 dissociation takes place on the active metallic site, while CO_2 conversion is initiated on the support surface (Chang et al., (2000); Verykios, (2003); Tsipouriari and Verykios, (2001)). No CO_2 conversion was detected on the Al-Ox supported Co monometallic catalyst, even though its nature of support, textural properties and basicity were the same as CopCat-Ni3-Mg/Al-0. This showed that the conversion of both CH_4 and CO_2 in DRM reaction could be synergetic. There was an obvious increase in the CO_2 conversion rate when these catalysts were modified with MgO. There was also an increase from 0 to 4.3 mmol s^{-1} g^{-1} for Co catalyst, and a corresponding increase from 2.0 to 4.0 mmol s^{-1} g^{-1} in the Ni catalysts when the support changed from Al-Ox to Mg-Al-Ox. In addition to the availability of surface metal, structure also plays an important role in the catalytic behavior of catalysts for DRM (Segner et al., (1984); Bradford and Vannice et al., (1999); Ruckenstein and Wang, (2002); Yamaguchi and Iglesia, (2010)). The presence of MgO is believed to accelerate the decomposition and dissociation of CH_4 and CO_2, which facilitates the formation of more formate ($HCOO^-$) (Son et al., 2014), that helps in the conversion of deposited carbon (from CH_4 dissociation) to CO. Presence of MgO can also transform the nature of spinel from inactive/less active $CoAl_2O_4$ and $NiAl_2O_4$ to mixed inverse spinel ($NiMgAl_2O_4$ and $CoMgAl_2O_4$), which are active for DRM reaction (Son et al., 2014). Similar trend was observed in the performance of the bimetallic catalysts for the rate of conversion of CO_2 and CH_4 as presented in Figures 5.3 and 5.4.

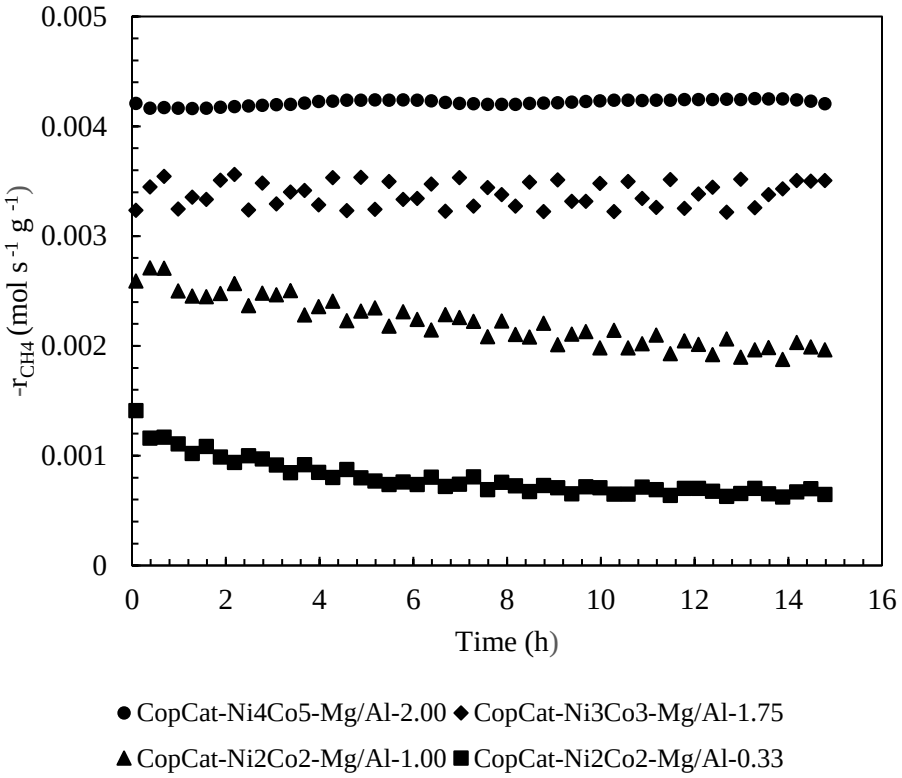

Figure 5.3. Rate of CH_4 conversion over the bimetallic catalysts

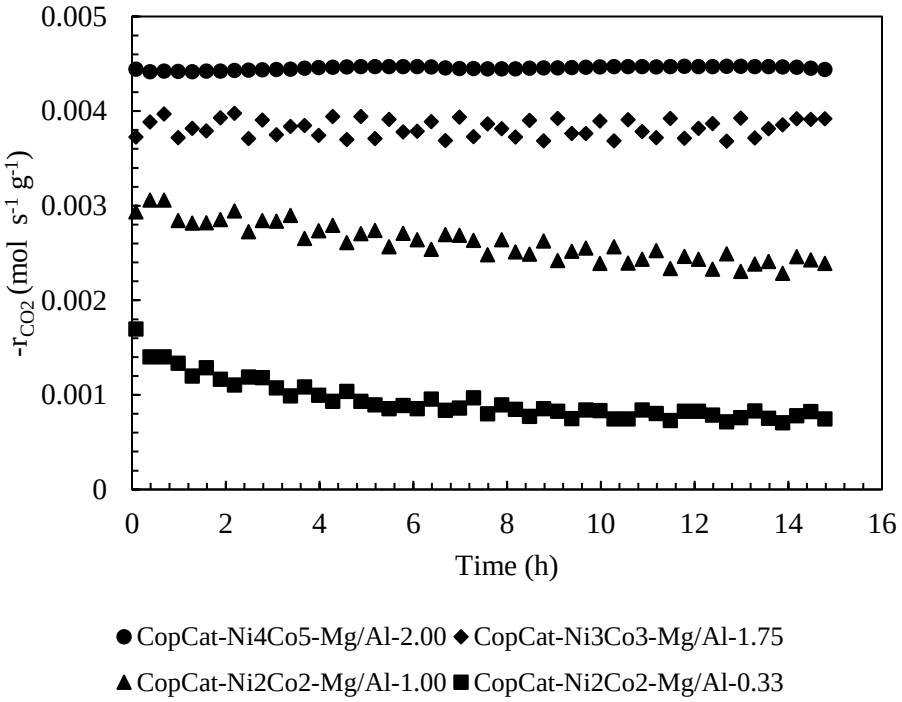

Figure 5.4. Rate of CO_2 conversion over the bimetallic catalysts

There was an increase in the initial rate of CH_4 conversion from 1.5 to 4.2 mmol s^{-1} g^{-1} as the Mg/Al ratio increased from 0.3 to 2. An increase from 1.8 to 4.5 mmol s^{-1} g^{-1} was observed in the rate of CO_2 conversion based on this ratio modification in the support of the bimetallic catalysts. While the trend in the performance of the monometallic catalysts followed the order of the basicity, the performance of the bimetallic catalysts followed the order of the extent of metal reduction and basicity. All these properties got improved solely because of the structural and compositional changes in the support. Irrespective of the group (monometallic or bimetallic), catalysts with higher Mg/Al in the support maintained good activity and stability over the entire TOS for the conversions of both CO_2 and CH_4 in the DRM reaction. Better performance of the higher Mg/Al ratio catalysts can be attributed to the availability of sufficient active sites that can accelerate the activation of CH_4, and enough basic sites that can hasten the activation of CO_2, which subsequently helped in the conversion of deposited carbon to CO.

5.1.2 Selectivity of H_2 and CO for DRM over the catalysts

The selectivity of catalysts towards the desired product for this reaction was measured by the H_2/CO ratio. The results of the H_2/CO ratio obtained for the catalysts used in this study are presented in Figures 5.5 and 5.6 for the monometallic and bimetallic catalysts respectively. There was difference in this ratio for the two groups of catalysts, and the observable trend was not different from the performance results in each group of catalysts. For the monometallic catalysts, no product selectivity was recorded for the Al-Ox supported monometallic Co catalyst (CopCat-Co4-Mg/Al-0), since there was no CH_4 and CO_2 conversion observed in this catalyst. An initial value of 0.85 was recorded for the CopCat-Ni3-Mg/Al-0, 0.93 for CopCat-Ni-Mg/Al-1.60 and 0.98 for CopCat-Co5-Mg/Al-1.55.

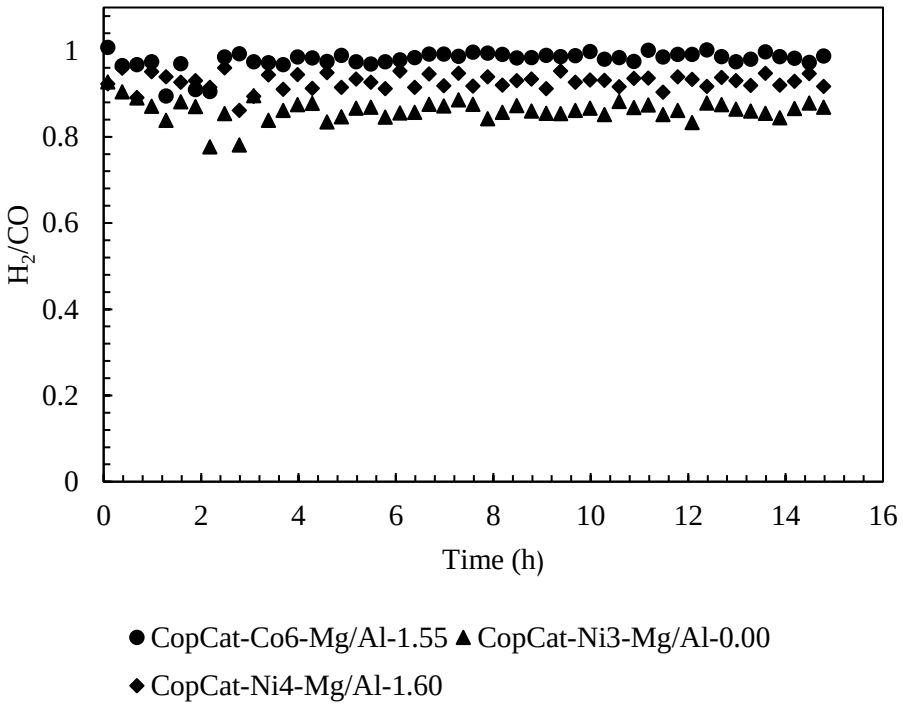

Figure 5.5. H_2/CO for the monometallic catalysts

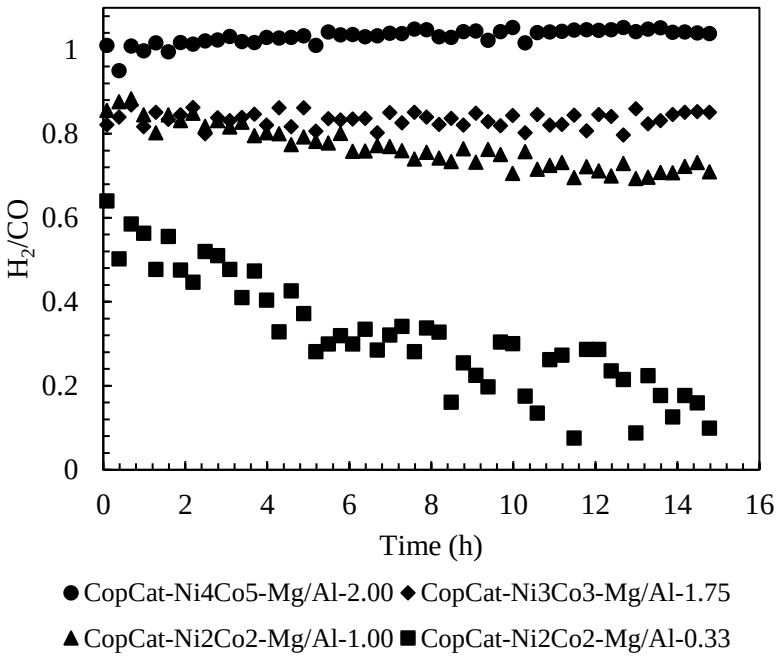

Figure 5.6. H_2/CO for the bimetallic catalysts

Similar trend was also observed in the results of H_2/CO ratio for the bimetallic catalysts as the H_2/CO increased from 0.64 to approximately 1 as the Mg/Al ratio increased from 0.3 to 2.0; like the observed trend in the activity results of the catalysts. CopCat-Ni4Co5-Mg/Al-2.0 and CopCat-Ni3Co3-Mg/Al-1.75 catalysts retained their H_2/CO ratio value of close to 1, while the ratio for CopCat-Ni2Co2-Mg/Al-1.0 and CopCat-Ni2Co2-Mg/Al-0.3 decreased over the TOS. Specifically, CopCat-Ni2Co2-Mg/Al-1.0 showed a decrease from 0.85 to 0.71, while CopCat-Ni2Co2-Mg/Al-0.3 experienced a significant decrease from 0.64 to 0.10 over the TOS. Decrease in product selectivity could be related to reduction in reactant conversion, resulting from catalyst deactivation. For most of the catalysts, the H_2/CO ratio was less than the stoichiometry value of 1, based on the reaction equation, which could be related to the presence of some side reactions competing with DRM reaction, to a different extent in the catalysts. For instance, reverse water gas shift (RWGS) is a prominent side reaction associated with DRM reaction and its degree of severance is measured by the H_2/CO ratio, as well as comparison between CO_2 and CH_4 conversions. Higher CO_2 conversion compared to CH_4, and H_2/CO ratio lower than 1 are indications of RWGS (Shi and Zhang, 2015). Other possible side reactions as stated from previous work by Zhang et al., (2008); Edwards and Maitra, (1995); include

$$CO_2 + H_2 \rightleftharpoons H_2O + CO \quad \text{(RWGS)} \qquad 5.4$$

$$CH_4 \rightleftharpoons C + 2H_2 \qquad 5.5$$

$$2CO \rightleftharpoons CO_2 + C \qquad 5.6$$

$$CO + H_2 \rightleftharpoons H_2O + C \qquad 5.7$$

Additionally, the degree of fluctuation in the reactants conversion and products selectivity plots was different for all the catalysts, an indication of the occurrence of side reactions to a different extent in the catalysts (Shi and Zhang, 2015), or periodic deposition and removal of carbon on and from the surface of the catalysts. (Wei, 2003). Thus, significant changes were observed in the

reactants conversion, products selectivity and stability of catalysts as the Mg/Al ratio changed in both the monometallic and bimetallic catalysts.

5.2 Turnover Frequency (TOF)

To differentiate the bulk performance of the catalysts from the site activity, TOF was calculated (based on site generated during reduction and CO uptake) for the catalysts using equations 5.8 and 5.9.

$$TOF_1\ (mol\ mol_{metal}^{-1}\ min^{-1}) = \frac{X\ \times\ n_{methane}^{inlet}}{(k\ L_{Ni} + y\ L_{Co}) \times W_{catalyst}} \qquad 5.8$$

$$TOF_2\ (site\ site^{-1}\ \ min^{-1}) = \frac{X\ \times\ n_{methane}^{inlet}}{(\ U_{CO}) \times W_{catalyst}} \qquad 5.9$$

where X is the conversion of reactant; n is the flow rate of methane (mol min^{-1}); L is the loading of the active metal(s) (mol g^{-1}); U_{CO} is the CO uptake (mol g^{-1}); $W_{catalyst}$ is the weight of catalyst; h = extent of Ni of reducibility (%); y is the extent of Co reducibility (%),

TOF also offers the opportunity of comparing the activity of sites generated by the catalysts (after reduction) for DRM. From the TOF results of the catalysts presented in Tables 5.1 and 5.2 for both groups of catalysts, two main trends were observed:

1) The TOF results followed an opposite trend to the extent of metal reduction, rate of CH_4 conversion, metal dispersion, as well as the Mg/Al ratio in the catalysts.

2) Higher Mg/Al ratio catalysts showed stable TOF value, while a significant decrease was observed in the lower Mg/Al ratio catalysts.

The observed trends in TOF with respect to the properties of the catalysts could be related to either one or more of these factors namely; redundancy of some during reaction, bigger size of site and low dispersion per reduced metal, or smaller particle size at higher reduction.

Table 5.1. Relationship between the CH_4 conversion rate and TOF for monometallic catalysts

Catalysts	Initial rate (mmol s^{-1} g^{-1})	Final rate (mmol s^{-1} g^{-1})	Initial TOF_1 (mol min^{-1} mol_{met}^{-1})	Final TOF_1 (mol min^{-1} mol_{met}^{-1})	Initial TOF_2 (site $site^{-1}$ min^{-1})	Final TOF_2 (site $site^{-1}$ min^{-1})
CopCat-Ni3-Mg/Al-0.00	1.9	1.2	571	491	21661	18653
CopCat-Co4-Mg/Al-0.00	0.0	0.0	0	0	0	0
CopCat-Ni4-Mg/Al-1.60	3.4	3.4	228	228	13683	13683
CopCat-Co6-Mg/Al-1.55	4.2	4.2	379	379	30507	30507

Table 5.2. Relationship between CH_4 conversion rate and TOF for bimetallic catalysts

Catalysts	Initial rate (mmol s^{-1} g^{-1})	Final rate (mmol s^{-1} g^{-1})	Initial TOF_1 (mol min^{-1} mol_{met}^{-1})	Final TOF_1 (mol min^{-1} mol_{met}^{-1})	Initial TOF_2 (site $site^{-1}$ min^{-1})	Final TOF_2 (site $site^{-1}$ min^{-1})
CopCat-Ni2Co2-Mg/Al-0.33	1.2	0.7	267	267	10301	10301
CopCat-Ni2Co2-Mg/Al-1.00	2.9	2.0	414	414	11222	11222
CopCat-Ni3Co3-Mg/Al-1.75	3.2	3.2	1139	851	17845	13333
CopCat-Ni4Co5-Mg/Al-2.00	4.3	4.3	1930	865	9288	4164

Low TOF at higher reduction could be related to redundancy of some sites during CO uptake, as well as during DRM reaction. Since adsorption of CO does not always happen on all site and there is also the tendency of not having all the metallic sites on the surface of catalysts during the reaction, the lower values observed at higher active metal reduction could be related to these factors. Another factor could contribute to the observed TOF trend is the size of metallic site. Different sizes of sites might generate different TOF, but bigger sites (particle sizes) are susceptible to carbon deposition leading to catalyst deactivation (Tang et al., (2000); Kim et al.; (2000)), as observed in the lower Mg/Al ratio catalysts. With the assumptions that reduced metals were on the surface and took part in the reaction, and equal metallic sites generated during reduction, another factor that could contribute to the TOF trend is the dispersion per reduced metal. A summary of the rate of CH_4 conversion and dispersion per reduced metal are shown in Tables 5.3 and 5.4. The results showed that based on the value of dispersion per reduced metal, the lower Mg/Al ratio catalysts displayed higher dispersion compared to the higher Mg/Al ratios in both group of catalysts. The nature of site generated by the catalysts could also be a factor. Some catalysts generated majorly Ni site, or Co site, while some generated both. These sites could interact differently with the reactants during DRM, as observed in the difference in TOF of the monometallic and bimetallic catalysts. Decrease in TOF of some catalysts over the TOS could be attributed to site deactivation, as similar observation was observed in the bulk activity and stability of the same catalysts during DRM. Stability of the other catalysts could be related to availability of sufficient basicity in the support, which can convert deposited carbon to CO during DRM reaction (Xu et al., (2011); Zhu et al., (2011)).

Table 5.3. Dispersion per reduced metal results for monometallic catalysts

Catalysts	Average reduced metal (%)	Dispersion (%)	Dispersion/Average reduced metal ($\times 10^{-2}$)
CopCat-Ni3-Mg/Al-0.00	33	0.9	2.6
CopCat-Co4-Mg/Al-0.00	0	0	-
CopCat-Ni4-Mg/Al-1.60	88	1.5	1.7
CopCat-Co6-Mg/Al-1.55	54	1.3	2.4

Table 5.4. Dispersion per reduced metal results for bimetallic catalysts

Catalysts	Average reduced metal (%)	Dispersion (%)	Dispersion/Average. reduced metal ($\times 10^{-2}$)
CopCat-Ni2Co2-Mg/Al-0.30	7	1.6	20.1
CopCat-Ni2Co2-Mg/Al-1.00	21	2.0	6.3
CopCat-Ni3Co3-Mg/Al-1.75	57	1.3	3.5
CopCat-Ni4Co5-Mg/Al-2.00	61	1.4	2.6

.

5.3 Catalysts Characterization after Reaction

The catalysts were subjected to further characterization after reaction to determine the major source of deactivation.

5.3.1 XRD of used catalysts

The XRD results of the used catalysts are presented in Figures 5.7 and 5.8. Compared to the XRD of the reduced catalysts, no observable difference was seen in the XRD results of catalysts with higher Mg/Al ratio for both monometallic and bimetallic catalysts, which could be an indication that no prominent change occurred in the structure of these catalysts over the reaction TOS. A broad peak was observed between 20^o and 30^o 2θ angle for catalysts with lower Mg/Al ratio (CopCat-Ni3-Mg/Al-0, CopCat-Ni2Co2-Mg/Al-0.3 and CopCat-Ni2Co2-Mg/Al-1.0) over the reaction TOS. Also, peak related to the active metal at $2\theta = 52^o$ became bigger in size for these catalysts in the following order; CopCat-Ni2Co2-Mg/Al-0.3 (17 nm) > CopCat-Ni2Co2-Mg/Al-1.0 (13nm) > CopCat-Ni3-Mg/Al-0 (12.5nm). Such increase in crystallite size suggestively indicated sintering of active metal (Shi and Zhang, 2015). The broad peak between 20^o and 30^o was associated with graphitic carbon (JCPDS 89-849). Thus, sintering and carbon deposition were identified as the cause of gradual deactivation in both group of catalysts, with non-stable activity over the TOS. The stability (resistance to deactivation) of the other catalysts could be attributed to synergetic effect of factors such as small particle size, good dispersion, good metal support interaction and basicity, all of which resulted from the structural and compositional changes in the catalysts support.

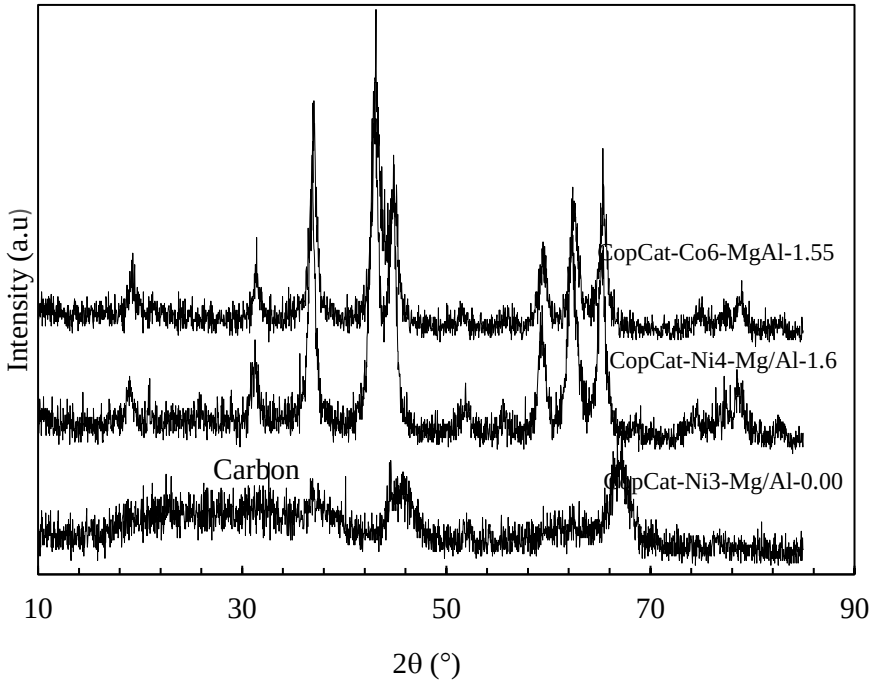

Figure 5.7. XRD of used monometallic catalysts

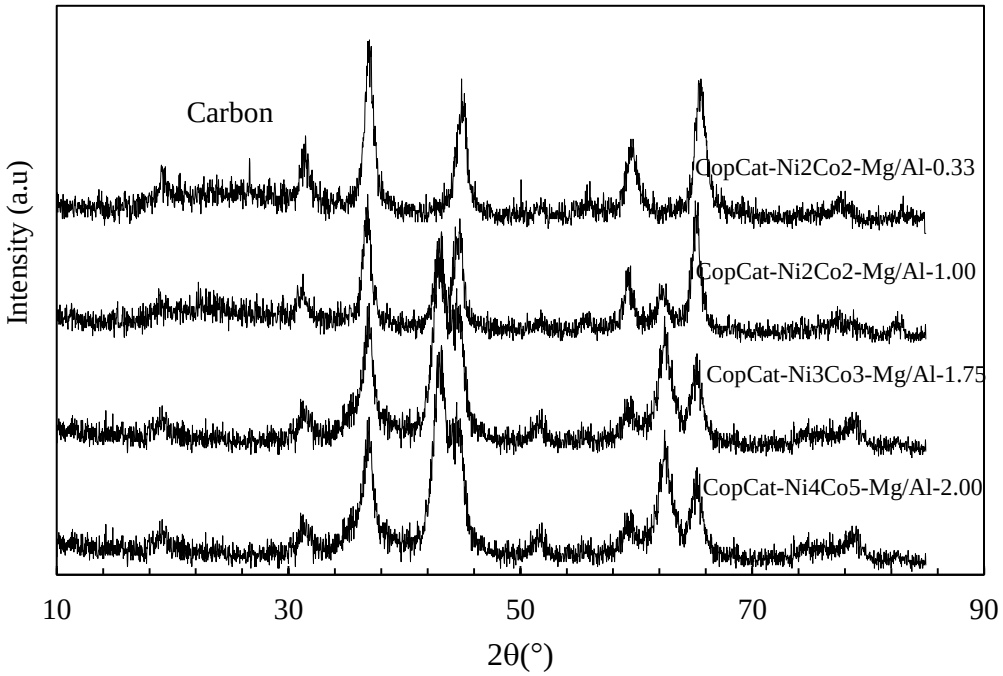

Figure 5.8. XRD of used bimetallic catalysts

5.3.2 Temperature programmed oxidation (TPO) of used catalyst

To establish the nature of deposited carbon on the catalysts, TPO was also carried out on the used catalysts. The obtained results are shown in Figures 5.9 and 5.10 for the monometallic and bimetallic catalysts respectively. No carbon oxidation peak was observed in the Mg rich catalysts (CopCat-Ni4-Mg/Al-1.60, CopCat-Co6-Mg/Al-1.55, CopCat-Ni3Co3-Mg/Al-1.75 and CopCat-Ni4Co5-Mg/Al-2.00), an indication that there was no significant carbon deposition to be detected on these catalysts. For other catalysts, their TPO profiles showed different oxidation peaks, related to different types of carbonaceous species deposited on the catalysts. A minor peak at around 390 ^{o}C, a broad peak at 500 ^{o}C and a major peak at 680 ^{o}C were found in the TPO of used CopCat-Ni3-Mg/Al-0. CopCat-Ni2Co2-Mg/Al-1.0 showed two peaks; a major peak at around 280 ^{o}C and a minor peak at 700 ^{o}C. CopCat-Ni2Co2-Mg/Al-0.3 showed a broad unresolved peak between 200 ^{o}C- 380 ^{o}C and two distinctive peaks at 500 ^{o}C and 700 ^{o}C. Low temperature peaks between 180 ^{o}C and 250 ^{o}C could be ascribed to active carbon specie or reaction intermediates that could be easily oxidized. Peaks between temperature ranges 350 ^{o}C - 400 ^{o}C could be attributed to amorphous and/or graphitic carbon, while higher temperature peaks could be for filamentous carbon deposition (Juan-Juan et al., 2009). The major form of carbon deposition on CopCat-Ni2Co2-Mg/Al-1.0 was active carbon species, whereas all types of carbon deposition could be seen on CopCat-Ni2Co2-Mg/Al-0.3. Overall, based on the area integration of peaks, the amount of carbon deposition on used CopCat-Ni2Co2-Mg/Al-0.3 was greater than CopCat-Ni2Co2-Mg/Al-1. This result support the good performance and XRD result of the used catalysts. Low dispersion could be responsible for sintering, while inadequate basicity could cause carbon deposition.

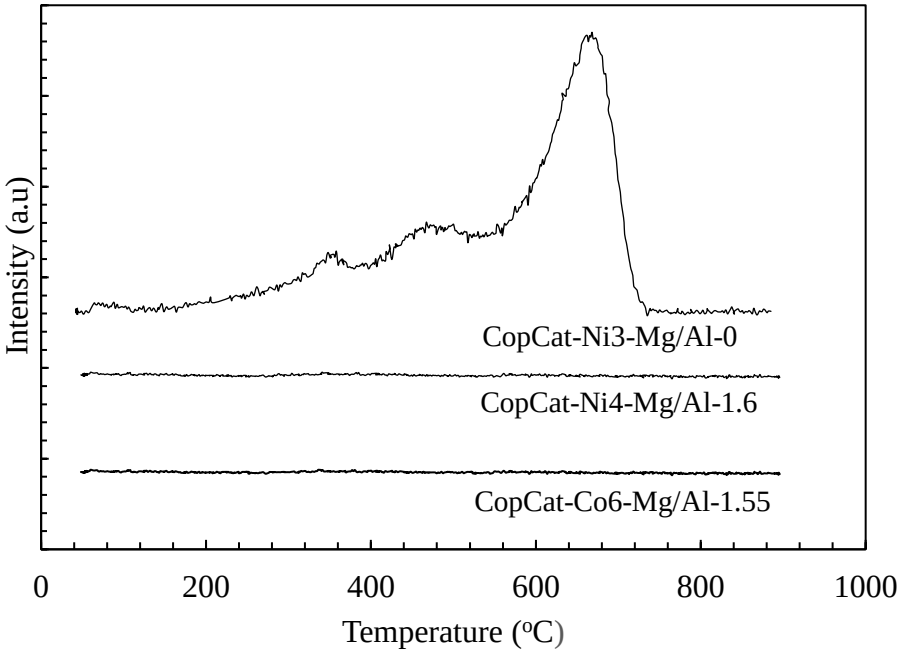

Figure 5.9. TPO of used monometallic catalysts

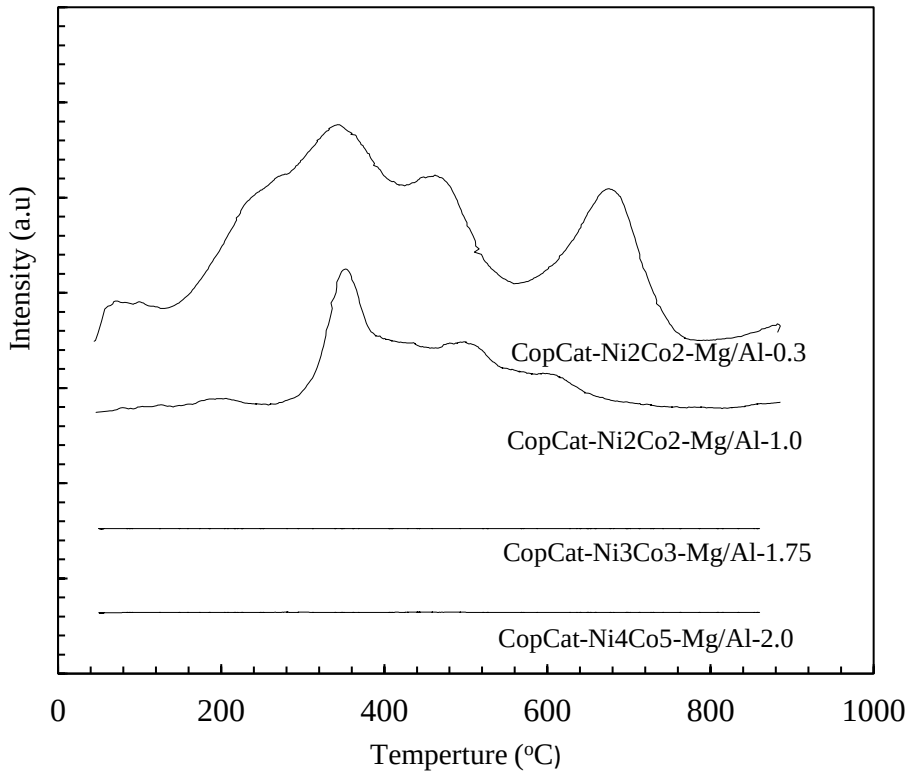

Figure 5.10. TPO of used bimetallic catalysts

5.4 Conclusions

From the results discussed in this chapter, the following conclusions were made:

- Increase in Mg/Al ratio made better and stable catalysts due to easy metal reduction and sufficient basicity that can convert deposited C to CO.
- Ni and Co interacted with Al-ox differently, which resulted in the different catalytic performance shown by the two catalysts.
- While bulk performance improved with Mg/Al ratio in the catalysts, the site activity decreased possibly due to low dispersion per reduced metal.
- Co showed good activity and stability in the presence MgO due to the nature of interaction and the presence of sufficient basicity.
- Structural changes due variation of Mg/Al ratio resulted in different catalytic properties and performance.
- Carbon deposition is the major cause of catalysts deactivation in the lower Mg/Al ratio catalysts.

CHAPTER SIX

CO_2 REFORMING OF CH_4 USING COAL GAS AND IDEAL FEED

The results of dry reforming reaction using coal and ideal feed gas are discussed in this chapter. A brief thermodynamic analysis and calculation of rate parameter using previously established model are discussed here in. Effect of the type of reactant feed on carbon deposition (on the catalyst) are also analyzed in this chapter.

This chapter has been published in Catalysis Today as "A Study of CO_2 Reforming of CH_4 for Ideal and Coal Delivered Gases over Ni-Based Catalysts". Prof. Wang reviewed the paper before submission.

6.1 Introduction and Motivation of Study

The contribution of China in the international energy market has been a huge success. This is even more evident in the last decades because of the set industrial structure and government's new developmental policy in favor of western China that is rich in coal, oil and other natural resources (Wei, 2003). As much as coal is considered as the cheapest and readily available energy source, its massive utilization is related to the increasing environmental concern due to air pollution and CO_2 emission (Minchener, 2005). In response to environmental demands, cleaner and more efficient coal conversion technologies are being developed in the province of Shanxi. Coal gasification and pyrolysis have emerged as clean and effective ways of producing gaseous fuel or as a synthesis liquid fuel precursor. Since coal gasification and pyrolysis process could yield up to almost equal amount of CO_2 and CH_4 in their exit gas, upgrade of these gaseous products was proposed. This involves the effective conversion of these products (CH_4 and CO_2) to useful fuel (syngas), and the chemistry is known as DRM.

The use of fossil fuels as the major sources of energy to produce syn-gas (H_2 and CO) is the first step synthesis of many chemicals. Steam reforming of CH_4 and coal gasification are the two commonly used methods to produce syngas, which form the backbone of the modern chemical industries (Wu et al., 2005). Also, different H_2/CO ratios in syngas is required for the downstream synthesis of different chemicals. This ratio is usually dictated by the H/C ratio of the primary feedstock and the reaction routes of the syngas production.

In recent years, much attention has been given to CO_2 reforming of CH_4, because it has the potential advantages of lower theoretical H_2/CO ratios and reuse of CO_2 (Wu et al., 2005). The incorporation of dry reforming in to the coal process is a good development, but getting the right catalyst has been a major problem in the industrialization of the process. A critical difficulty of this process is its greater potential for carbon deposition, which rapidly deactivates the catalyst (Armor, (1999); Qin et al, (1994); Xu et al., (1999); Tang, (1995)).

Following the successful synthesis and extensive study of Ni based catalyst with good activity, product selectivity and resistance to carbon deposition for DRM using pure feed (Zhang et al., (2006; 2007; 2008) and Wang et al., (2012)), there is need to extend our study to industrially feasible feed and condition, to test the strength and the properties that make the catalyst better. Due to the endothermic nature of the reaction, high temperature is believed to facilitate sintering and carbon deposition from higher CH_4 decomposition (Khoshtinat and Amin, (2011); Tan et al., (2014)). Industrially feasible feed like coal gas consists of more carbon atoms and other gases that could facilitate other side reactions which could affect catalyst performance and stability for DRM (Khoshtinat and Amin, (2011); Tan et al., (2014)). Thus, the focus of this chapter is as stated above. *Note: The coal gas feed was a simulated coal gas feed based on the average composition of coal gas in Taiyuan*

6.2 Experimental

Experiment was conducted using both mono Ni and bimetallic (Ni and Co) composite catalysts with different Mg/Al ratio in the support. The catalysts used in this study are CopCat-Ni3-Mg/Al-0.00, CopCat-Ni4-Mg/Al-1.60, CopCat-Ni2Co2-Mg/Al-0.30 and Ni3Co3-Mg/Al-1.75. The synthesis method and properties of these catalysts are as described in chapter 4. Evaluation of catalyst performance was carried out in a fixed–bed quartz reactor (Tianjin Tian Yi Technology Co. Ltd) with ID 8 mm, OD 12 mm and length 60 cm. For each experimental run, 150 mg of catalyst was mixed with 750 mg of sand. Equimolar reactant feed composition of CH_4 (99.99 %), CO_2 (99.99 %) and N_2 (99.99 %) mixture was introduced into the reactor at a pressure of 89.83 kPa, 900 ^oC and a GHSV = 1.2×10^5 mL g^{-1} h^{-1}. The coal gas feed composed of CH_4 (6.6 %), CO_2 (6.7 %), N_2 (2.6 %), CO (32.36 %), H_2 (51.34 %) and O_2 (0.4 %). Catalyst was activated by H_2 and N_2 gas mixture with a molar ratio of 1:4 at 900 ^oC for 4 h before activity test. All gases were supplied by Jining Xieli Special Gas Co. Ltd. Evaluation was carried out at 900 ^oC and the mixture of catalyst and sand was loaded at the middle of the reactor. The product gas from the CO_2 reforming of CH_4 reaction (for both coal and ideal gas) was analyzed using a gas chromatography (Haixin GC-950) on packed column (TDX-01) with Ar as carrier gas, equipped with a thermal conductivity detector after passing a cold trap.

6.3 Thermodynamics Analysis Base on Feed Effect

Based on previous study by Zhang et al., 2012; (from this group) during CO_2 reforming of CH_4, in addition to the main reaction (Equation 6.1), other possible side reactions are as listed in Equations 6.2 to 6.8.

$$CH_4 + CO_2 \rightleftharpoons 2H_2 + 2\,CO \qquad 6.1$$

$$CO_2 + H_2 \rightleftharpoons H_2O + CO \qquad 6.2$$

$$CH_4 + H_2O \rightleftharpoons 3H_2 + CO \quad (6.3)$$

$$CH_4 \rightleftharpoons 2H_2 + C \quad (6.4)$$

$$C + CO_2 \rightleftharpoons 2\,CO \quad (6.5)$$

$$C + H_2O \rightleftharpoons H_2 + CO \quad (6.6)$$

$$CH_4 + 2CO_2 \rightleftharpoons H_2 + 3\,CO + H_2O \quad (6.7)$$

$$CH_4 + 3CO_2 \rightleftharpoons 2H_2O + 4\,CO \quad (6.8)$$

$$CH_4 + 0.5O_2 \rightleftharpoons 2H_2 + CO \quad (6.9)$$

$$C + O_2 \rightleftharpoons CO_2 \quad (6.10)$$

$$C + 0.5O_2 \rightleftharpoons CO \quad (6.11)$$

With the presence of oxygen in the coal gas feed, other side reactions such as equations 6.9 to 6.11 are thermodynamically possible. The extent of occurrence of these side reactions depend on the experimental condition and nature of catalyst. Also, reactants conversion, products selectivity as well as the H_2/CO in the product stream depend on these side reactions (to some extent), as well as the nature of catalysts (Zhang et al., 2012).

6.4 Kinetics Analysis Base on Feed Effect

The performance results of the catalysts for both CO_2 and CH_4 conversion, as well as the H_2/CO ratio using ideal and the coal gas feed are presented section 6.5. Even though the experimental conditions, catalyst composition and reactor size were different, estimation of kinetic parameters and reaction rate of CopCat-Ni3Co3-Mg/Al-1.75 was done using the model developed for Ni-Co/Mg-Al-O by Zhang et al., 2009. The two models used in this study are the Power model and Langmuir -Hinshelwood model. For the Power model, the reaction rate was estimated using the formula;

$$-r_{CH4} = kP_{CH4}{}^{m}P_{CO2}{}^{n} \quad (6.12)$$

where $k = k_o\, e^{\frac{-E_a}{RT}}$ 6.13

$$k_o = \quad 0.089 \quad \text{mol}\,\frac{\text{mol}}{\text{s.g}_{cat}}\,\text{kPa}^{(m+n)} \qquad 6.14$$

$$E = 63.3\,\frac{\text{kJ}}{\text{mol}} \qquad 6.15$$

$$m = 0.483 \; and \; n = 0.291 \qquad 6.16$$

The Langmuir-Hinshelwood model is given as;

$$-r_{CH4} = \frac{aP_{CH4}P_{CO2}}{bP_{CH4}+cP_{CO2}} \qquad 6.17$$

where

$$a = a_o\, e^{\frac{-E_a}{RT}} \qquad 6.18$$

$$b = b_o\, e^{\frac{-E_a}{RT}} \qquad 6.19$$

$$c = c_o\, e^{\frac{-E_a}{RT}} \qquad 6.20$$

$$a_0 \; = \; 1.35 \text{ x } 10^{-8}\ (\text{mol}/\ (\text{g.s}))^2.\ (\text{kPa})^{-2} \qquad 6.21$$

$$E_a = \; 25.9\,\frac{\text{kJ}}{\text{mol}} \qquad 6.22$$

$$b_0 \; = \; 9.25 \text{ x } 10^{-8}(\text{mol}/\ (\text{g.s}))\ .\ (\text{kPa})^{-1} \qquad 6.23$$

$$E_b = \; -40.6\,\frac{\text{kJ}}{\text{mol}} \qquad 6.24$$

$$C_0 \; = \; 2.46 \text{ x } 10^{-7}(\text{mol}/\ (\text{g.s}))\ .\ (\text{kPa})^{-1} \qquad 6.25$$

$$E_c = \; -38.3\,\frac{\text{kJ}}{\text{mol}} \qquad 6.26$$

All these parameters were obtained from the previous work of Zhang et al., 2009. The ideal feed composition was CO_2, CH_4, and N_2 (33.33 % each). For the coal gas feed, the composition was given as CH_4 (6.6 %), CO_2 (6.7 %), N_2 (2.6 %), CO (32.36 %), H_2 (51.34 %) and O_2 (0.4 %).

Plugging these parameters into the rate equations 6.12 and 6.17 (under the reaction condition (T = 1173 K, P = 89.83 kPa) the reaction rate obtained using the two models, as well as the experimental values are shown in Table 6.1. Regardless of the differences between predicted and experimental values of reaction rate, the ratio of the rate for the coal gas feed to the ideal feed from the experiment was almost equal to the predicted value by the L-H model (1/6 vs. 1/5). This is an indication that the smaller reaction rate observed using the coal gas feed, was due to the smaller partial pressures of CO_2 and CH_4 in the coal gas feed.

Table 6.1. Experimental and predicted reaction rates for CopCat-Ni3Co3-Mg/Al-1.75

Feed	Experimental reaction rate*, mmol $g^{-1}s^{-1}$	Predicted reaction rate, mmol $g^{-1}s^{-1}$	
		L-H model	Power law model
	(10^{-1})	(10^{0})	(10^{0})
Coal gas feed	0.80	0.30	0.54
Ideal feed	4.80	1.50	1.90
Coal gas feed/Ideal feed	1/6.04	1/5.02	1/3.50

*The average reaction rate is obtained by the mean of all the data during the 24 h TOS.

6.5 Catalyst Performances for Dry Reforming

The rates of reactants conversion (CO_2 and CH_4), as well as the H_2/CO ratio using ideal and the coal gas feed over the selected catalysts are presented in Figures 6.1 - 6.6. The observed order of the catalyst activity, selectivity and stability over the TOS is given as: CopCat-Ni3Co3-Mg/Al-1.75 > CopCat-Ni5-Mg/Al-1.60 > CopCat-Ni3-Mg/Al-0.0 > CopCat-Ni2Co2-Mg/Al-0.33. This trend contrasts with the extent of metal reduction as observed in the catalysts, was in line with the trend of basicity and metal dispersion, with CopCat-Ni2Co2-Mg/Al-0.3 catalyst being the only exception. Even though MgO was present in this catalyst, it was not enough to interact with the active metals (no MgO-solid phase) or facilitate Ni-Co interaction in this catalyst. Thus, MgO did not have any significant effect on the performance of this catalyst for DRM. This also support the fact that active metal alone is not sufficient for better catalytic performance, the support also contributes in terms of basicity for the activation of CO_2. These observations agreed with the reaction mechanism suggested by the L-H model that stipulated that CH_4 dissociates on the metallic sites, while the activation of CO_2 takes place on the basic sites (Zhang et al., 2009). Bimetallic CopCat-Ni3Co3-Mg/Al-1.75 showed better stability than monometallic CopCat-Ni5-Mg/Al-1.60 due to the possibility of the formation of NiCo alloy, which can enhance the formation of smaller metallic site and resist carbon deposition (Wang et al., 2012). At higher reaction temperature, the reverse water-gas shift reaction becomes the main side reaction, as some CO_2 reacts with the produced H_2 (Zhang et al., 2012). This explains the lower H_2/CO from the coal gas feed, as well as in the performance of some of the catalysts using ideal feed, as better catalyst mitigates the occurrence of some side reactions, making the H_2/CO ratio closer to 1.

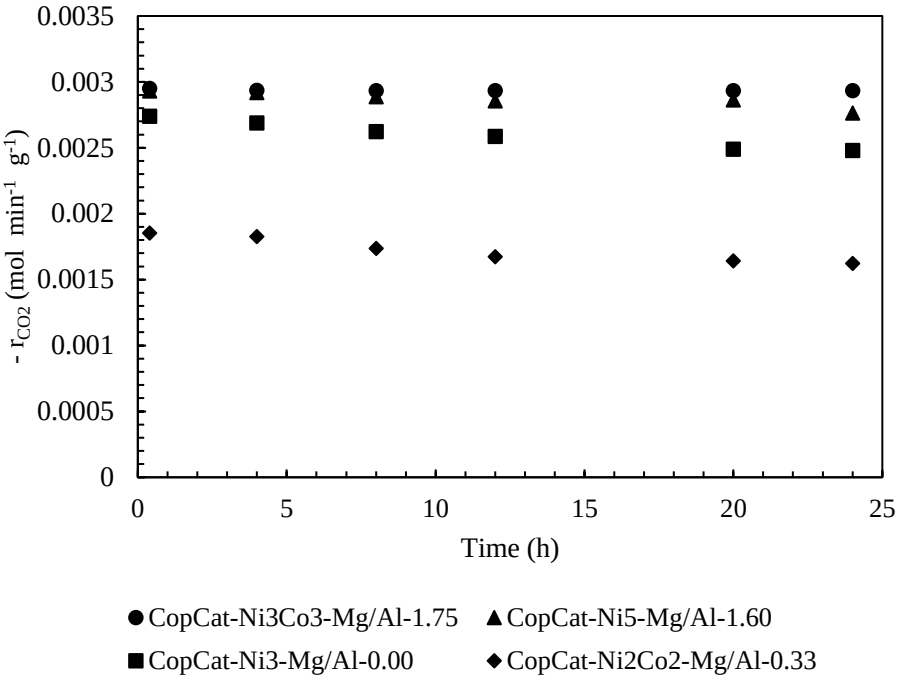

Figure 6.1. Rate of CO_2 conversion for the catalysts using pure gas feed

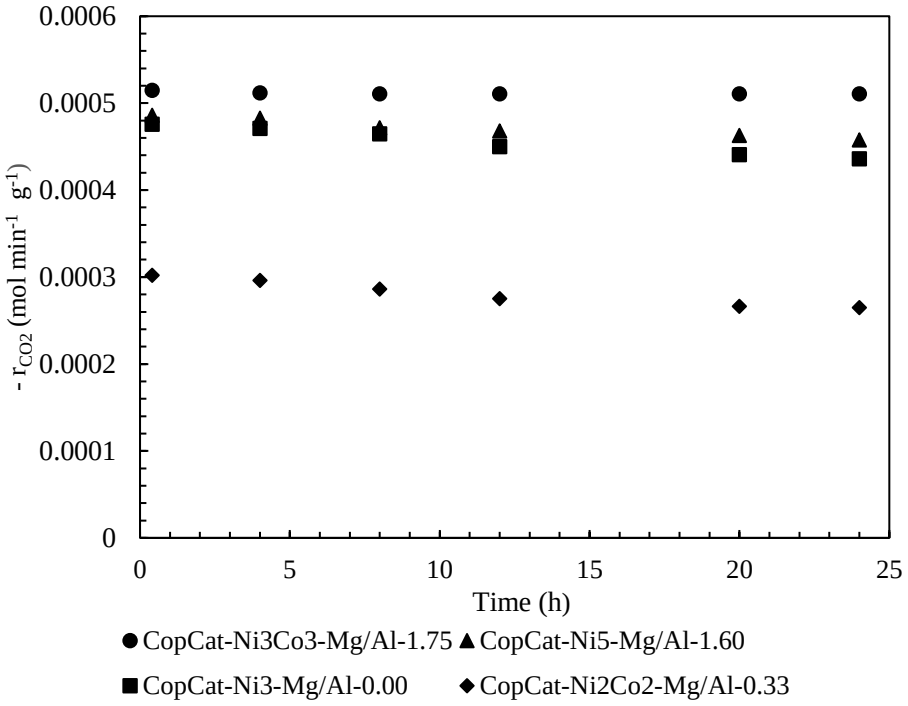

Figure 6.2. Rate of CO_2 conversion for the catalysts using coal gas feed

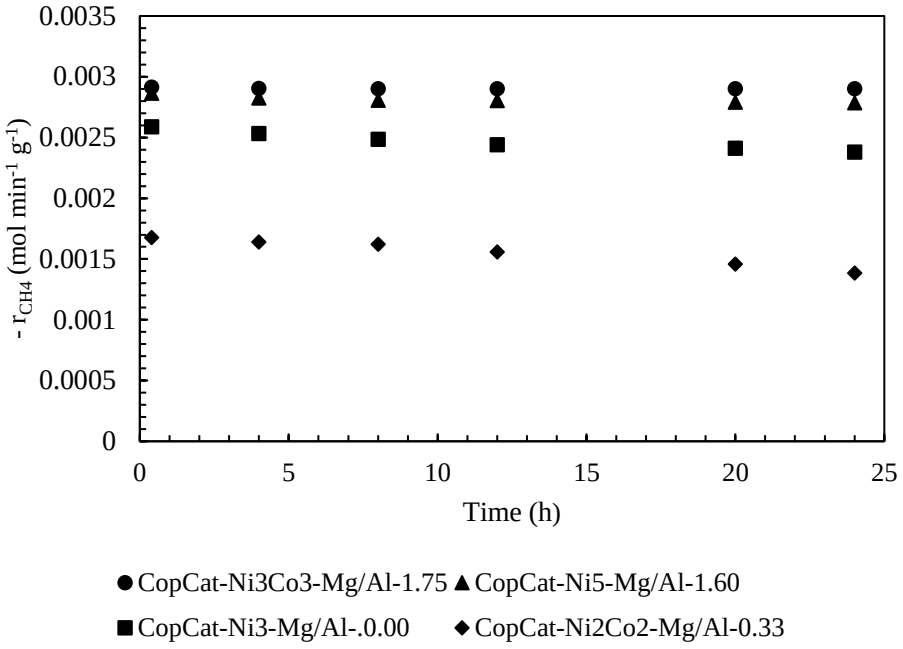

Figure 6.3. Rate of CH_4 conversion for the catalysts using pure gas feed

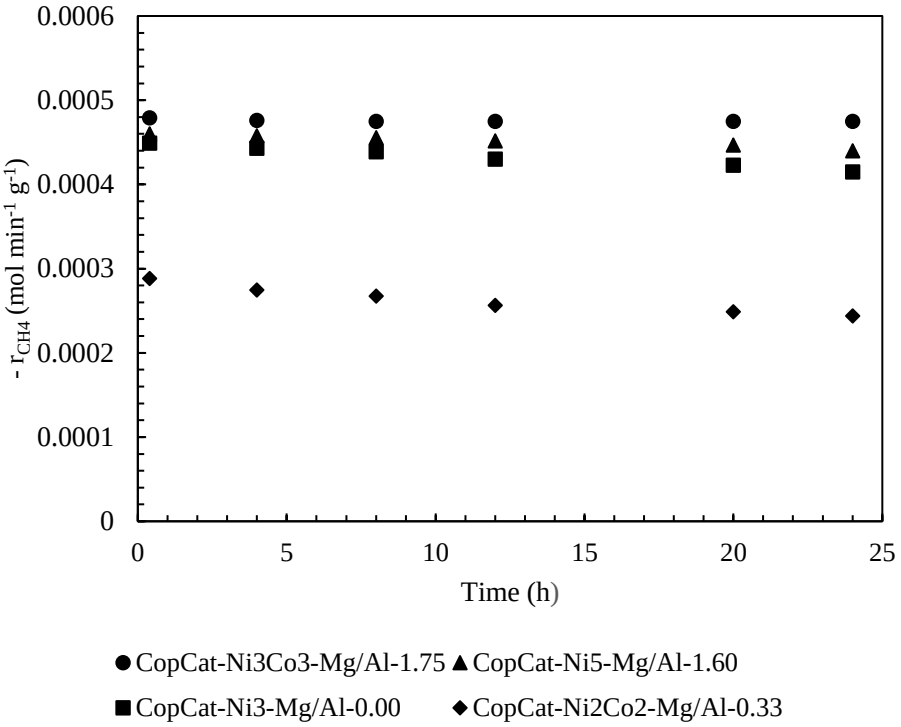

Figure 6.4. Rate of CH_4 conversion for the catalysts using coal gas feed

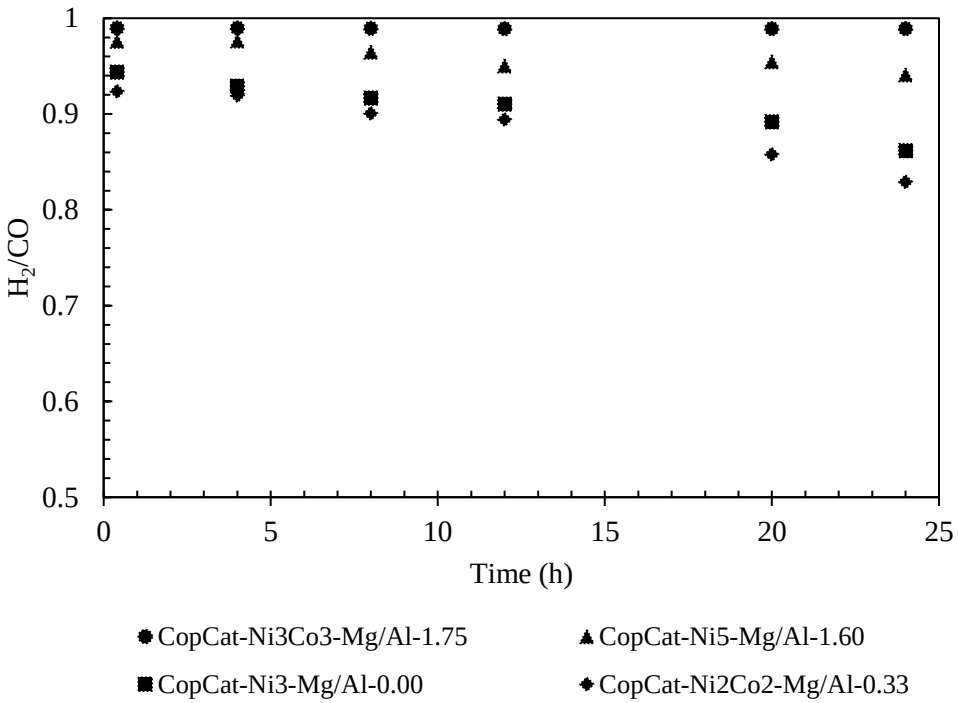

Figure 6.5. H_2/CO ratio for the ideal gas feed

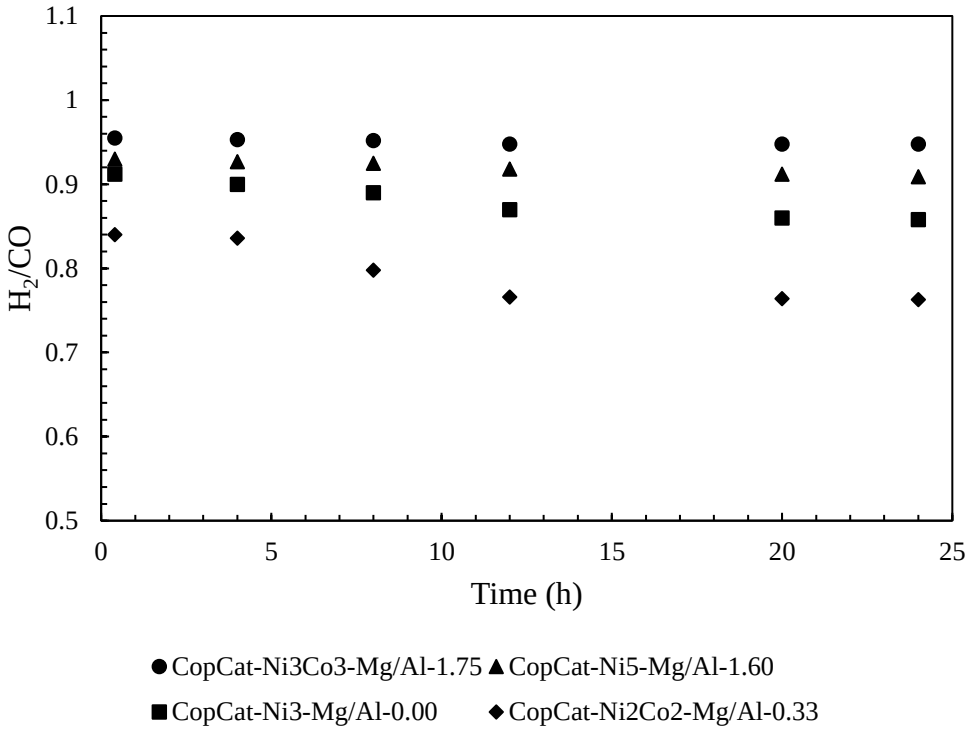

Figure 6.6. H_2/CO ratio for the coal gas feed

6.6 Carbon Deposition on Spent Catalysts

Figures 6.7 and 6.8 showed the Temperature-Programmed Oxidation (TPO) profiles of the spent catalysts for the ideal feed and coal gas feed respectively. The temperature range of the CO_2 oxidation peak can be used to determine the type of carbon species formed on the surface of the catalyst after DRM. Zhang and Verykios, 1994; denoted CO_2 peaks in the temperature range of 150 - 220 ^{o}C, 530 - 600 ^{o}C and > 650 ^{o}C in their TPO result from DRM as C_α, C_β, and C_γ respectively. Hao et al., 2009; represented the peaks from their profile over the temperature range < 250 ^{o}C (C_α), 250 – 600 ^{o}C (C_β), and > 600 ^{o}C (C_γ) as atomic carbon, amorphous carbon, and graphitic carbon respectively. While, atomic and amorphous carbon are easily oxidized to CO at lower and higher temperatures respectively, graphitic carbon can lead to catalyst deactivation. Guo et al., 2007; attributed C_α, (peak at 360 ^{o}C) and C_β (peak at 470 ^{o}C) detected over Ni/γ-Al_2O_3 and Ni/$MgAl_2O_4$ catalysts to polymeric and filamentous carbons. From the TPO profile results presented in this study, no carbon oxidation peak was observed in the profile of CopCat-Ni3Co3-Mg/Al-1.75, which is an indication that no significant carbon was deposited on the surface of this catalyst. For CopCat-Ni2Co2-Mg/Al-0.3 using deal feed, various carbon species (atomic, polymeric, filamentous and graphitic) were discovered on this catalyst. Mainly graphitic, with small filamentous and polymeric carbon were detected on CopCat-Ni3-Mg/Al-0 catalyst from the TPO profile result. Only small amount of filamentous carbon was found on the CopCat-Ni5-Mg/Al-1.60. The presence of the MgO phase in CopCat-Ni5-Mg/Al-1.60 catalyst increased the basicity of the catalyst surface, thereby mitigating the formation of graphitic carbon. The possibility of growing bigger Ni particles during reduction (at higher temperature) could be the major cause of the filamentous carbon, as previously observed by Zhang et al., 2008.

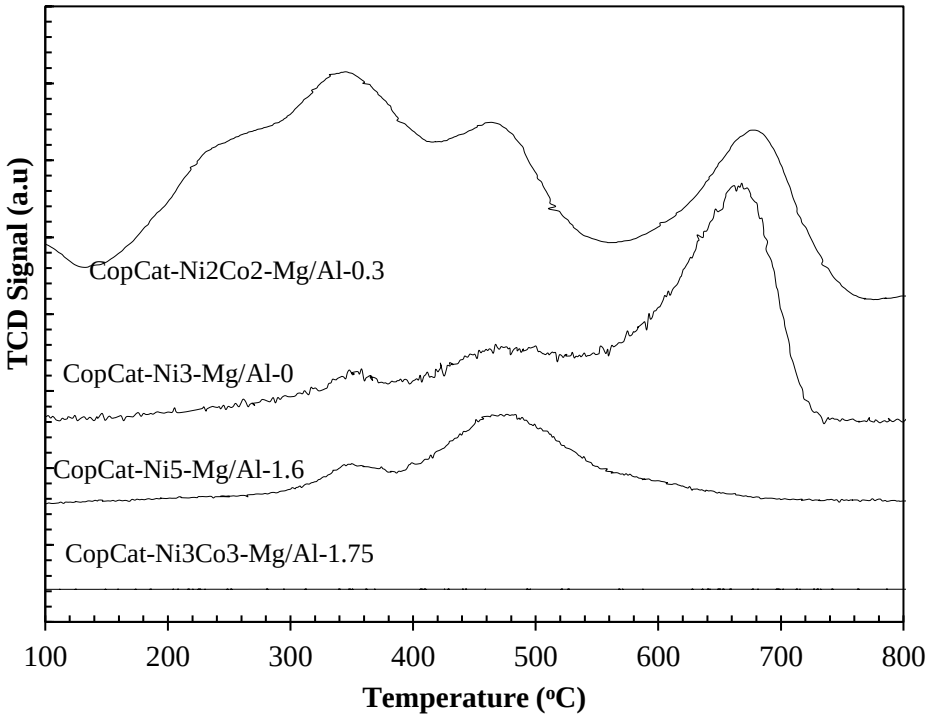

Figure 6.7. TPO profiles of catalysts for ideal gas feed.

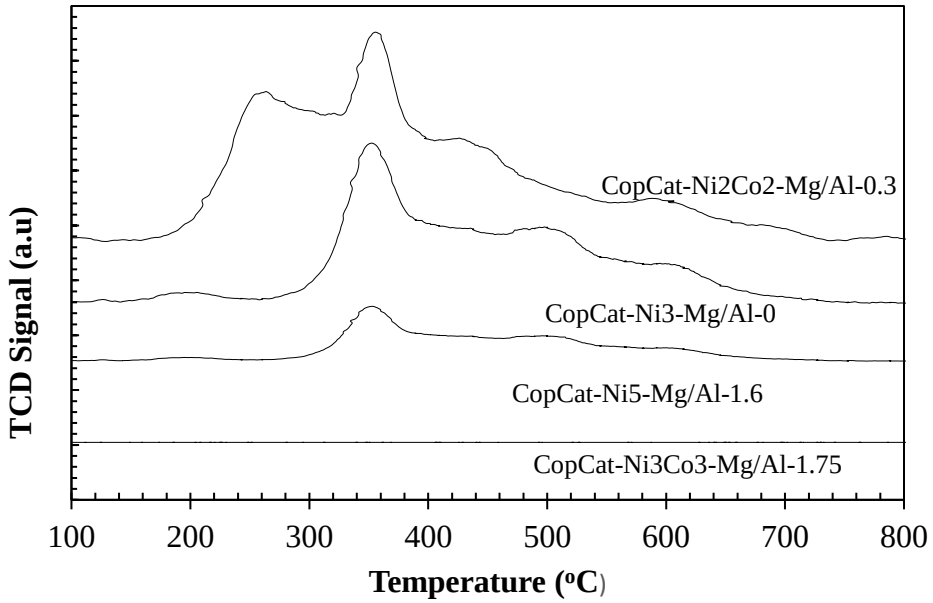

Figure 6.8. TPO profiles of catalysts for coal gas feed.

For the coal gas feed, the TPO profiles (Figure 6.8) of CopCat-Ni5-Mg/Al-1.6, CopCat-Ni3-Mg/Al-0, and CopCat-Ni2Co2-Mg/Al-0.3 showed no significant graphitic carbon, possibly due to the presence of O_2 in the coal gas, which can convert some of the carbon species to CO during reaction. Filamentous carbon was seen on these three catalysts, but much smaller in CopCat-Ni4-Mg/Al-1.60. The existence of MgO phase is believed to mitigate carbon formation on this catalyst. Atomic carbon observed on CopCat-Ni2Co2-Mg/Al-0.3 catalyst was supposed to be an active species for the formation of CO with an active O (from the activated CO_2). With weak basicity, there was no sufficient O species formed around this carbon. Thus, the accumulation of these carbon species could possibly have led to gradual deactivation of the catalyst. These results confirmed that an active and stable catalyst need not only the active metallic sites in the right size (for CH_4 activation), but also need the presence of basic sites to activate CO_2. The MgO phase in the catalyst could help the formation of both sites, while the presence of Co can promote better catalytic properties and performance for DRM.

6.7 Conclusions

From the above results, the following conclusions were drawn;

- All the chosen catalysts this study showed significant activity for DRM using coal gas feed.
- The kinetic study results showed that the difference in reaction rates between the ideal feed and the coal gas feed was mainly caused by the difference in the partial pressures of CO_2 and CH_4 in the feeds.
- CopCat-Ni3Co3-Mg/Al-1.75 showed the best activity and stability in both feeds due to its high ability to activate both CO_2 and CH_4 molecules, which resulted in no carbon deposition.
- The nature of deposited carbon differed for catalysts and feed type, and less carbon deposition was observed on the catalysts with coal gas feed.

CHAPTER SEVEN

CO_2 REFORMING of ETHANE

CO_2 reforming of ethane (CRE) was explored and reported in this chapter. Associated side reaction such as ethane dissociation was studied over the selected catalysts. Competition between side and main reactions are studied, and what made the catalysts selective towards the desired reaction are presented in this chapter.

7.1 Introduction

This reaction offers another route to limit the emission of CO_2 (principal global warming gas) to the environment by converting it to useful syn-gas. Additionally, natural gas usually contains some appreciable amount of higher hydrocarbon like C_2H_6, thus this study could help explain or provide an insight into the result of CO_2 reforming of such gas.

Based on thermodynamic study and results presented by Laosiripojana et al., 2006, at temperature above 700 ^oC, dissociation of C_2H_6 (to C_2H_4, H_2 and CH_4) can occur, and the associated equations as given by Lasoripojana et al., (2006); Twigg, (1989); are shown below:

$$C_2H_6 \rightleftharpoons C_2H_4 + H_2 \qquad 7.1$$

$$C_2H_4 \rightleftharpoons 2C + 2H_2 \qquad 7.2$$

$$C + 2H_2 \rightleftharpoons 2C + 2H_2 \qquad 7.3$$

With reference to these literature, this part of study was designed as follows:

- Study of C_2H_6 dissociation with and without catalysts
- CO_2 reforming of C_2H_6
- CO_2 reforming after C_2H_6 dissociation

- Catalysts characterization for carbon deposition study.

7.2 Experimental

Evaluation of the catalyst activity and stability for CRE was carried out in a fixed-bed quartz reactor (Autoclave Engineers) with ID 3.9 mm, OD 6.35 mm and length 30 cm. For each experimental run, 40 mg of catalyst was mixed with approximately 200 mg of silicon carbide and reactant feed composition of C_2H_6 (99.2 %), CO_2 (99.9 %) and N_2 (99.9 %) in a ratio 1:2:1.5 was introduced into the reactor at atmospheric pressure and GHSV = 6×10^5 mL g^{-1} h^{-1} (flow rate 400 ml min^{-1}). Catalyst was activated in H_2 (99.9 %) and N_2 (99.9 %) mixture with a molar ratio of 1:4 at 800 ^oC for 4 h before activity test. All the gases were supplied by Praxair Canada Inc. Evaluation test was carried out at 800 ^oC with the mixture of catalyst and silicon carbide loaded in the middle of the reactor during evaluation test. The product gas from the CO_2 reforming of C_2H_6 reaction was analyzed by an on-line Agilent 6890N GC equipped with TCD and a GS-GASPRO capillary column (J&W Scientific) of 60 m in length and 0.32 mm in inner diameter using GC Chemstation software. Helium (Ultra high purity 5.0, PRAXAIR Canada Inc.) was used as the carrier gas. C_2H_6 dissociation study, mixture of C_2H_6 and N_2 totalling 225 ml min^{-1} were fed in a ratio of 1: 1.5. The selected catalysts are from the earlier synthesized catalysts, with their compositions and properties highlighted in chapter 4.

7.3 Data analysis, Reactant Conversion and Product Selectivity

The Equations used for reactant conversion (X), products selectivity (S), rate of reaction -r (reactant conversion) and r (production formation) are shown in Equations 7.4 – 7.9.

$$X_j = \frac{F_j^i - F_j^f}{F_j^i} \times 100 \qquad 7.4$$

$$S_{H_2} = \frac{F^f_{H_2}}{3\times (F^i_{C_2H_6} - F^f_{C_2H_6})} \times 100 \quad 7.5$$

$$S_{CO} = \frac{F_{co}}{2\times (F^i_{C_2H_6} - F^f_{C_2H_6}) + \left(F^i_{CO_2} - F^f_{CO_2}\right)} \times 100 \quad 7.6$$

$$S_{CH_4} = \frac{F^f_{CH_4}}{2\times (F^i_{C_2H_6} - F^f_{C_2H_6}) + \left(F^i_{CO_2} - F^f_{CO_2}\right)} \times 100 \quad 7.7$$

$$S_{C_2H_4} = \frac{F^f_{C_2H_4}}{(F^i_{C_2H_6} - F^f_{C_2H_6}) + 0.5\times\left(F^i_{CO_2} - F^f_{CO_2}\right)} \times 100 \quad 7.8$$

$$-r_i\ (\text{mol g}^{-1}\ \text{s}^{-1}) = \frac{n^i_j - n^f_j}{60\times m_{cat}} \quad 7.9$$

$$r_i\ (\text{mol g}^{-1}\ \text{s}^{-1}) = \frac{n^f_j}{60\times m_{cat}} \quad 7.10$$

m_{cat} = mass of catalyst in gram, n = molar flow rate (mol min^{-1})

7.4 Results and Discussion

The results of C_2H_6 dissociation and CRE on the selected catalysts are presented in sub-sections 7.4.1 and 7.4.2 respectively.

7.4.1 C_2H_6 dissociation study

The results of C_2H_6 dissociation study are presented in Figure 7.1, while the average products selectivity over the TOS is shown in Table 7.1. Compared to the blank run, the presence of catalyst did not seem to have significant effect on the dissociation of C_2H_6. Even though the higher Mg/Al ratio catalysts showed an average increase of around 5% in C_2H_6 dissociation compared to the support and blank, no distinctive trend was observed in the dissociation results of C_2H_6 over the catalysts. This could an indication that C_2H_6 dissociation is thermally controlled and must have started occurring before getting in contact with the catalyst.

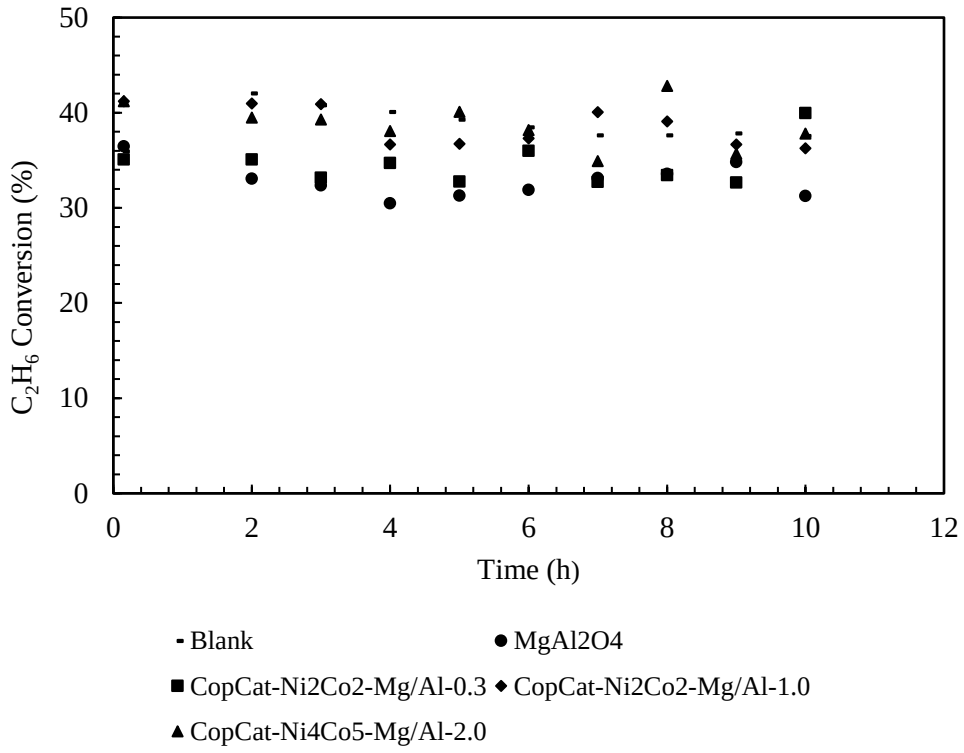

Figure 7.1. C_2H_6 conversion over the TOS at 800 °C, 1atm and GHSV = 3.3×10^5 mL g^{-1} h^{-1}

Table 7.1. Average selectivity of products from C_2H_6 dissociation

Catalyst	Average Product selectivity (%)		
	C_2H_4	H_2	CH_4
Blank	81	23	2
$MgAl_2O_4$	78	20	3
CopCat-Ni2Co2-Mg/Al-0.3	80	22	2
CopCat-Ni2Co2-Mg/Al-1.0	80	22	3
CopCat-Ni4Co5-Mg/Al-2.0	82	21	3

With respect to product selectivity, from Table 7.1, all the catalysts showed approximately equal selectivity towards the products, but a trend could be observed with respect to the selectivity of CH_4 and H_2. A slightly higher selectivity of H_2 resulted in a slightly lower CH_4 selectivity. Additionally, as the Mg/Al increased, CH_4 selectivity increased, while H_2 selectivity decreased. This might be an indication that reaction 7.3 was favored in the presence of catalysts. Similar results had been reported for C_2H_6 dissociation by Kim et al., (2011); Mulla and Choudhary, (2003).

7.4.2 CO_2 reforming of C_2H_6 results

The main Equation for this reaction is given as

$$CO_2 + C_2H_6 \rightleftharpoons 4CO + 3H_2 \qquad 7.11$$

In addition to Equations 7.1-7.3, some other possible side reactions (depending on reaction condition and the performance of catalysts) can include;

$$CO_2 + C \rightleftharpoons 2CO \qquad 7.12$$

$$2CO + 2H_2 \rightleftharpoons CH_4 + CO_2 \qquad 7.13$$

$$C_2H_4 + 2CO_2 \rightleftharpoons 4CO + 2H_2 \qquad 7.14$$

The results of the performance tests are shown in Figures 7.2 to 7.4 for the conversions of C_2H_6, CO_2 and H_2/CO ratio respectively, while the average products selectivity is presented in Table 7.2. From Figures 7.2 and 7.3, the order of performance of the catalysts for both C_2H_6 and CO_2 conversions followed an increasing order of the Mg/Al ratio in the catalyst system. The lesser conversion of CO_2 compared to C_2H_6 might be attributed to equation 7.14. Additionally, increase in C_2H_6 conversion was recorded with the presence of CO_2 (in CRE) when compared to dissociation of C_2H_6.

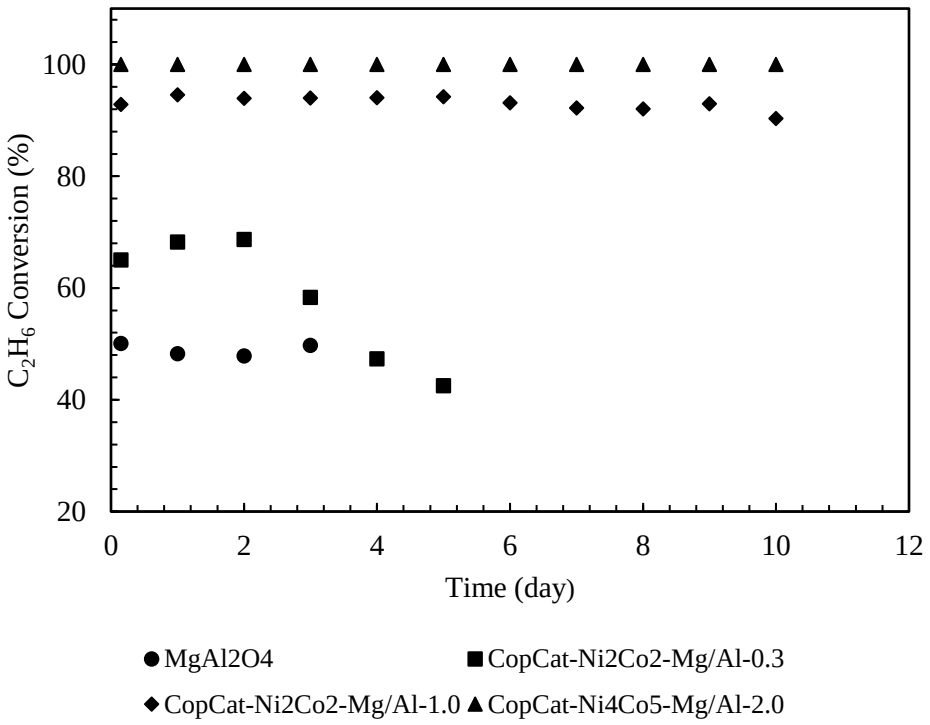

Figure 7.2. C_2H_6 conversion as a function of TOS at 800 °C, 1atm, GHSV= 6×10^5 mL g^{-1} h^{-1}

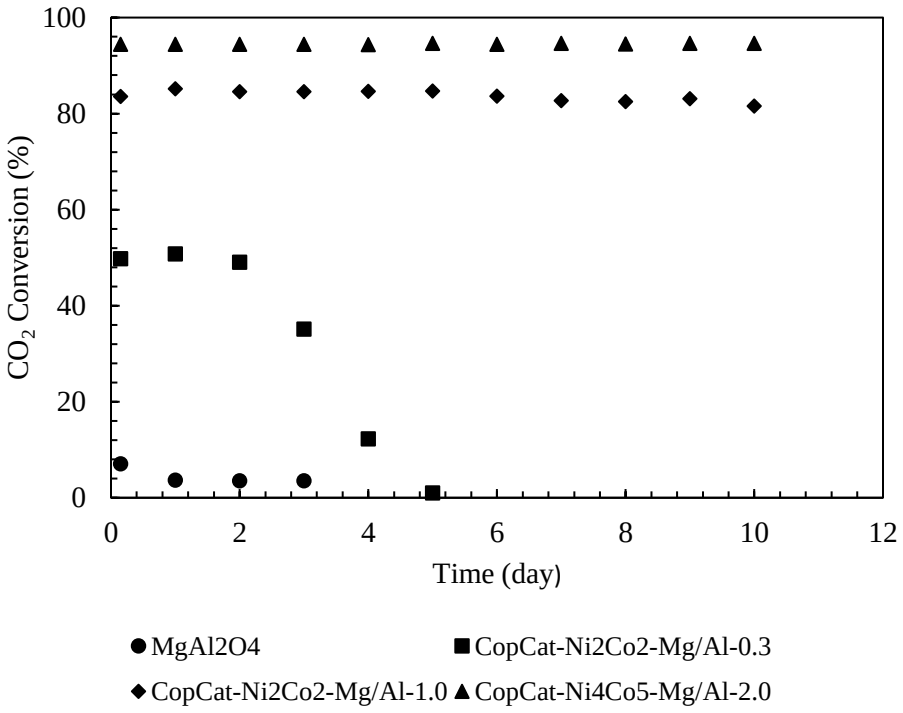

Figure 7.3. CO_2 conversion as a function of TOS at 800 °C, 1atm, GHSV = 6×10^5 mL g^{-1} h^{-1}

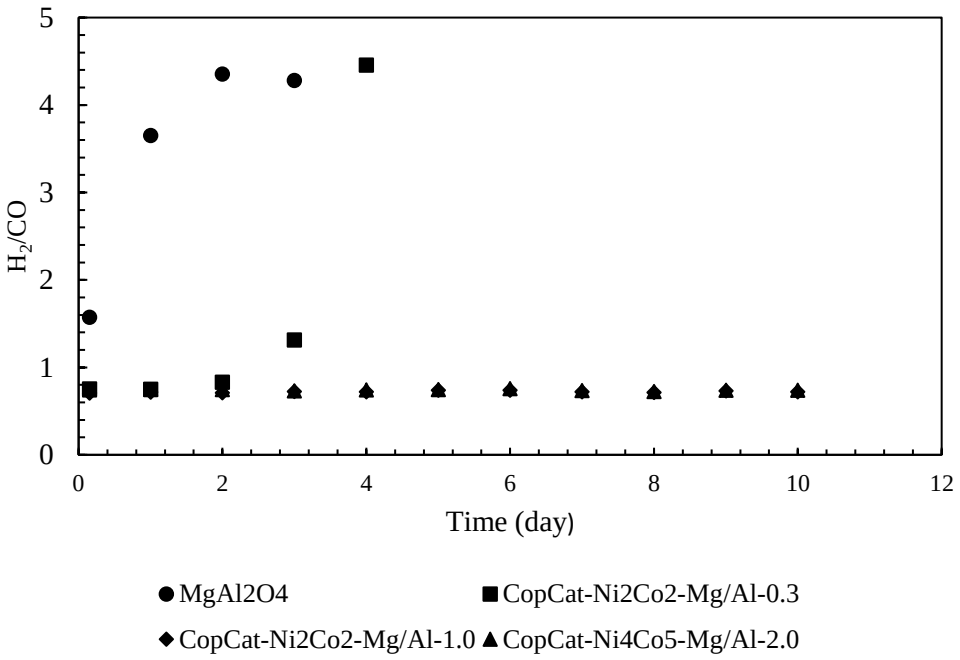

Figure 7.4. H_2/CO ratio a function of time-on-stream at 800 °C, 1atm, GHSV = 6×10^5 mL g^{-1} h^{-1}

Table 7.2. Average selectivity of products from CO_2 reforming of C_2H_6

Catalysts	Average product selectivity (%)			
	C_2H_4	H_2	CH_4	CO
$MgAl_2O_4$	70	18	3	8
CopCat-Ni2Co2-Mg/Al-0.3	30	61	1	54
CopCat-Ni2Co2-Mg/Al-1.0	3	89	1	94
CopCat-Ni4Co5-Mg/Al-2.0	0	99	2	99

This is an indication that CRE was occurring in addition to C_2H_6 dissociation, which is even substantiated by the higher conversion of CO_2 recorded as compared to zero conversion shown by CO_2 dissociation study. Also, appreciable amount of activity was shown by support only ($MgAl_2O_4$) for this reaction, an indication that nature of support could play an important for this reaction. The selectivity of the desired products from main reaction was measured by the H_2/CO ratio, and based on stoichiometry of reaction, the expected H_2/CO ratio is 0.75. Only CopCat-Ni2Co2-Mg/Al-0.3 showed a value greater than 0.75 from Figure 7.4. Additionally, this catalyst showed the highest C_2H_4 selectivity, an indication that C_2H_6 dissociation could be competing with CO_2 reforming. Higher CO and H_2 with no C_2H_4 selectivity was recorded for CopCat-Ni4Co5-Mg/Al-2.0, and stability of catalysts was also in the same order as the Mg/Al ratio. Notable to say is increase in selectivity of catalysts towards CO and H_2, and decrease in selectivity towards C_2H_4 as Mg/Al ratio in the catalysts increase. This shows the preference of these catalysts for CRE over C_2H_6 dissociation. Thus, the nature and composition of support played an important role in the performance of catalysts for CRE. In the presence of adequate basicity, CO_2 is easily activated leading to CRE and even deposited C_2H_4 (from thermal dissociation of C_2H_6) could be converted to CO and H_2. From, this study, support, metal oxides and metal sites are active for CRE, compared to DRM in which only metal can catalyze the reaction.

7.5 Conclusions

Highlighted below are some of the conclusions from this chapter;

- Catalysts do not have any significant effect on thermal dissociation of C_2H_6.
- Higher Mg/Al ratio catalysts promote CRE and limit the occurrence of side reaction such as C_2H_6 dissociation.
- Higher Mg/Al ratio catalysts showed no deactivation over the TOS.

CHAPTER EIGHT

CONCLUSIONS AND RECOMMENDATIONS

Conclusions drawn from this work was summarized in this chapter. Recommendations for future work were also mentioned in this concluding chapter.

8.1 Conclusions

Although previous work reported Ni-Co-Mg-Al-Ox to be an active and stable catalyst for dry reforming reaction (DRM), yet desire to understand more about the catalyst, and to answer some more questions about the properties of the catalyst motivated this research work. What controls active metal reduction, role of each component of the catalyst, why Ni reduces more than Co in the catalyst system and the effect of support composition on the structure, metal distribution, metal reduction and performance of both monometallic and bimetallic catalysts need to be understood.

Variation of Mg/Al ratio in the support led to changes in the bulk structure, active metal distribution, reduction and performance of bimetallic Ni-Co-Mg-Al-Ox catalyst for DRM. A change from complete spinel through spinel + MgO-solid and finally to $NiCoO_2$ + spinel + MgO-solid phases was observed as the Mg/Al ratio increased from 0.3 to 2. This consequently affected the distribution and reduction of the active metals within the sites of the support. A change from a more regular spinel to an inverse spinel was also observed as the ratio increased. The presence of MgO-solid phase and spinel inversion offered more octahedral site occupancy for the metal, making their reduction easier, with more active sites for CH_4 dissociation. Basicity of support also improved with the introduction of more MgO. This enhanced more CO_2 chemisorption and

facilitated the conversion of deposited C to CO. With these properties, the performance of catalyst was enhanced with increase in Mg/Al ratio in the support.

Similar trend was also observed in the structure of Al-Ox supported monometallic Ni and Co catalysts with the introduction of MgO, except that $NiCoO_2$ phase was absent in the Mg-Al-Ox supported monometallic catalysts. Characterization results showed all the properties of Ni-Al-Ox and Co-Al-Ox are similar, but they showed different extent of metal reduction and performance for DRM. Co showed neither reduction nor activity, while appreciable metal reduction and performance were observed with Ni-Al-Ox for DRM. This observed difference was related to the interaction of the active metal with Al based on their electronic configuration. The desire of Co for tetrahedral site and Ni for octahedral site could be a possible reason for the difference. With the presence of MgO, Co reduction increased from 0 to 54%, while Ni reduction attained 88% from 33%. The basicity results showed the presence of strong basic site in Co-Mg-Al-Ox compared to Ni-Mg-Al-Ox. Such site could result from stronger Co-Mg as compared to Ni-Mg interaction. A slightly better performance was observed in Mg-Al-Ox supported Co catalyst compared to Ni, even though more active sites were present in Ni-Mg-Al-Ox catalyst. This confirmed that good catalytic behaviour not only depended on active metal, but rather on synergetic effect of both active site and basicity of support. Thus, nature of support affected the performance of catalysts for this reaction. Also, in addition to be a promoter, Co can also be an active metal for this reaction with the right support. Easier reduction of Ni (compared to Co) could be attributed to the presence of isolated NiO, preference of Ni for octahedral site and less stronger interaction with support as compared to Co.

Site performance was distinguished from the bulk catalytic performance by calculation of the TOF. The TOF results showed a contrasting trend to the bulk performance. Increase in Mg/Al

ratio (more reduction) led to decrease in the site performance. This was related to decrease in dispersion per reduced metal in the catalyst as Mg/Al ratio increased.

Dry reforming reaction using coal gas simulated feed was compared to the ideal gas feed using some selected catalysts with different Mg/Al ratio. Better performance was observed in the bimetallic catalyst with higher Mg/Al ratio for both feeds. Additionally, better activity was observed using ideal feed compared to the coal gas feed. This difference was related to lower composition of CH_4 and CO_2 in the coal gas feed. Low carbon deposition was observed using coal gas feed compared to ideal gas feed for each corresponding catalyst. This was due to the presence of O_2 in the feed that could convert deposited carbon to CO and the presence of sufficient basicity to activate CO_2 reaction with C to give CO.

Examination of CO_2 reforming of C_2H_6 was done in the last part of this work. Dissociation of C_2H_6 was observed with or without catalyst, while CO_2 reforming of C_2H_6 observed on support as well. Higher Mg/Al ratio catalysts showed preference for CO_2 reforming of C_2H_6 over dissociation. Additionally, CO_2 reforming of C_2H_6 can proceed on catalysts without reduction unlike CO_2 reforming of CH_4.

8.2 Recommendations

After presenting the above conclusions from this present work, the following highlighted points could be of interest for future work;

- Detailed mechanism and kinetics of carbon deposition on catalyst for both CO_2 reforming of C_2H_6 and CH_4 needs to be examined. Also, the nature of carbon deposition leading to catalyst deactivation needs to be examined, since not all deposited carbon leads to catalyst deactivation.

- Mechanism and kinetics of CO_2 reforming of C_2H_6 reaction on catalysts needs to be examined and compared to CO_2 reforming of CH_4, since C_2H_6 can be activated on support, metal and metal oxide, while CH_4 can only be activated on active metal alone.
- During catalyst synthesis, the initial pH of salt solution changed with changes in the ratio of the Mg and Al salt in the solution. This could possibly affect the extent of metal precipitation. A detailed correlation between initial pH, precipitating pH and extent of metal precipitation should be deeply examined.
- The pH of the precipitation process and precipitation speed can be varied, to know their effect on the properties of the catalyst.

REFERENCES

1. Adris, A. M., Pruden, B. B., Lim, C. J., Grace, J. R. (1996), "On the Reported Attempts to Radically Improve the Performance of the Steam Methane Reforming Reactor", Canadian Journal of Chemical Engineering 74,177–186 (1996).

2. Aditya, A. A., "Spinel Structure and Factors Affecting the Types of Spinel Structure", www.adichemistry.com/inorganic/cochem/spinels/spinel-structures.html. (Accessed January 2017).

3. Al-Fatesh, A., "Suppression of Carbon Formation in CH_4–CO_2 Reforming by Addition of Sr into Bimetallic Ni–Co/γ-Al_2O_3 Catalyst", Journal of King Saud University-Engineering Sciences 27, 101-107 (2015).

4. Alyea, E.C., He, D., Wang, J., "Alcohol Synthesis from Syngas. I: Performance of alkali promoted Ni-Mo (MOVS) Catalysts", Applied Catalysis A 104, 77-85 (1993).

5. Arena, F., F. Frusterl, F., Giordano, N., "Temperature-Programmed Reduction study of NiO–MgO Interactions in Magnesia-Supported Ni Catalysts and NiO–MgO Physical Mixture", Journal of the Chemical Society, Faraday Transactions 86, 2663-2669 (1990).

6. Armor, A. N., "The Multiple Roles for Catalysis in the Production of H_2", Applied Catalysis A 176, 159-176 (1999).

7. Ashcroft, A. T., Cheetham, A. K., Green, M. L. H., Vernon, P. D. F., "Partial Oxidation of Methane to Synthesis gas using Carbon dioxide", Nature 352, 225-226 (1991).

8. Bhattacharyya, A., and Chang, V.W., "Rapid Catalytic Reforming of Methane with CO_2 and its Application to Other Reactions", Studies in Surface Science and Catalysis 88, 207-213 (1994).

9. Blom, R., Dahl, I.M., Slagtern, A., Sortland, B., Spjelkavik, A., and Tangstad, E., "Carbon Dioxide Reforming of Methane Over Lanthanum-Modified Catalysts in a Fluidized-bed Reactor", Catalysis Today 21, 535-543 (1994).

10. Bradford, M.C.J., and Vannice, M.A., "Catalytic Reforming of Methane with Carbon Dioxide Over Nickel Catalysts II. Reaction kinetics", Applied Catalysis A 142, 97-122 (1996).

11. Bradford, M.C.J., and Vannice, M.A., "CO_2 Reforming of CH_4 Over Supported Pt Catalysts", Journal of Catalysis 173, 151-157 (1997).

12. Bradford, M.C.J. and Vannice, M.A., "CO_2 Reforming of CH_4", Catalysis Reviews: Science and Engineering 41, 1-42 (1999).

13. Brinen, J. S., Armstrong, W.D., "Surface Chemistry of Activated Hydro-Desulfurization Catalysts by X-ray Photoelectron Spectroscopy", Journal of Catalysis 54, 57-65 (1978).

14. Burch, R. and Petch, M.I., "Investigation of the Synthesis of Oxygenates from Carbon monoxide/Hydrogen Mixtures on Supported Rhodium Catalysts", Applied Catalysis A 88, 39-60 (1992).

15. Chang, J., Park, S., Yoo, J., Park, J.-M., "Catalytic Behavior of Supported KNiCa Catalyst and Mechanistic Consideration for Carbon Dioxide Reforming of Methane", Journal of Catalysis 195, 1-11 (2000).

16. Chang, Z., Wu, Q., Li, J., and Zhu, Q., "Effects of Promoters and Preparation Procedures on Reforming of Methane with Carbon Dioxide Over Ni/Al_2O_3 Catalyst", 30, 147-155 (1996).

17. Chen, W., Zhao, G.F., Xue, Q.S., Chen, L., Lu, Y., "High Carbon-resistance $Ni/CeAlO_3$-Al_2O_3 Catalyst for CH_4/CO_2 Reforming", Applied Catalysis B 260, 136-137 (2013).

18. Chein, R.Y., Chen, Y.C., Yu, C. T., J. N. Chung, J.N., "Thermodynamic Analysis of Dry Reforming of CH_4 with CO_2 at high Pressures", Journal of Natural Gas Science and Engineering 26, 617-629 (2015).

19. Cheng, W.-H. and Kung, H. H., "In Methanol Production and Uses", Published by Marcel Dekker: New York, pp 1-18 (1994).

20. Chin, R.L., Hercules, D.M., "Surface Spectroscopic Characterization of Cobalt-Alumina catalysts", Journal of Physical Chemistry 86, 360-367 (1982).

21. Cho, J.H., Park, J.H., Chang, T.S., Seo, G., Shin, C.H.," Reductive Amination of 2-propanol to Mono-isopropyl Amine Over Co/γ-Al_2O_3 Catalysts", Applied Catalysis A 417-418, 313-319 (2012).

22. Choi, M.-J., Cho, D.-H., "Research Activities on the Utilization of Carbon Dioxide in Korea", Clean Journal 36, 426 – 432 (2008).

23. Cimino, A., Lo Jacono, M., Schiavello, M., "Effect of Zinc, Gallium, and Germanium ions on the Structural and Magnetic Properties of Nickel Ions Supported on Alumina", Journal of Physical Chemistry 79, 243-249 (1975).

24. Crisafulli, C., Scirè, S., Minicò,S., Solarino, L.,"Ni–Ru Bimetallic Catalysts for the CO_2 Reforming of Methane", Applied Catalysis A 225, 1-9 (2002).

25. Damyanova, S., Pawelec, B., Arishtirova, K., Fierro, J.L.G., Sener, C.,Dogu, T., "MCM-41 Supported PdNi Catalysts for Dry Reforming of Methane",Applied Catalysis B 92, 250–261 (2009).

26. Debecker, D.P., Gaigneaux, E.M., Busca, G., "Exploring, Tuning, and Exploiting the Basicity of Hydrotalcites for Applications in Heterogeneous Catalysis", Chemistry: A European Journal 15, 3920-3935 (2009).

27. Dias, J.A.C., Assaf, J.M., "Influence of Calcium Content in $Ni/CaO/\gamma$-Al_2O_3 Catalysts for CO_2 Reforming of Methane", Catalysis Today 85, 59-68 (2003).

28. Di-Cosimo, J.I., Diez, V.K., Xu, M., Iglesia, E., Apeesteguna, C.R., "Structure and Surface and Catalytic Properties of Mg-Al Basic Oxides," Journal of Catalysis 178, 499 – 510 (1998).

29. Dillard, J.G., Schenck, C.V., Koppelman, M.H., "X-ray Photoelectron Spectroscopic Surface Characterization of Cobalt on the Surface of Kaolinite", Surface Chemistry of Cobalt in Calcined Cobalt-Kaolinite Materials", Clays and Clay Minerals, 31, 69-72 (1983).

30. Edwards, J.H., Maitra, A.M., "The Chemistry of Methane Reforming with Carbon dioxide and its Current and Potential Applications", Fuel Processing Technology 42, 269-289 (1995).

31. Euler, B., "Solubility Product", Online Chemistry 112, University of Rhode Island, 2006. www.bilbo.chm.uri.edu. (Accessed December 2nd, 2016).

32. Fei, J. Hou, Z., Zheng, X., and Yashima, T., "Doped Ni Catalysts for Methane Reforming with CO_2", Catalysis Letter 98, 241-246 (2004).

33. Ferreira-Aparicio, P., Guerrero-Ruiz A., RodroAguez-Ramos, I., "Comparative Study at Low and Medium Reaction Temperatures of Syngas Production by Methane Reforming with Carbon dioxide over Silica and Alumina Supported Catalysts", Applied Catalysis A 170,177-187 (1998).

34. Foo, S.Y., Cheng, C.K., Nguyen, T.-H., Adesina, A.A., "Syngas Production from CH_4 Dry Reforming Over Co–Ni/Al_2O_3 Catalyst: Coupled Reaction-Deactivation Kinetic Analysis and the Effect of O_2 Co-feeding on H_2:CO Ratio" International Journal of Hydrogen Energy 37, 17019 - 17026 (2012).

35. Gadalla, A.M. and Bower, B., "The Role of Catalyst Support on the Activity of Nickel for Reforming Methane with CO2", Chemical Engineering Science, 43, 3049-3062 (1988).

36. Gadalla, A.M. and Sommer, M.E., "Synthesis and Characterization of Catalysts in the System Al_2O_3-MgO-NiO-Ni for Methane Reforming with CO_2", Journal of the American Ceramic Society 72, 683-687 (1989).

37. Garcıa-Dieguez, M., Herrera, M.C., Pieta, I.S., Larrubia, M.A., Alemany,l., "NiBa catalysts for CO_2 Reforming of Methane", Catalysis Communications 11, 1133-1136 (2010).

38. Gronchi, P., Fumagalli, D., Rosso, R.D., Centola, P., "Carbon Deposition in Methane Reforming with Carbon Dioxide", Journal of Thermal Analysis and Calorimetry 7, 227-234 (1996).

39. Guo, J., Lou, H., Zhao, H., Chai, D., Zheng, X., "Dry Reforming of Methane Over Nickel Catalysts Supported on Magnesium Aluminate Spinels", Applied Catalysis A, (2004) 75–82 (2004).

40. Guo, J.J., Lou, H., Zhao, H., Zheng, X., "Improvement of Stability of Out-layer $MgAl_2O_4$ Spinel for a Ni/$MgAl_2O_4$/Al_2O_3 Catalyst in Dry Reforming of Methane", Reaction Kinetics and Catalysis Letters 84,93-100 (2005).

41. Guo, J.J., Lou, H., Mo, L., Zheng, X., "The Reactivity of Surface Active Carbonaceous Species with CO_2 and its Role on Hydrocarbon Conversion Reactions", Journal of Molecular Catalysis A 316, 1-7 (2010).

42. Guo, J., Lou, H., Zheng, X., "The Deposition of Coke from Methane on a Ni/$MgAl_2O_4$ Catalyst", Carbon 45, 1314–1321 (2007).

43. Hao, Z.-P., Hu, C., Jiang, Z., Lu, G.Q., "Preparation and Catalytic Properties of ZrO_2-Al_2O_3 Composite Oxide Supported Nickel Catalysts for Methane Reforming with Carbon Dioxide", Journal of Environmental Science China 16, 316-320 (2004).

44. Hao, Z., Zhu, Q., Jiang, Z., Hou, B., Li, H., "Characterization of Aerogel Ni/Al_2O_3 Catalysts and Investigation on their Stability for CH_4-CO_2 Reforming in a Fluidized Bed", Fuel Processing Technology 90, 113-121 (2009).

45. Horiuchi, T., Sakuma, K., Fukui, T., Kubo, Y., Osaki, T., and Mori T., "Suppression of Carbon Deposition in the CO_2 Reforming of CH_4 by Adding Basic Metal Oxides to a Ni/Al_2O_3 Catalyst", Applied Catalysis A 144, 111-120 (1996).

46. Hou, Z., Yokota, O., Tanaka, T., Yashima, T., "A Novel KCaNi/α-Al_2O_3 Catalyst for CH_4 Reforming with CO_2", Catalysis Letter 87, 37-42 (2003).

47. Hou, Z., Yokota, O., Tanaka, T., and Yashima, T., "Investigation of CH_4 Reforming with CO_2 on Meso-porous Al_2O_3-Supported Ni Catalyst", Catalysis Letter 89, 121-127 (2003).

48. Huang, T.J., Li, H.J, and Yu, T.C., "A Comparison of Oxygen-Vacancy Effect on Activity Behaviors of Carbon Dioxide and Steam Reforming of Methane Over Supported Nickel Catalysts", Catalysis Letter 105, 239-247 (2005).

49. Hu, C., Gao, Z., Yang, X., "Fabrication of Mesoporous Ni-8YSZ and Its Catalytic Activity for Carbon Dioxide Reforming of Methane", Energy Fuels 21, 2950-2954 (2007).

50. Hu, Y.H., "Solid-Solution Catalysts for CO_2 Reforming of Methane", Catalysis Today 148, 206-211 (2009).

51. Hu, Y.H., Ruckenstein, E., "Binary MgO-Based Solid Solution Catalysts for Methane Conversion to Syngas", Catalysis Reviews Science and Engineering 44,423-453 (2002).

52. Hu, Y., Xu, R., Dynes, J., Blyth, R., Yu, G., Kozak, L., Huang, P., "Coordination Nature of Aluminum (Oxy)Hydroxides Formed Under the Influence of Tannic Acid Studied by X-ray Absorption Spectroscopy", Geochemical et Cosmochimica Act 72, 1959-1969 (2008).

53. Hu. Y.H., Ruckenstein E., "An optimum NiO content in the CO2 Reforming of CH4 with NiO/MgO Solid Solution Catalysts", Catalysis Letter 36, 145-149 (1996).

54. Hu. Y.H., Ruckenstein E., "The Characterization of a Highly Effective NiO/MgO Solid Solution Catalyst in the CO_2 Reforming of CH_4", Catalysis Letter 43, 71-77 (1997).

55. Intergovernmental Panel on Climate Change, "Mitigation of Climate Change Report 2014" Web Source: www.ipcc.ch/report/ar5/wg3. (Accessed May, 2017).

56. Ji, L., Tang, S., Zeng, H.C., Lin, J., Tan, K.L., "CO_2 Reforming of Methane to Synthesis Gas over Sol–gel-made Co/γ-Al_2O_3 Catalysts from Organometallic Precursors", Applied Catalysis A 207, 247-255 (2001).

57. Jing, Q.S., Fei, J.H., Lou, H., Mo, L.Y., Zheng, X., "Reforming of CH_4 with CO_2 and O_2 to Produce Syngas Over CaO Modified Ni/SiO_2 Catalysts in a Fluidized Bed Reactor", Reaction Kinetics and Catalysis Letter 83, 291-298 (2004).

58. Jing, Q.S., Fei, J.H., Lou, H., Mo, L.Y., Zheng, X., "Combination of CO_2 Reforming and Partial Oxidation of Methane over Ni/BaO-SiO_2 Catalysts to Produce low H_2/CO Ratio Syngas using a Fluidized Bed Reactor", Journal of Molecular Catalysis A 212, 211-217 (2004).

59. Jóźwiak,W.K., Nowosielska, M., Rynkowski,J., " Reforming of CH_4 with CO_2 Over Supported Bimetallic Catalysts Containing Ni and Noble Metal: Characterization and Activity of SiO_2 Supported Ni-Rh Catalysts. Applied Catalysis A 280,233-244 (2005).

60. Juan-Juan, J., Roman-Martinez, M.C., Illan-Gomez, M.J., "Ni Catalyst Activation in CO_2 Reforming of CH_4: Effect of Pre-treatment", Applied Catalysis A 355, 27–32 (2009).

61. Juan-Juan, J., Román-Martínez, M.C., Illán-Gómez, M.J., "Effect of potassium content in the activity of K-promoted Ni/Al_2O_3 catalysts for the dry reforming of methane", Applied Catalysis A 264, 9-15 (2004).

62. Khoshtinat, M., Amin, N.A.S., "Thermodynamic Analysis of Carbon Dioxide Reforming of Methane in view of Solid Carbon Formation", Fuel Processing Technology 92, 678-691 (2011).

63. Kim, G.J., Cho, D.S., Kim, K.H., and Kim, J.H., "The Reaction of CO_2 with CH4 to Synthesize H_2 and CO over Nickel-loaded Y-Zeolites", Catalysis Letter 28, 41-52 (1994).

64. Kim, J.-H., Suh, D.J., Park, T.-J., Kim, K.-L., "Effect of Metal Particle Size on Coking during CO_2 Reforming of CH_4 over Ni–Alumina Aerogel Catalyst", Applied Catalysis A 197, 191-200 (2000).

65. Kim, K.S., "X-ray-Photoelectron Spectroscopic Studies of the Electronic Structure of CoO", Physical Review B 11, 2177-2185 (1975).

66. 1. Kim, M.S., Lee, S.Y., Kwak, J.H., Han, G.Y., Yoon, K.J., "Hydrogen Production by Decomposition of Ethane-Containing Methane over Carbon Black Catalysts", Korean Journal Chemical Engineering 28, 1833-1838 (2011).

67. Koo, K.Y., Roh, H.-S., Seo, Y.T., Seo, D.J., "Coke study on MgO-Promoted Ni/Al_2O_3 Catalyst in Combined H_2O and CO_2 Reforming of Methane for Gas to Liquid (GTL) process", Applied Catalysis A 340,183-190 (2008).

68. Lasoripojana, N., Sangtongkitcharoen, W., Assabumrungrat, S., "Catalytic Steam Reforming of Ethane and Propane over CeO_2-doped Ni/Al_2O_3 at SOFC Temperature: Improvement of Resistance Toward Carbon formation by the Redox Property of Doping CeO_2 ", Fuel 85, 323-332 (2009).

69. LeBlanc, J. R., Schneider, R. V., Strait, R. B., "In Methanol Production and Uses"; Published by Marcel Dekker: New York, pp 51-131 (1994).

70. Lee, J.-H., Lee, E.-G., Joo, O.-S., Jung, K.-D., "Stabilization of Ni/Al_2O_3 Catalyst by Cu Addition for CO_2 Reforming of Methane", Applied Catalysis A 269,1-6 (2004).

71. Lemonidou, A. A. and Vasalos, I.A., "Carbon Dioxide Reforming of Methane Over 5 wt.% $Ni/CaO-Al_2O_3$ Catalyst", Applied Catalysis A 228, 227-235 (2002).

72. Louise, S., Aleksander, J., Mattias, E., Danielle, M.-L, Seo, D.-K., F. Javier, F. G.-G., Ulrich, H., "Structural analysis of highly porous γ-Al_2O_3", Journal of Solid State Chemistry 217, 1–8 (2014).

73. Matienzo, L.J., Yin, L.I., Grim, S.O., Swartz, W.E., "X-ray Photoelectron Spectroscopy of Nickel Compounds", Inorganic Chemistry 12, 2770-2778 (1973).

74. Michalkiewicz, B., Sreńscek-Nazzal, J., Ziebro, J., "Optimization of Synthesis Gas Formation in Methane Reforming with Carbon Dioxide", Catalysis Letter 129, 142-148 (2009).

75. Minchener, A.J., "Coal Gasification for Advanced Power Generation" Fuel 84, 2222-2235 (2005).

76. Millard, R.L., Peterson, R.C., Hunter, B.K., "Temperature Dependence of Cation Disorder in $MgAl_2O_4$ spinel using ^{27}Al and 17O Magic-Angle Spinning NMR", American Mineralogist 77, 44-52 (1992).

77. Mulla, S.A.R., Choudhary, V.R., "Conversion of Ethane in the Presence of Limited O2 Over supported SrO Promoted Sm2O3 Catalyst", Indian Journal of Chemical Technology 10, 615-618 (2003).

78. Mo, L., Zheng, X., Jing, Q., Lou, H., Fei, J., "Combined Carbon Dioxide Reforming and Partial Oxidation of Methane to Syngas over $Ni{-}La_2O_3/SiO_2$ Catalysts in a Fluidized-Bed Reactor", Energy and Fuels 19, 49-53 (2005).

79. Munoz, M., Moreno, S., Molina, R., "Synthesis of Ce and Pr-Promoted Ni and Co Catalysts from Hydrotalcite Type Precursors by Reconstruction Method", International Journal of Hydrogen Energy 37, 18827-18842 (2012).

80. Myint, M., Yan, B., Wan, J., Zhao, S., Chen, J.G., "Reforming and oxidative dehydrogenation of ethane with CO2 as a soft oxidant over bimetallic catalysts", Journal of Catalysis 343, 168–177 (2016).

81. National Geography, "Climate Change" Web Source: wwwnationalgeographic.com/environment/global-warming/global-warming-overview. (Accessed May,2017)

82. Nagaoka, K., Takanabe, K., Aika, K., "Modification of Co/TiO_2 for Dry Reforming of Methane at 2 MPa by Pt, Ru or Ni" Applied Catalysis A 268,151-158 (2004).

83. Nagaoka, K., Takanabe, K., Aika, K., "Influence of the Reduction Temperature on Catalytic Activity of Co/TiO_2 (anatase-type) for High Pressure Dry Reforming of Methane", Applied Catalysis A 255, 13-21 (2003).

84. Neuville, D.R., de Ligny, D., Cormier, L., Henderson, G.R., Roux, J., Flank, A.-M., Lagarde, P., "The Crystal and Melt Structure of Spinel and Alumina at High Temperature: An in-situ XANES Study at the Al and Mg K-edge", Geochimica et Cosmochimica Acta 73, (2009) 3410–3422 (2009).

85. Nichio, N.N., Casella, M.L., Santori, G.F., Ponzi, E.N., Ferritti, O.A., "Stability Promotion of $Ni/\alpha\text{-}Al_2O_3$ Catalysts by Tin Added via Surface Organometallic Chemistry on Metals: Application in Methane Reforming Processes", Catalysis Today 62 231-240 (2000).

86. Oh, Y.-S., Roh, H.-S., Jun, Ki. -W., Baek, Y.-S., "A Highly Active Catalyst, $Ni/Ce–ZrO_2/\theta\text{-}Al_2O_3$, for On-Site H_2 Generation by Steam Methane Reforming: Pretreatment Effect", International Journal of Hydrogen Energy 28, 1387-1392 (2003).

87. Osaki, T., Masuda, H., Mori, T., "Intermediate Hydrocarbon Species for the CO2-CH4 reaction on supported Ni catalysts", Catalysis Letter.29, 33-37 (1994).

88. Osaki, T., Masuda, H., Horiuchi, T., Mori, T., "Highly Hydrogen-deficient Hydrocarbon Species for the CO_2 Reforming of CH_4 on Co/Al_2O_3 Catalyst", Catalysis Letter 34, 59-63 (1995).

89. Osaki T., Mori, T., "Role of Potassium in Carbon-free CO_2 Reforming of Methane on K-Promoted Ni/Al_2O_3 Catalysts", Journal of Catalysis 204, 89-97 (2001).

90. Osaki, T., Horiuchi, T., Suzuki, K., Mori T., "Kinetics, Intermediates and Mechanism for the CO_2 Reforming of Methane on Supported Nickel Catalysts", Journal of the Chemical Society, Faraday Transactions 92, 1627-31 (1996).

91. Osaki, T., "Effect of reduction temperature on the CO2-reforming of methane over TiO2-supported Ni catalyst", Journal of the Chemical Society, Faraday Transactions 93, 643-647 (1997).

92. Pompeo, F., Nichio, N.N., Souza, M.V.M., Cesar,D.V., Ferretti, O.A., Schmal , M., "Study of Ni and Pt Catalysts Supported on $\alpha\text{-}Al_2O_3$ and ZrO_2 Applied in Methane Reforming with CO_2", Applied Catalysis A 316, 175-183 (2007).

93. Qin, D., Lapszewicz, J., "Study of Mixed Steam and CO_2 Reforming of CH_4 to Syngas on MgO-Supported Metal", Catalysis Today 21, 551-560 (1994).

94. Quincoces, C.E., Dicundo, S., Alvarez, A.M., González, M.G., "Effect of Addition of CaO on Ni/Al_2O_3 Catalysts Over CO_2 Reforming of Methane", Materials Letter 50,21-27 (2001).

95. Quincoces, C.E., Vargas, S.P.D., Grange, P., and Gonzales, M.G., "Role of Mo in CO_2 Reforming of CH_4 over Mo promoted Ni/Al2O3 catalysts", Material Letters 56 698-704 (2002).

96. Ramaswamy, V., Boucher, O., Haigh, J., Hauglustaine, D., Haywood, J., Myhre, G.,Nakajima, T., Shi, G.Y., Solomon, S., "Contribution of Working Group I to the Third Assessment Report of the Intergovernmental Panel on Climate Change", Cambridge University Press, Cambridge, United Kingdom and New York, NY, USA, 2001.

97. Ranjbar, A., Rezaei, M., "Preparation of Nickel Catalysts Supported on $CaO-Al_2O_3$ for Methane Reforming with Carbon dioxide", International Journal of Hydrogen Energy 37,6356-6362 (2012).

98. Reitmeier, R., Atwood, K., Bennet, H., and Baugh, H., "Production of Synthesis Gas by Reacting Light Hydrocarbons with Steam and Carbon Dioxide," Industrial and Engineering Chemistry 40, 620-626 (1948).

99. Richardson, J. T., "Principles of Catalyst Development: Fundamental and Applied Catalysis'', Plenum Press: New York, 1989.

100. Rodriguez, G., Roger, A.C., Bedel, L., Udron, L., Carballo, L., Kiennemann, A., "Dry Reforming of Ethane on Tri-Metallic Perovskites (LaCoxFe1-xO3). Characterisations and Reactivity", Fuel Chemistry Division Preprints 47, 260 (2002).

101. Rostrup-Nielsen, J. R., "Industrial Relevance of Coking", Catalysis Today 37, 225-232 (1997).

102. Ruckenstein E., and Hu. Y.H., "Carbon Dioxide Reforming of Methane Over Nickel/alkaline earth metal oxide catalysts", Applied Catalysis A 133, 149-161 (1995).

103. Ruckenstein E., and Hu. Y.H., "Role of Support in CO_2 Reforming of CH_4 to Syngas Over Ni Catalysts", Journal of Catalysis 162, 230-238 (1996).

104. Ruckenstein, E., Wang, H.Y., "Carbon Dioxide Reforming of Methane to Synthesis Gas Over Supported Cobalt Catalysts", Applied Catalysis A 204, 257-263 (2000).

105. Ruckenstein, E., Hu, Y.H., "Highly Efficient Catalysts for CO_2 Reforming of Methane*",* Chemical Innovation 30, 39-44 (2000).

106. Ruckenstein, E. and Wang, H.Y., "Carbon Deposition and Catalytic Deactivation During CO_2 Reforming of CH_4 over $Co/\gamma-Al_2O_3$ Catalysts", Journal of Catalysis 205, 289-293 (2002).

107. SanJose´-Alonso, C., Illa´n-Go´mez, M. J., and Roma´n-Martı´nez, M. C.," K and Sr Promoted Co Alumina Supported Catalysts for the CO_2 Reforming of Methane", Catalysis Today 176, 187-190 (2011).

108. Schreyeck, L., Wlosik, A., Fuzellier, H., "Influence of the Synthesis Route on $MgAl_2O_4$ Spinel Properties", Journal of Material Chemistry 11, 483-486 (2001).

109. Segner, J., Campbell, C.T., Doyen, G., Ertl, G., "Catalytic Oxidation of CO on Pt(111): The Influence of Surface Defects and Composition on the Reaction Dynamics", Surface Science138, 505-523 (1984).

110. Seok, S.H., Choi, S.H., Park, E.D., Han, S.H., and Lee, J.S., "Mn-Promoted Ni/Al_2O_3 Catalysts for StableCarbon Dioxide Reforming of Methane", Journal of Catalysis 209, 6-15 (2002).

111. Seshan, K., Barge, H.W., Hally, W., Keulen, A.N.J., Ross, J.R.H., "Natural gas conversion" Elsevier, Amsterdam, page 285 (1994).

112. Shi, C., Zhang, P., "Role of MgO over γ-Al_2O_3-Supported Pd Catalysts for Carbon Dioxide Reforming of Methane", Applied Catalysis B 170-171, 43-52 (2015).

113. Sing, K.S.W., Everett, D.H.G., Haul, R.A.W., Moscou, L., Pierotti, R.A., Rouquerol, J., Siemieniewska, T., "Reporting Physisorption Data for Gas/Solid System: International Union of Pure and Applied Chemistry, IUPAC", Pure Applied Chemistry 57, 603-619 (1985).

114. Slagtern, A., Olsbye, U., Blom, R.,Dahl, I.M., "The Influence of Rare Earth Oxides on Ni/Al_2O_3 Catalyst During CO_2 Reforming of CH_4", Studies in Surface Science and Catalysis 107, 497-502 (1997).

115. Son, I.H., Lee, S.J., Song, I.Y., Jeon, W.S., Jung, I.D., Yunc, J., Jeong, D.-W., Shim, J.-O., Jang, W.-J., Rohd, H.-S., "Study on Coke Formation Over Ni/γ-Al_2O_3, Co-Ni/γ-Al_2O_3, and Mg-Co-Ni/γ-Al_2O_3 Catalysts for Carbon Dioxide Reforming of Methane", Fuel 136, 194-200 (2004).

116. Son, I., Lee, S., Song, I., Jeon, W., Jung, I., Yunc, D., Jeong, D.-W., Shim, J.-O.,Jang, W.-J., Rohd, H.-S., "Study on Coke Formation over Ni/γ-Al_2O_3, Co-Ni/γ-Al_2O_3, and Mg-Co-Ni/γ-Al_2O_3 Catalysts for Carbon Dioxide Reforming of Methane",Fuel 136, 194-200 (2014).

117. Song, S.H., Lee, S.B., Bae, J.W., Prasad, P.S.S., Jun, K.W., "Influence of Ru Segregation on the activity of Ru-Co/γ-Al_2O_3 during FT synthesis: A Comparison with that of Ru-Co/SiO2 Catalysts. Catalysis Communication 9, 2282–2286 (2008).

118. Stöcker, M., Jens, K.-J., Riis, T., Grepstad, J.K., "Characterization of Ni Exchanged Montmorillonites by X-ray Photoelectron Spectroscopy", Journal of the Chemical Society, Faraday Transactions 1: 84, 1863-1870 (1988).

119. Souza, M.V.M., Clavé, L., Dubois, V., Pelez, C.A.C., Schmal, M., "Activation of Supported Nickel Catalysts for Carbon Dioxide Reforming of Methane", Applied Catalysis A 272, 133-139 (2004).

120. Suzuki, K., Wargadalam, V.J., Onoe, K., Yamaguchi, T., CO_2 Reforming of Methane by Thermal Diffusion Column Reactor with Ni/Carbon-Coated Alumina Tube Pyrogen", Energy and Fuels 15, 571-574 (2001).

121. Suzuki. D., "Global Warming" Web Source: David Suzuki.org/issues/climate-change/science/climate-change-basics/greenhouse-gases. (Accessed April, 2017).

122. Swaan, H.M., Kroll, V.C.H., Martin, G.A., and Mirodatos, C., "Deactivation of Supported Nickel Catalysts During the Reforming of Methane by Carbon Dioxide", Catalysis Today 21, 571-578 (1994).

123. Takanabe, K., Nagaoka K., Aika, K., "Improved Resistance against Coke Deposition of Titania Supported Cobalt and Nickel Bimetallic Catalysts for Carbon Dioxide Reforming of Methane", Catalysis Letter 102, 153-157 (2005).

124. Takanabe, K., Nagaoka, K., Nariai, K., Aika, K., "Titania-supported Cobalt and Nickel Bimetallic Catalysts for Carbon Dioxide Reforming of Methane", Journal of Catalysis 232, 268-275 (2005).

125. Takano, A., Tagawa, T., and Goto, S., "Carbon Dioxide Reforming of Methane on Supported Nickel Catalysts", Journal of Chemical Engineering, Japan 27, 727-731 (1994).

126. Takayasu, O., Hongo, N., Masuura,I., "Noble Metal Promoted Ni0.03Mg0.97O Solid Solution Catalysts for the Reforming of CH_4 with CO_2", Studies in Surface Science and Catalysis 77, 305-309 (1993).

127. Tan, P., Gao, Z., Shen, C., Du, Y., Li, X., Wei, H., "Ni-Mg-Al Solid Basic Layered Double Oxide Catalysts Prepared using Surfactant-Assisted Coprecipitation Method for CO2 Reforming of CH_4", Chinese Journal of Catalysis 35, 1955-1971 (2014).

128. Tang, S.B., Qiu, F.L., Lu, S.J., "Effect of Supports on the Carbon Deposition of Nickel Catalysts for Methane Reforming with CO_2", Catalysis Today 24, 253-255 (1995).

129. Tang, S., Ji, L., Lin, J., Zeng, H.C., Tan, K.L., Li, K., "CO_2 Reforming of Methane to Synthesis Gas over Sol–gel-made Ni/γ-Al_2O_3 Catalysts from Organometallic Precursors", Journal of Catalysis 194, 424- 430 (2000).

130. Therdthianwong, S., Therdthianwong, A., Siangchin, C., "Synthesis Gas Production from Dry Reforming of Methane Over Ni/Al_2O_3 stabilized by ZrO_2", International Journal of Hydrogen Energy 33, 991-999 (2008).

131. Tichit, D., Medina, F., Coq, B., Dutartre, R., "Tichit, D., Medina, F., Coq, B., and Dutartre, R., "Activation Under Oxidizing and Reducing Atmospheres of Ni-Containing Layered Double Hydroxides", Applied Catalysis A 159, 241-258 (1997).

132. Tomishige, K., Kanazawa, S., Sato, M., Ikushima, K., Kunimori, K., "Catalyst Design of Pt-Modified Ni/Al_2O_3 Catalyst with Flat Temperature Profile in Methane Reforming with CO_2 and O_2", Catalysis Letter 84, 69-74 (2002).

133. Trcera, N., Cabaret, D., Rossano, S., Farges, F., Flank, A.-M., Lagarde, P., "Experimental and Theoretical Study of the Structural Environment of Magnesium in Minerals and Silicate Glasses using X-ray Absorption Near-Edge Structure", Physics and Chemistry of Minerals 36, 241-257 (2009).

134. Tsipouriari, V.A., Verykios, X.E., "Kinetic Study of the Catalytic Reforming of CH_4 with CO_2 to Syn Gas Over Ni/La2O3 Catalyst", Catalysis Today 64, 83-90 (2001).

135. Twigg, M.V., Catalyst Handbook, 2nd Edition, Wolfe Publishing, London, (1989).

136. U. S. Department of Energy, "Carbon Cycling and Bio-sequestration", Integrating Biology and Climate Through Systems Science: Report from the March 2008 Workshop, DOE/SC-108. U.S. Department of Energy Office of Science, 2008.

137. U.S. Environmental Protection Agency, "Greenhouse Gases Emission", Web Source: www.epa.gov/ghgemissions/global-greenhouse-gas-emissions-data. (Accessed May, 2017).

138. Vernon, P.D.F., Green, M.L.H., Cheetham, A.K., and Ashcroft A.T., "Partial Oxidation of Methane to Synthesis gas, and Carbon Dioxide as an Oxidising Agent for Methane Conversion", Catalysis Today13, 417-426 (1992).

139. Verykios, X.E., "Catalytic Dry Reforming of Natural Gas for the Production of Chemicals and Hydrogen", International Journal of Hydrogen Energy 28, 1045-1063 (2003).

140. Wang, H.Y., Ruckenstein, E., "Conversions of Methane to Synthesis Gas over $Co/\gamma\text{-}Al_2O_3$ by CO_2 and/or O_2", Catalysis Letters 75,13-18 (2001).

141. Wang, H.Y. and, Ruckenstein, E., "CO_2 Reforming of CH_4 Over Co/MgO Solid Solution Catalysts - Effect of Calcination Temperature and Co loading", Applied Catalysis A 209, 207-215 (2001).

142. Wang, H. and Sameen, Z., "Catalyst Development for CO_2 Activation to Produce Syn-Gas through CO_2 Reforming of CH_4: Mitigation of Carbon Formation on Ni-Based Catalysts'', Published by Elsevier page 455-479 (2013).

143. Wang, H., Miller, J.T., Shakouri, M., Xi, C., Wu, T., Zhao, H., Akatay, M.C., "XANES and EXAFS Studies on Metal Nanoparticle Growth and Bimetallic Interaction of Ni-Based Catalysts for CO_2 reforming of CH_4" Catalysis Today 207, 3-12 (2013).

144. Wang, S., Lu G.Q.M., Millar, G.J. "Carbon Dioxide Reforming of Methane to Produce Synthesis Gas over Metal-Supported Catalysts: State of the Art", Energy and Fuel 10,896-904 (1996).

145. Wang, S., Lu, G.Q., "Effects of promoters on catalytic activity and carbon deposition of $Ni/\gamma\text{-}Al_2O_3$ catalysts in CO_2 reforming of CH_4", Journal of Chemical Technology and Biotechnology 75, 589-595 (2000).

146. Wang, Y.H., Liu, H.M., Xu, B.Q., "Durable Ni/MgO Catalysts for CO_2 Reforming of Methane: Activity and Metal–support interaction", Journal of Molecular Catalysis A 299, 44-52 (2009).

147. Wei, J.-M., Xu, B.-Q., Li, J.-L., Cheng, Z.-X., Q.-M. Zhu, Q.-M., "Highly Active and StableNi/ZrO2 Catalyst for Syngas Production by CO_2 Reforming of CH_4", Applied Catalysis A 196, 167-172 (2000).

148. White, G.A., Roszkowski, T.R., Stanbridge, D.W., "Catalytic Conversion of Methane to Syn Gas", Hydrocarbon Process 54,130 (1975).

149. Wu, M., Hercules, D.M., "Studies of Supported Nickel Catalysts by X-ray Photoelectron and Ion Scattering Spectroscopies", Journal of Physical Chemistry 83, 2003–2008 (1979).

150. Wu, J., Yitian F., Yang W., "Combined coal Gasification and Methane Reforming for Production of Syngas in a Fluidized-Bed Reactor", Energy & Fuels 19, 512-516 (2005).

151. Xiong, H., Zhang, Y., Liew, K., Li, J., "Catalytic Performance of Zirconium-Modified Co/Al_2O_3 for Fischer–Tropsch Synthesis", Journal of Molecular Catalysis. A 231,145-151 (2005).

152. Xu, L. L., Song, H.L., Chou, L.J., "Carbon Dioxide Reforming of Methane Over Ordered Mesoporous NiO–MgO–Al_2O_3 Composite Oxides ", Catalysis B 108, 177-190 (2011).

153. Xu, G., Shi, K., Gao, Y., Xu, H., Wei, Y., "Studies of Reforming Natural Gas with Carbon Dioxide to Produce Synthesis Gas: X. The Role of CeO_2 and MgO Promoters", Journal of Molecular Catalysis A 147, 47-54 (1999).

154. Yamaguchi, A., Iglesia, E., "Catalytic Activation and Reforming of Methane on Supported Palladium Clusters", Journal of Catalysis 274, 52-63 (2010).

155. Yoshimura, T., Tamenori, Y., Iwasaki, N., Hasegawa, H., Suzuki, A., Kawahata, H., "Magnesium K-edge XANES Spectroscopy of Geological Standards", Journal of Synchrotron Radiation 20, 734-740 (2013).

156. Yu, J.J., Jiang, Z., Zhu, L., Hao, Z.P., Xu, Z.P., "Adsorption/Desorption Studies of NOx on Well-Mixed Oxides Derived from Co-Mg/Al Hydrotalcite-like Compounds", Journal of Physical Chemistry B 110, 4291–300 (2006).

157. Zhang, J., Wang, H., Dalai, A. K., 19th Canadian Symposium on Catalysis, Saskatoon, Saskatoon, Canada, May 14-17, 2006, p. 159.

158. Zhang, J., Wang, H., Dalai, A.K., "Development of Stable Bimetallic Catalysts for Carbon Dioxide Reforming of Methane", Journal of Catalysis 249, 300–310 (2007).

159. Zhang, J., Wang, H., Dalai, A.K., "Effects of Metal Content on Activity and Stability of Ni-Co Bimetallic Catalysts for CO_2 Reforming of CH_4", Applied Catalysis A 339,121-129 (2008).

160. Zhang, J., Wang, H., Dalai, A.K., "Kinetic Studies of Carbon Dioxide Reforming of Methane over NiCo/AlMgO Bimetallic Catalyst", Industrial Engineering Chemistry 48,677-684 (2009).

161. Zhang, J., Wang, H., Xi, C., Hu, Y., Dalai, A.K., "Design and Preparation of Ni-Co Bimetallic

Nanocatalyst for Carbon Dioxide Reforming of Methane", in: A.K. Dalai (ed), Nanocatalysis for Fuels and Chemicals, ACS Symposium Series, American Chemical Society, Washington, DC, pages.196–221 (2012).

162. Zhang, J., Wang, H., Dalai, A.K.,", US Patent 7.985,710 B2, 2011.

163. Zhang, J., "Research and Development of Nickel Based Catalysts for Carbon Dioxide Reforming of Methane", Ph.D. Thesis, University of Saskatchewan, Saskatoon, Canada, 2008.

164. Zhang, Z., and Verykios, X.E., "Mechanistic Aspects of Carbon Dioxide Reforming of Methane to Synthesis gas over Ni Catalysts", Catalysis Today 21, 589 (1994).

165. Zhang, Z.L., and Verykios, X.E., "A Stableand Active Nickel-based Catalyst for Carbon Dioxide Reforming of Methane to Synthesis Gas", Journal of the Chemical Society, Chemical Communications 71-72 (1995).

166. Zhu, J., Peng, X., Yao, L., Tong, D., Hu, W., "CO_2 Reforming of Methane Over Mg-Promoted Ni/SiO2 Catalysts: The Influence of Mg Precursors and Impregnation Sequences", Catalysis Science and Technology 2, 529-537 (2012).

167. Zhu, J., Peng, X., Yao, L., Shen, J., Tong, D., Hu,C., " The Promoting Effect of La, Mg, Co and Zn on the Activity and Stability of Ni/SiO_2 Catalyst for CO_2 Reforming of Methane",International Journal of Hydrogen Energy 36,7904-7104 (2011) .

168. Zhu, J.Q., Peng, X.X., Yao, L., Shen, J., Tong, D.M., Hu, C.W., "The Promoting Effect of La, Mg, Co and Zn on the Activity and Stability of Ni/SiO_2 Catalyst for CO_2 Reforming of Methane", International Journal of Hydrogen Energy 36,7094-7104 (2011).

APPENDICES

APPENDIX A: SCHEMATIC DIAGRAM OF CATALYST PREPARATION PROCEDURE

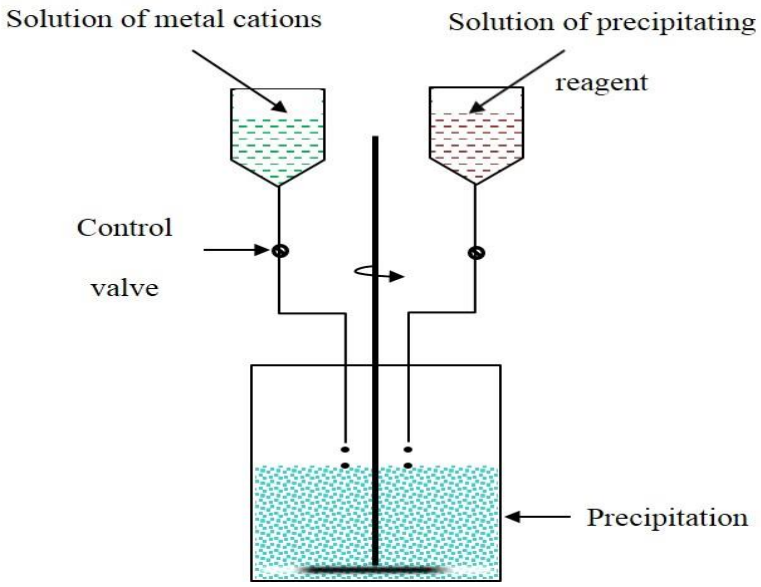

Figure A.1. Schematic diagram of catalyst preparation procedure

APPENDIX B: SCHEMATIC DIAGRAM OF CATALYST EVALUATION PROCEDURE

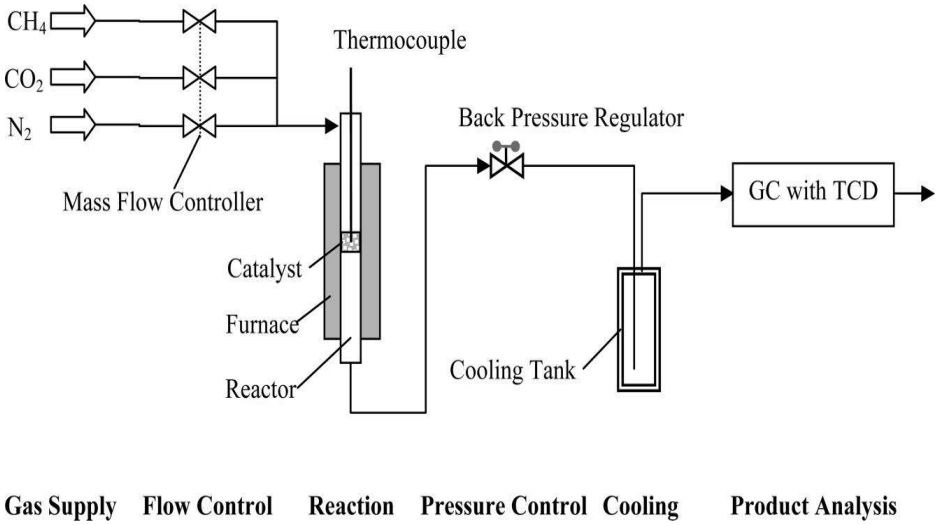

Figure B.1. Schematic diagram of catalyst evaluation procedure

APPENDIX C: MFC CALIBRATION

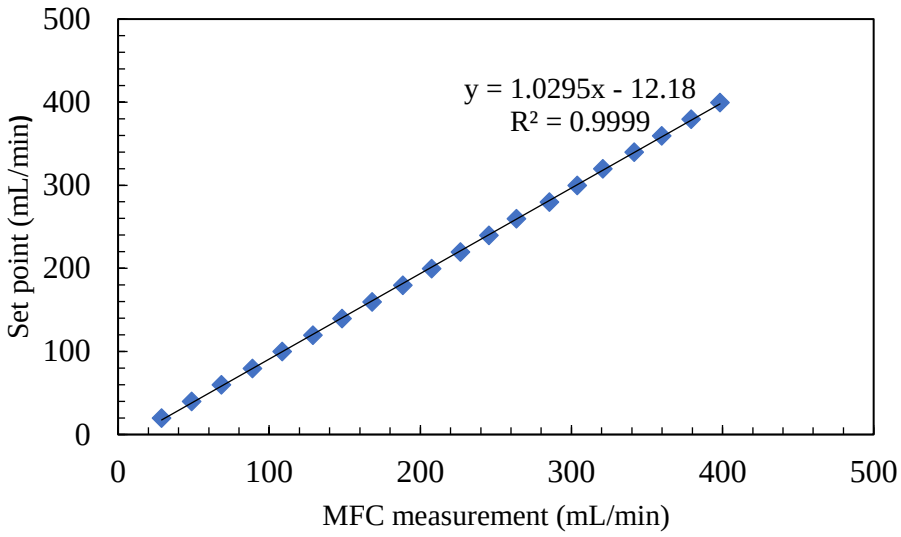

Figure C.1. N_2 mass flow controller (Set point vs MFC measurement at STP)

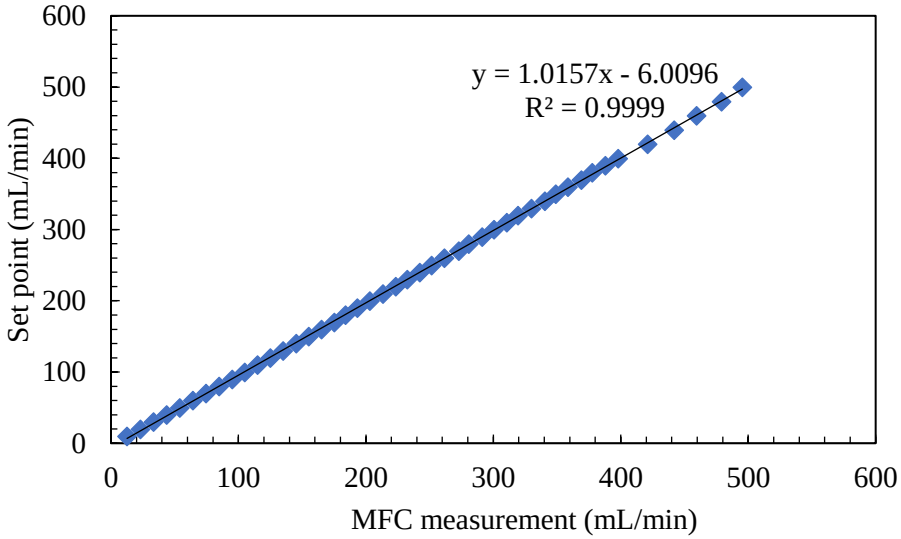

Figure C.2. CO_2 mass flow controller (Set point vs MFC measurement at STP)

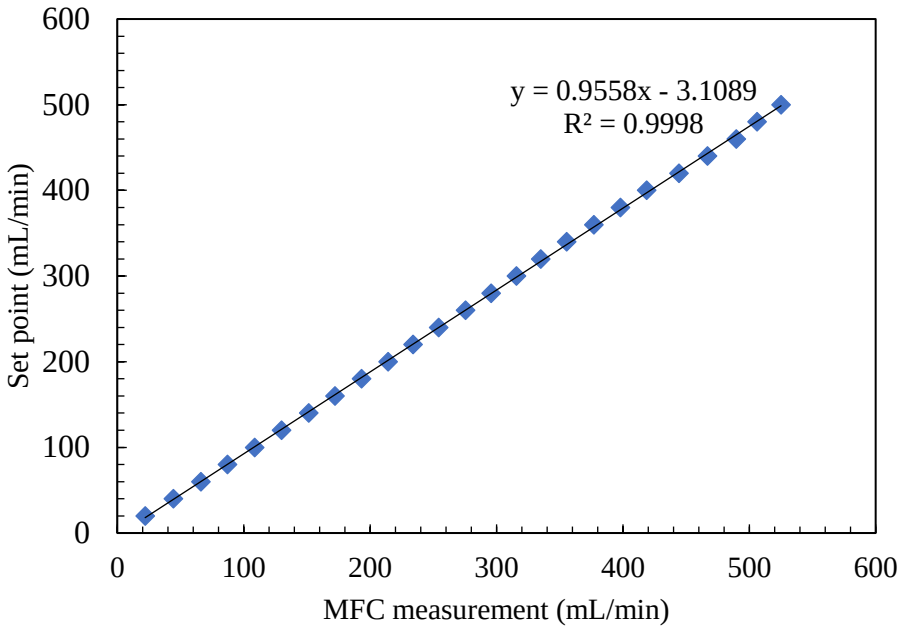

Figure C.3. CH_4 mass flow controller (Set point vs MFC measurement at STP)

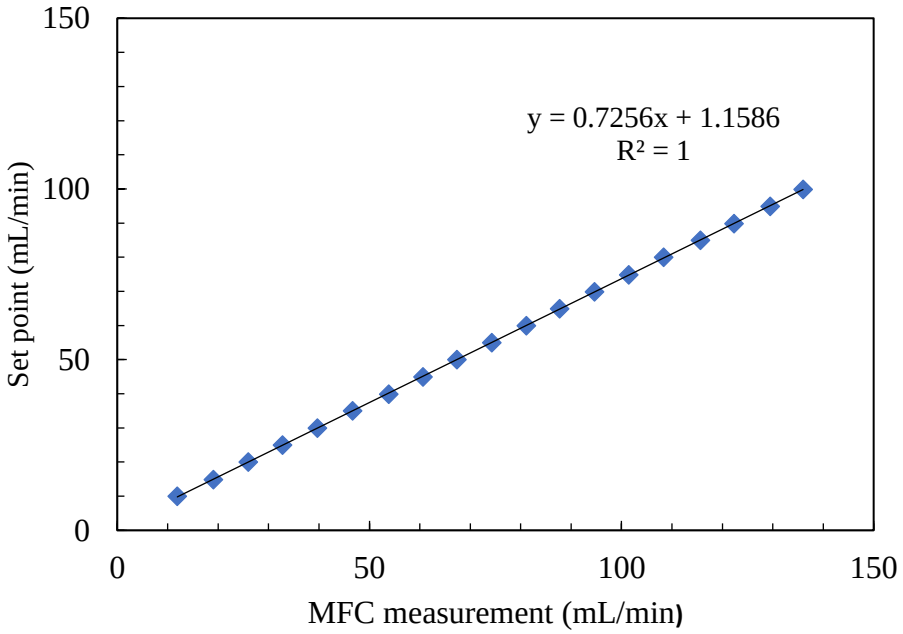

Figure C.4. H_2 mass flow controller (Set point vs MFC measurement at STP)

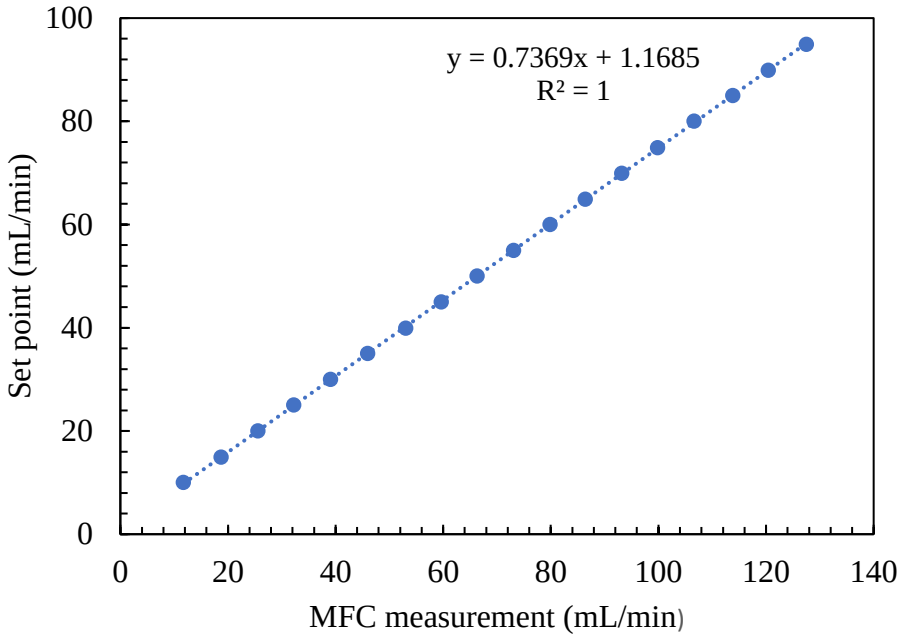

Figure C.5. CO mass flow controller (Set point vs MFC measurement at STP)

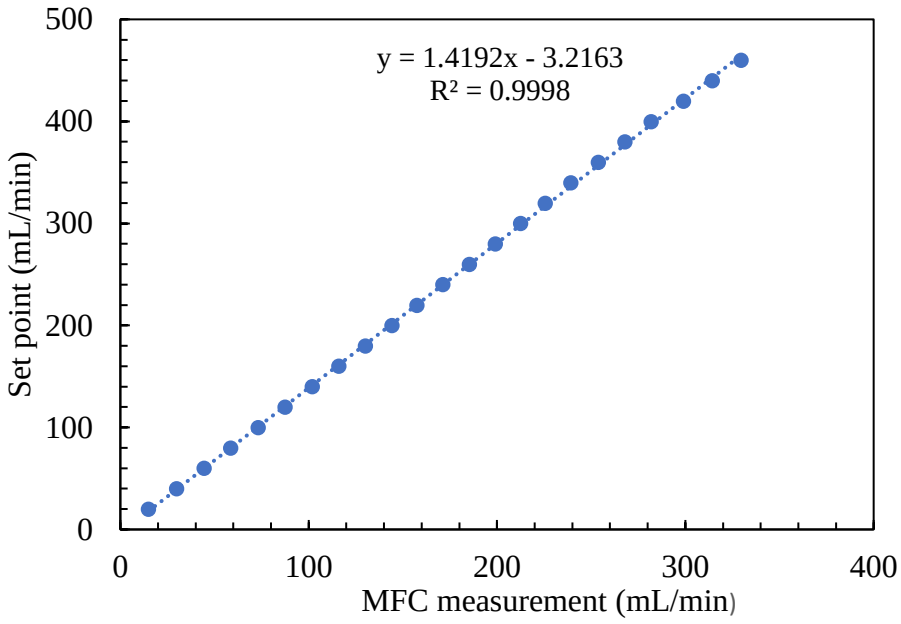

Figure C.6. C_2H_6 mass flow controller (Set point vs MFC measurement at STP)

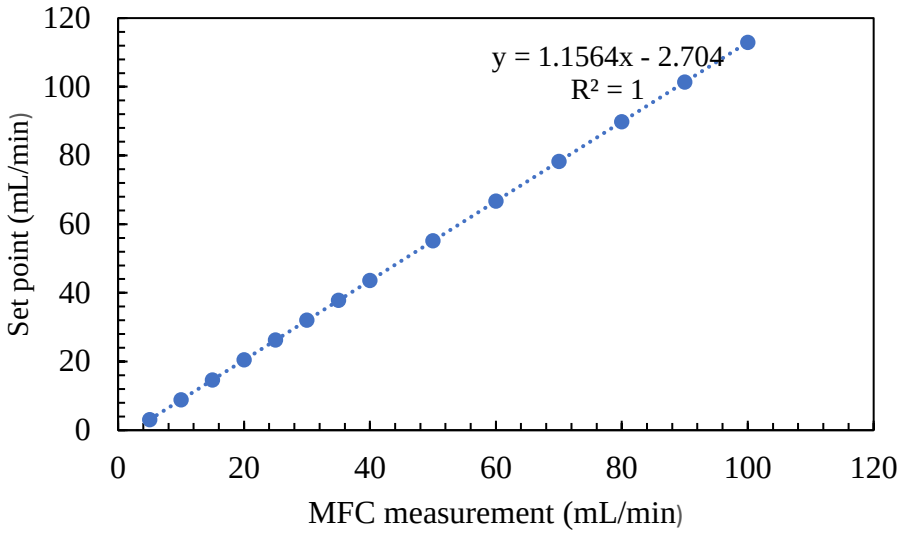

Figure C.7. C_2H_4 mass flow controller (Set point vs MFC measurement at STP)

APPENDIX D: GC CALIBRATION

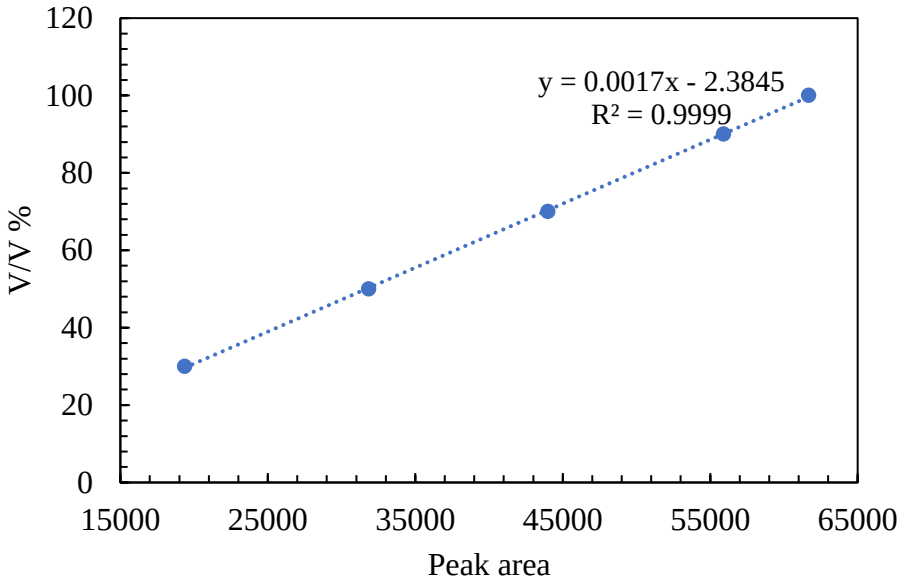

Figure D.1. N_2 GC calibration (V/V % vs Peak area)

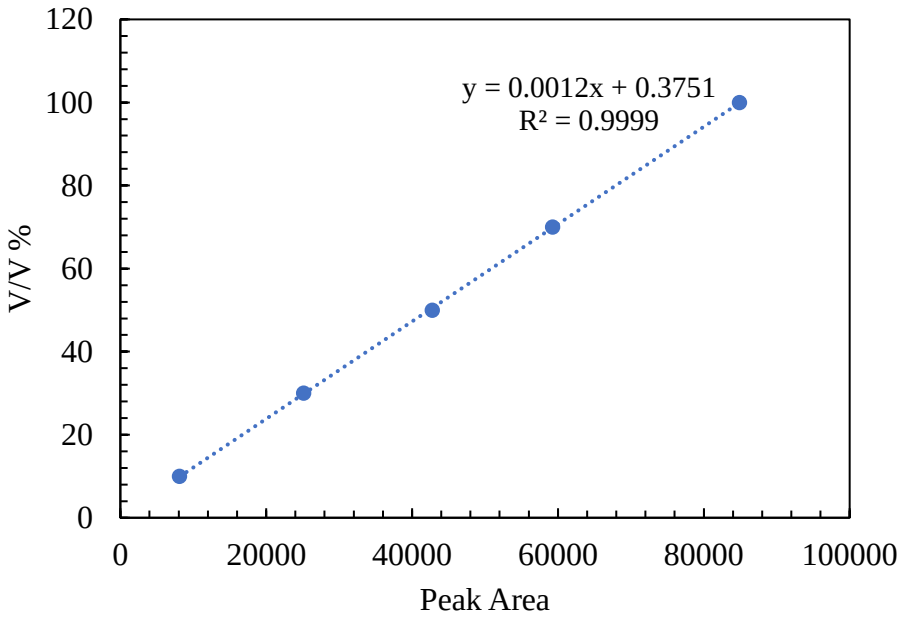

Figure D.2. CO_2 GC calibration (V/V % vs Peak area)

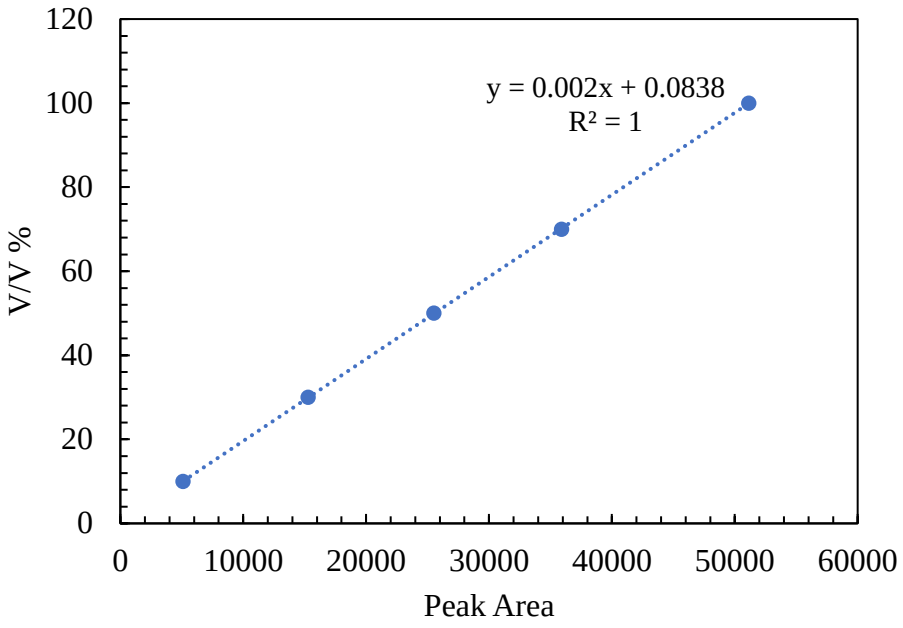

Figure D.3. CH_4 GC calibration (V/V % vs Peak area)

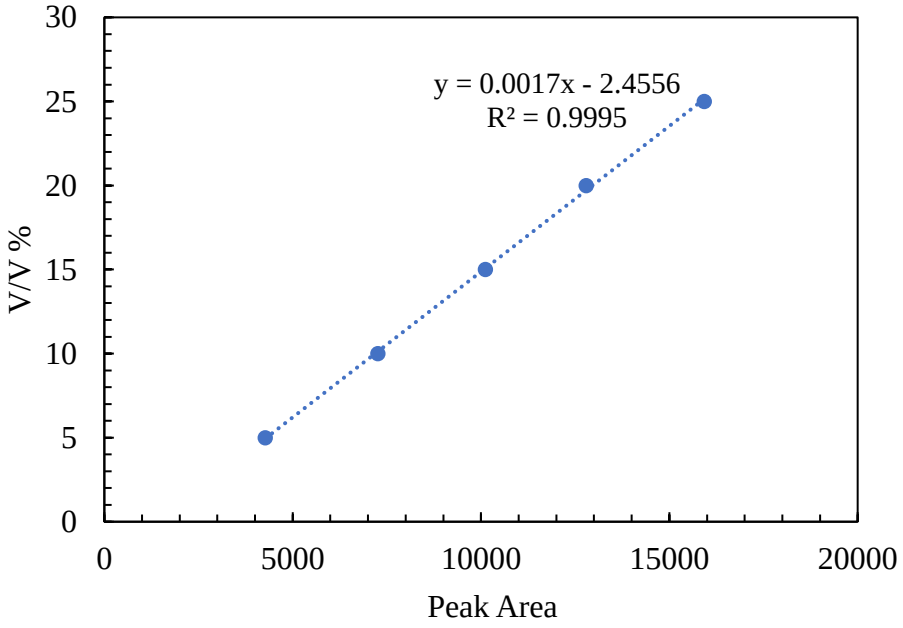

Figure D.4. CO GC calibration (V/V % vs Peak area)

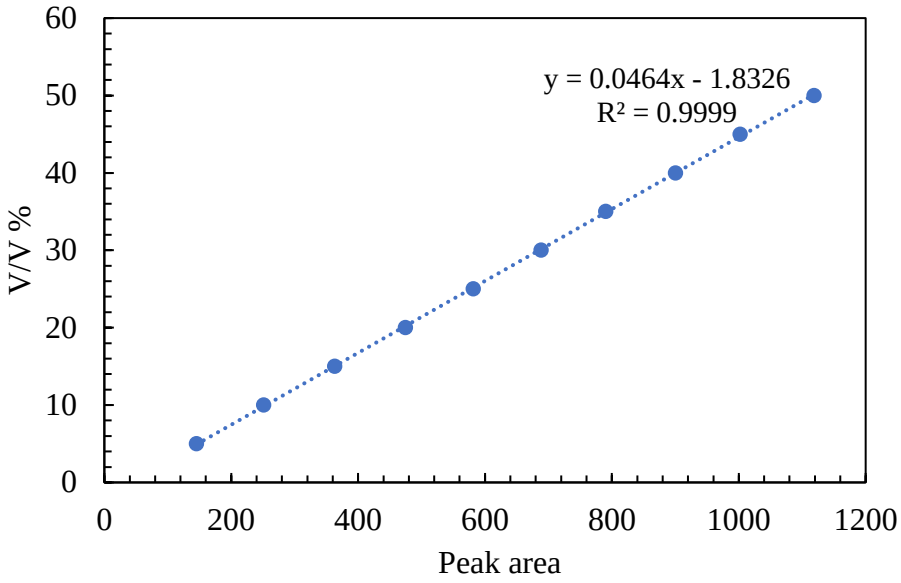

Figure D.5. H_2 GC calibration (V/V % vs Peak area)

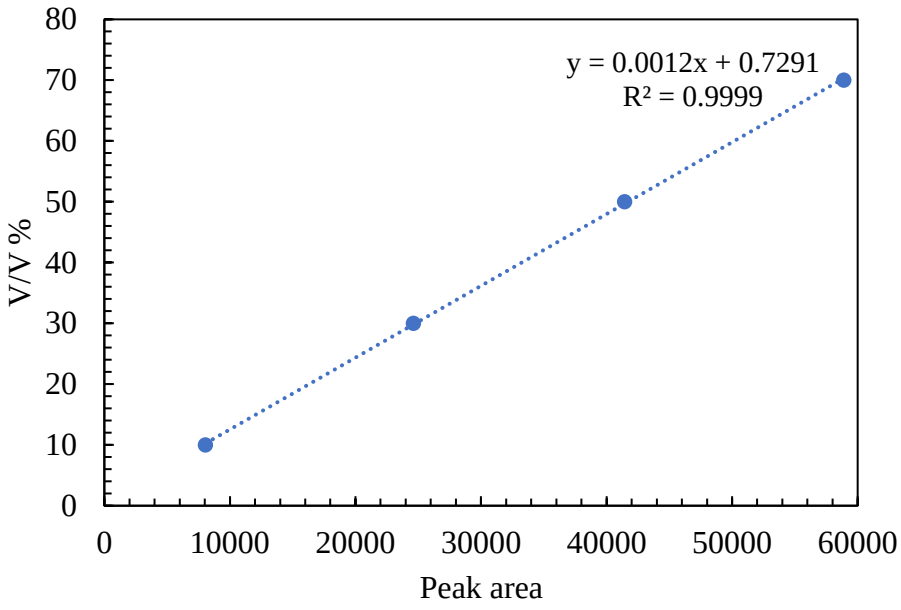

Figure D.6. C_2H_6 GC calibration (V/V % vs Peak area)

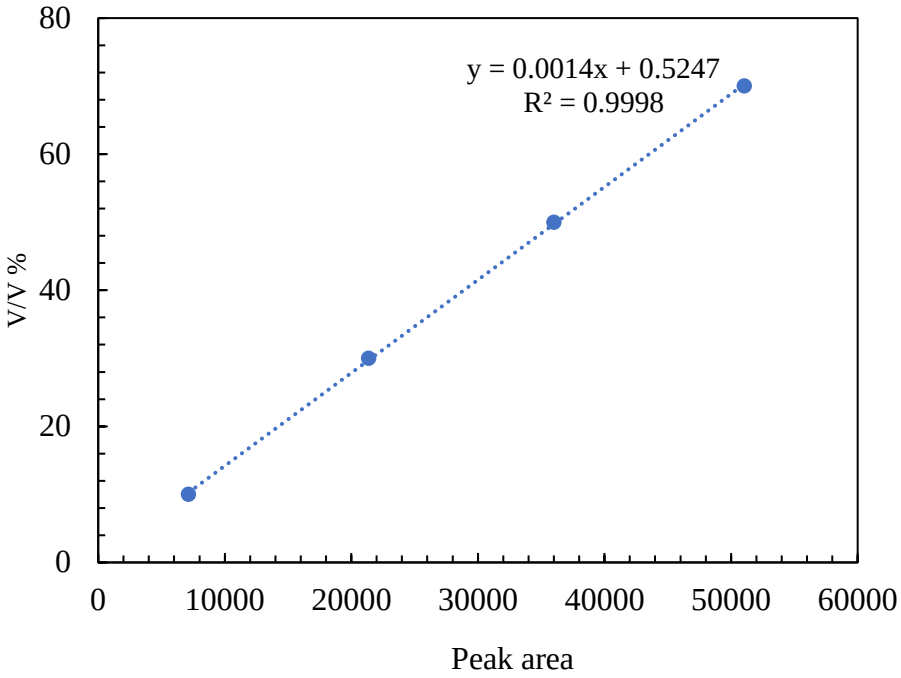

Figure D.7. C_2H_6 GC calibration (V/V % vs Peak area)

APPENDIX E: EFFECT OF INITIAL pH OF SALT SOLUTION ON METAL PRECIPITATION

Table E.1. Effect of initial pH of salt solution on metal precipitation for Mg-Al supported catalysts

Catalyst	Initial pH of salt solution	Target Mg/Al	Actual Mg/Al	% Composition			
				Ni	Co	Mg	Al
CopCat-Ni5-Mg/Al-1.60	2.8	3.6	1.6	4.8	-	59.0	36.2
CopCat-Co6-Mg/Al-1.55	3.2	3.6	1.5	-	6.1	56.8	37.1
CopCat-Ni2Co2-Mg/Al-0.30	1.2	0.3	0.3	1.6	1.7	21.5	75.2
CopCat-Ni2Co2-Mg/Al-1.00	1.7	1.0	0.9	1.7	1.8	45.6	50.9
CopCat-Ni3Co3-Mg/Al-1.75	2.5	4.0	1.8	2.6	3.1	59.9	34.4
CopCat-Ni4Co5-Mg/Al-2.00	3.6	8.0	2.0	3.9	4.9	60.8	30.4

Table E.2. Effect of initial pH of salt solution on metal precipitation for Mg or Al supported catalysts

Catalyst	Initial pH of salt solution	Target Composition (%)				Actual Composition (%)			
		Ni	Co	Mg	Al	Ni	Co	Mg	Al
CopCat-Ni3-Mg/Al-0.0	2.3	3.3	-	-	96.7	3.00	-	-	97.0
CopCat-Co4-Mg/Al-0.0	2.5	-	3.3	-	96.7	-	3.6	-	96.4
CopCat-Ni84-Mg/Al-#	6.3	3.3	-	96.7	-	83.9	-	16.1	-
CopCat-Co87-Mg/Al-#	6.7	-	3.3	96.7	-	-	87.1	12.90	-

Table E.3. Effect precipitation pH on metal precipitation for NiCoMgAlOx catalyst

Catalyst	Precipitation	Target composition (%)				Actual Composition (%)				Target	Actual
	pH	Ni	Co	Mg	Al	Ni	Co	Mg	Al	Mg/Al	Mg/Al
NiCoMgAlOx	5.5	1.6	1.6	75.9	20.9	4.1	4.3	15.9	75.7	3.6	0.2
NiCoMgAlOx	8.5	1.6	1.6	75.9	20.9	2.5	2.9	58.9	35.7	3.6	1.7
NiCoMgAlOx	10.0	1.6	1.6	75.9	20.9	0.8	2.0	71.9	25.3	3.6	2.8

Table E.4.: Effect on initial concentration of salts on metal precipitation

Catalyst	Conc. Of salt solution (g/cm^3)	Initial Ph of salt solution	Actual composition (%)				Target Mg/Al	Actual Mg/Al
			Ni	Co	Mg	Al		
NiCoMgAlOx	0.45	2.0	2.5	3.10	57.9	36.4	3.6	1.6
NiCoMgAlOx	0.23	3.4	2.5	3.0	58.	35.7	3.6	1.7
NiCoMgAlOx	0.09	3.0	3.2	3.5	50.90	42.4	3.6	1.2

APPENDIX F: REPEATABILITY RESULTS OF SOME EXPERIMENTS

Table F.1. Repeatability results for catalysts composition from ICP results

Catalyst	Composition from ICP result				Mg/Al
	Ni	Co	Mg	Al	ratio
CopCat-Ni4Co5-Mg/Al-2	3.9	4.9	60.9	30.3	2.0
CopCat-Ni4Co5-Mg/Al-2 repeat	3.9	4.9	60.8	30.4	2.0
CopCat-Ni2Co2-Mg/Al-0.3	1.6	1.7	21.5	75.2	0.3
CopCat-Ni2Co2-Mg/Al-0.3 repeat	1.6	1.7	21.7	75.0	0.3
CopCat-Ni1Co2-Mg/Al-2.8	0.8	2.0	72.0	25.2	2.9
CopCat-Ni1Co2-Mg/Al-2.8 repeat	0.8	2.0	72.1	25.1	2.9
CopCat-Ni3-Mg/Al-0.0	3.0	-	-	97.0	-
CopCat-Ni3-Mg/Al-0.0 repeat	3.0	-	-	97.0	-
CopCat-Co4-Mg/A-0.0	-	3.4	-	96.6	-
CopCat-Co4-Mg/A-0.0 repeat	-	3.4	-	96.6	-

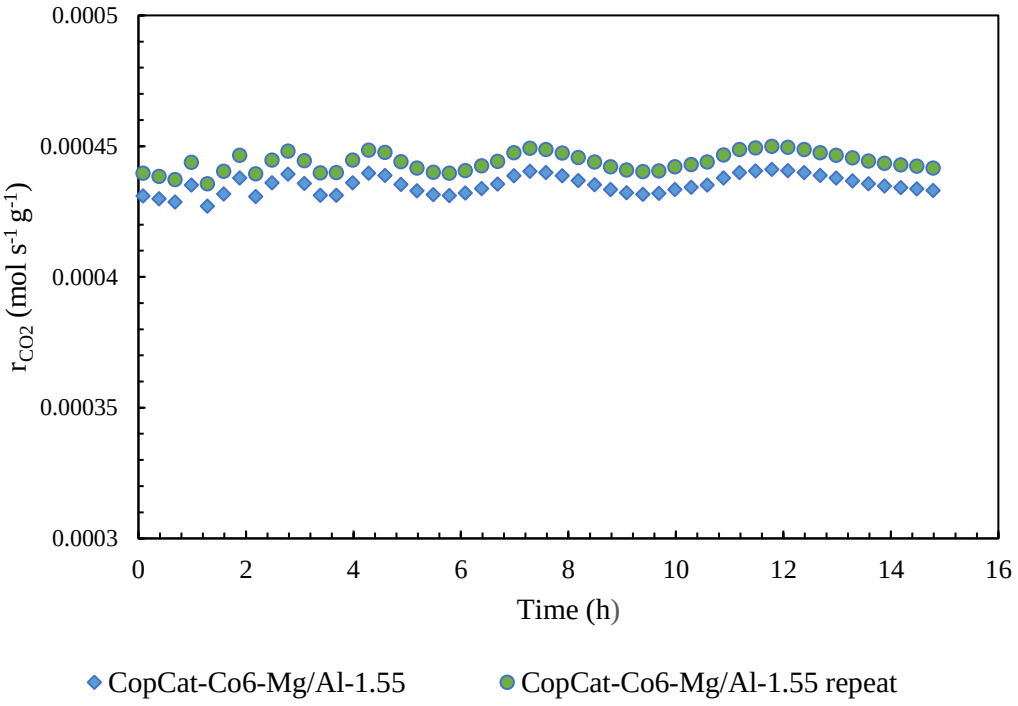

Figure F.1. Rate of CO_2 conversion for monometallic cobalt catalyst

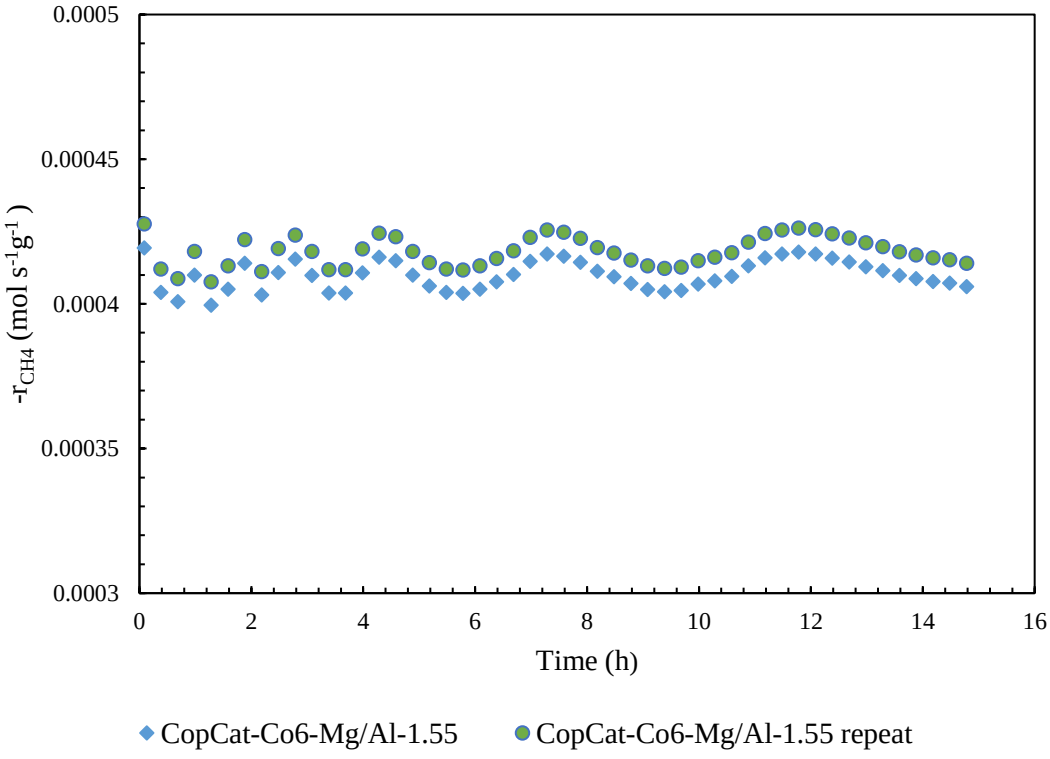

Figure F.2. Rate of CH_4 conversion for monometallic cobalt catalyst

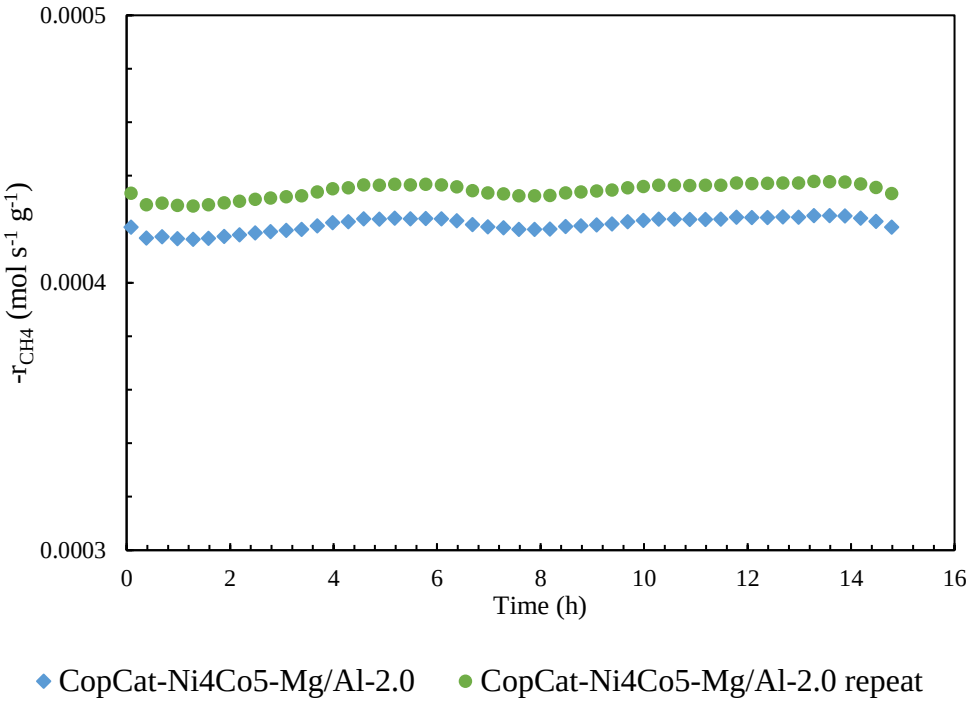

Figure F.3. Rate of CH_4 conversion for bimetallic Ni-Co catalyst

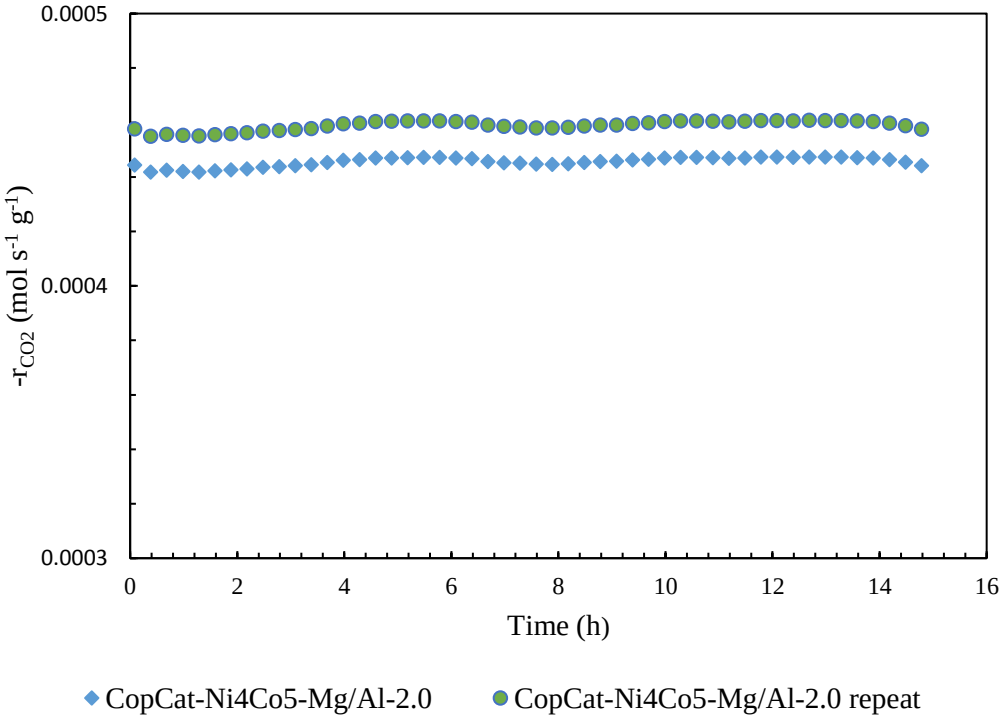

Figure F.4. Rate of CO_2 conversion for bimetallic Ni-Co catalyst

APPENDIX G: MASS AND KINETIC TRANSFER LIMITATION STUDIES

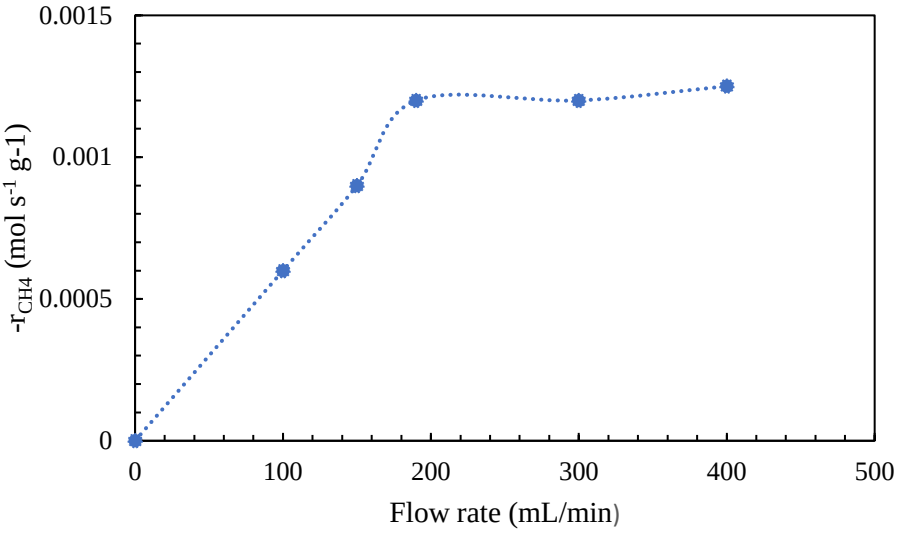

Figure G.1. External Mass Transfer Limitation

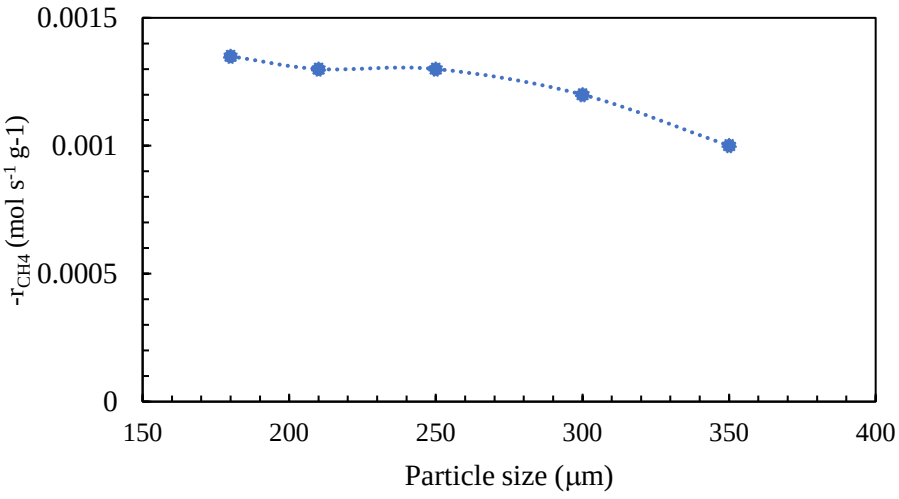

Figure G.2. Internal Mass Transfer Limitation

Reaction rate calculation formula:

$$r_i\ (\text{mol}\ g^{-1}s^{-1}) = \frac{n_j^i - n_j^f}{60 \times m_{cat}}$$